ABSTRACT

STAMM, LINDSEY BROOKS JERRIM. Meniscus-Directed Assembly of Biologically Active Coatings of Cells, Microparticles, and Nanoparticles. (Under the direction of Dr. Orlin D. Velev.)

Convective assembly principles and techniques were used in two complementary studies for depositing close packed yeast-coated surfaces and gold nanoparticle wires. Convective assembly at high volume fraction was used for the rapid deposition of uniform, close-packed coatings of *Saccharomyces cerevisiae* onto glass slides. A computational model was developed to calculate the thickness profiles of such coatings for various experimental conditions. Both experimentation and numerical simulations demonstrated that the deposition process is strongly affected by the presence of sedimentation. The deposition device was inclined to increase the uniformity of the coatings by causing the cells to sediment toward the three-phase contact line. In accordance with the simulation, the experiments showed that both increasing the angle of the device and decreasing the angle between the slides increased the uniformity of the deposited coatings. Finally, the “convective-sedimentation” assembly method was used to deposit composite coatings of live cells and large latex particles as an example of biologically active composite coatings. These coatings were allowed to proliferate and demonstrate a proof-of-concept of a self-cleaning surface.

Two methods were developed for the deposition of micro- and nanoparticles into linear assemblies that could be used in biosensors and biomaterials. In capillary-guided deposition, a capillary is withdrawn across a wettable substrate, resulting in the assembly of a particle line. We characterized the effects of particle concentration and withdrawal

speed and correlated them to structure of the deposited assemblies. The particles are assembled into one of three different structures, depending on the particle volume fraction and deposition speed. We demonstrate that the metallic nanoparticle lines are Ohmically conductive. Using wedge-templated deposition, linear assemblies were deposited from sessile droplets on moderately hydrophobic surfaces. The particles convectively assemble at the freely-receding three-phase contact line and are pulled into a line against the wedge. The deposited lines can be long and narrow with a few breaks or significantly wider and shorter but unbroken. These methods could be used for engineered patterning of nanoparticle structures on surfaces.

Meniscus-Directed Assembly of Biologically Active Coatings of Cells, Microparticles, and Nanoparticles

by
Lindsey Brooks Jerrim Stamm

A dissertation submitted to the Graduate Faculty of
North Carolina State University
in partial fulfillment of the
requirements for the Degree of
Doctor of Philosophy

Chemical Engineering

Raleigh, North Carolina

2009

APPROVED BY:

_____	_____
Jan Genzer	Christine Grant
_____	_____
Carol Hall	Anne Lazarides

_____

Orlin Velev
Chair of Advisory Committee

DEDICATION

This dissertation is dedicated

to my parents, John and Beverly Jerrim,

to my sister, Carley,

and to my husband, Josh,

for their unending love and support.

BIOGRAPHY

Lindsey was born on March 17, 1982 to John and Beverly Jerrim. She and her younger sister, Carley, grew up just north of Atlanta, in Duluth, GA. Lindsey has long loved playing piano, hiking, reading, cooking, and exercising. In recent years, all of these interests have served as stress relief from the mental rigors of college and graduate school.

Lindsey's interest in science was first piqued at a very young age by her mother, who taught her how to cook and accurately measure ingredients. Her interest grew and expanded as she was introduced to microscopy, chemistry, and astronomy while in elementary school. Her interest in science as a career was cemented while in 5^{th} and 6^{th} grades, when she was introduced to *Scientific American* and *Astronomy Magazine*. While most other kids in her careers class wanted to be doctors or teachers, Lindsey wanted to do chemistry-related research. By her sophomore year of high school, she had decided to become a chemical engineer.

Lindsey graduated from Duluth High School in 2000 and went off to Clemson University, much to her parents' delight. She wasted no time at Clemson, and graduated with her Bachelor of Science in Chemical Engineering in 2003. The summer prior to her senior year, Lindsey participated in an REU program at Clemson, through which she discovered that she really enjoyed research. Upon graduation, she became a graduate student at North Carolina State University, where she has since worked in the field of colloid science.

ACKNOWLEDGEMENTS

I am extraordinary grateful to a number of individuals who have supported me along this journey. First and foremost, I must thank my parents, John and Beverly Jerrim, who helped to make me who I am. They encouraged me to study science, to set high goals, and to find what it is that I love to do. They have supported me financially, emotionally, and in every other possible way throughout my life. I must also thank my sister, Carley Jerrim, who has been my closest confidante for many, many years. She has encouraged me in my goals, shared in my joys and in my disappointments, and held my hand through many struggles. I love you all so much.

I certainly could not have done this without the support of my husband, Josh Stamm. He has been my best friend and has supported me throughout this process. He has encouraged me when I needed it, cheered me on, prayed for me, and been extraordinarily patient. Josh has made this whole process much more enjoyable, and I couldn't imagine the last several years without him by my side. He, along with our three cats, Squeak, Ellie, and Bowen, have been vital to my relaxation and stress relief. I reserve for Josh my highest gratitude. I am unable to express just how much I love you.

Liz Lynch has been so supportive, and I am so glad that we bonded in the lab that day a couple of years ago, talking about Summer the dog. She has been my exercise buddy and my best friend over the last couple of years, has listened to me vent, held me through several

crises, edited my papers, and helped me plan my wedding. What more could I want in a friend? She has been such a joy to know and work with.

I must also thank my Delta Gamma sisters from Clemson: Lindsay Weathers, Stephanie Caddell, Laura Harley, and Lauren Virgo. Stephanie and I took many undergraduate Chem E classes together, worked on projects together, and have had many, many random conversations over the years. She introduced me to my husband and to most of my bridesmaids. Lindsay and I have had many chats commiserating over the toils associated with graduate school and writing a dissertation, in addition to all of our other fun chats. Lauren has been my blonde buddy for many recreated pictures that Stephanie wanted, and she has been such a joy to know. Laura has been my crazy, fun-loving friend who always knows how to make me laugh really, really hard. All of the sleepovers over the years have brought you all so close to me, and I am honored to have been your friend.

I would be remiss if I did not also acknowledge all of my friends from White Plains UMC. My friends in the Crossroads Sunday school class have been there for me since the beginning of this journey, and the many conversations and parties have been so fun. All of the youth counselors and youth have been great friends and have reduced my stress level by leaps and bounds. The choir gave me my musical outlet and my chance to goof off, and I am so grateful for that. The prayers of all of these people have been invaluable, and I could not have done this without you.

The entire Velev research group has been a wonderful source of information, help, and advice. They have edited my papers and presentations, helped me with my experiments,

fixed my computer, and introduced me to many foods and cultures I would not otherwise have experienced. Sandra Bailey, as well as the rest of the office staff, deserve recognition as well. They have taken care of every snag that has developed over the last five and a half years.

I am also extremely grateful to my advisor, Dr. Orlin Velev. He has been a wonderful mentor, and he has been so encouraging, supportive, and above all, patient over the years. His direction, suggestions, and input have been invaluable. Thank you so much!

TABLE OF CONTENTS

LIST OF TABLES

LIST OF FIGURES

Chapter 1. General Background on Patterning of Biomaterials

This dissertation is the culmination of my work in developing structures consisting of biomaterials. The primary focus of my research has been to develop techniques to deposit these materials in one- and two-dimensional structures and to understand the mechanisms underlying the deposition processes. This general overview sets the stage by summarizing the biological inspiration for many structured biomaterials, discussing the principles of convective self-assembly and the use of this technique to deposit biological particles, and reviewing the recent work in the deposition of one-dimensional structures.

1.1 Biological Inspiration for Structured Materials

Nature is the source of inspiration for a vast number of structured and composite materials that have been developed in recent years. To quote Leonardo da Vinci, "Where Nature finishes producing its own species, man begins, using natural things and with the help of this nature, to create an infinity of species."[1] It is through the study of many natural species that an understanding has been developed and used to create many nanostructured materials.

These materials frequently use micro- and nanoscale structure to enhance the properties of the components.[2] For example, superhydrophobic materials are frequently created from components that are less hydrophobic than the resultant material, just as weak components, with the proper structure, can be used to construct a material with much stronger mechanical properties.[3] Although innumerable micro- and nanoscale

structures exist in nature, I will be focusing on superhydrophobicity, optical properties, structural properties, adhesion and self-healing.

1.1.1 Superhydrophobic Properties

Superhydrophobic properties have been discovered on many different species spanning both the plant and animal kingdoms. These properties have been found on the leaves of a number of plants including lotus,[4-9] cabbage,[7] Indian cress,[7,8] and lady's mantle,[8,10] among many others.[4,6,11] All of these plant leaves exhibit surface roughness on several length scales, which is responsible for the water repellency.[4,6,8,11] Water striders are able to stand and move across the surface of water due to the structure of their legs. The legs are covered tiny hairs (microsetae) that have nanogrooves, making them superhydrophobic.[10,12-14] The wings of cicadas, as well, have been studied for their superhydrophobic properties.[10,14] The difference in the structure of cormorant feathers to that of other water birds was investigated, and it was found that the water birds had a network of barbs and smaller barbules that greatly increased the water-repellency of their feathers, while the cormorants did not.[15] That same structure has also been found in pigeon feathers.[16] The Stenocara beetle in the Namib Desert has patterned hydrophilic and superhydrophobic patches on its wings. These serve to collect small droplets of dew and thereby capture water for the beetle to drink.[17]

All of these natural superhydrophobic surfaces have hierarchical structures that enhance their water-repellency. Artificial superhydrophobic surfaces have taken

inspiration from these various natural surfaces and have used various means to create structures with multiple length scales on their surfaces. Superhydrophobic surfaces have been created by using a series of tall posts, upon which a water droplet would rest,[5,7,9,14,18-22] fractal surfaces,[23] roughened surfaces[7,10] and composite surfaces.[7,10,14,19,20] Additionally, the Namib desert beetle has been used as the inspiration for the development of substrates patterned with hydrophilic and superhydrophobic regions by depositing hydrophilic polyelectrolyte on a superhydrophobic surface.[17]

1.1.2 Optical Properties

The optical properties of various natural structures have been studied to provide inspiration for light-guiding components, antireflective coatings, as well as for technologies requiring specific wave frequency bands.[24] Optical properties include the iridescence of plants,[24] insects,[24-26] and various animals;[25] antireflective surfaces on insects;[24,25] structural coloring of insects,[24,27,28] birds,[24] and plants;[24] polarized colored reflection of insects;[24], and UV absorption of Edelweiss flowers.[27] For example, the microstructure of butterfly wings have been studied for their unique optical properties,[24-28] as well as their hydrophobicity,[10,19] and there has been some work on replicating their reflection of light, but only over small areas.[25] Also, the iridescent cuticle of a scarab beetle has a liquid crystal-like structure that has been replicated using titania films.[25]

1.1.3 Structural Properties

The deep-sea glass sponge *Euplectella* has a cylindrical structure with a square lattice of bundled silica spicules. These spicules consist of silica nanospheres surrounding a protein filament.[29,30] This hierarchical structure imparts a much greater strength to the structure than would otherwise be present.[29] Both the structural[29] and the optical properties[31] of these structures have been explored, as a possible source of bioinspiration.

Mollusk shells have an inner layer of nacre (mother of pearl), which is constructed of the aragonite form of calcium carbonate and biopolymers. The components layered and structured on multiple length scales in such a way that the resultant structure is extremely tough.[3,30,32-35] Artificial nacre can be developed by sequentially depositing layers of polyelectrolyte and clays, with structural properties approaching those of natural nacre.[36] The physics of ice formation has also been used to develop porous, layered materials to mimic nacre.[37]

1.1.4 Adhesive Properties

The surface of a gecko's foot consists of a series of microscopic hairs (setae), when then split into many smaller pads (spatulas). These spatulas adhere to surfaces via van der Waals forces.[19,38] In order to mimic this surface, patches of patterned multiwalled carbon nanotubes have been constructed to have large adhesion forces.[38] Another approach has used arrays of polypropylene fibers to achieve a similar result.[39]

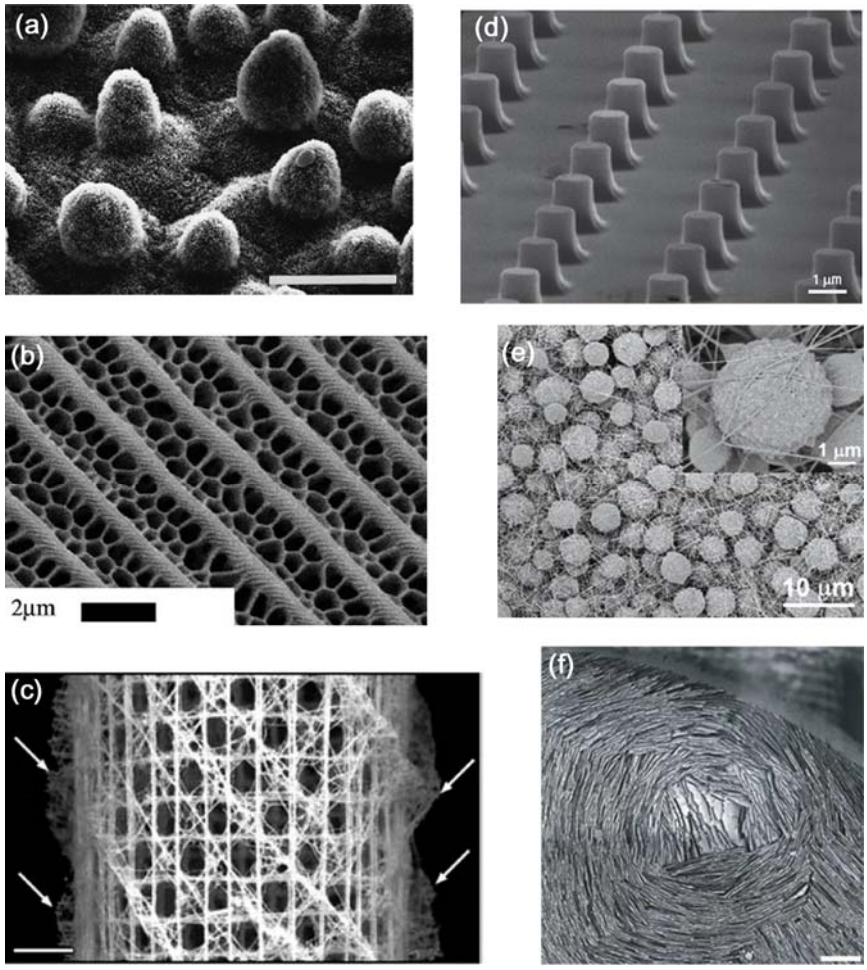

Figure 1.1. Natural and artificial hierarchically structured materials. (a) The rough surface of a lotus leaf, *N. nucifera*, characterized by papillose epidermal cells and epicuticular wax crystals, which make the surface superhydrophobic. Scale bar is 20 μm.[4] (b) The nanostructure of a butterfly wing, *P. ulysses*, resulting in an iridescent blue color.[27] (c) The cage structure of the sponge, *Euplectella* sp., showing the lattices constructed of spicule bundles, increasing the mechanical rigidity and stability of the structure. Scale bar is 5 mm.[29] (d) A series of pillars mimicking natural self-cleaning surfaces, made by plasma-etching on a silicon wafer, resulting in a superhydrophobic surface.[5] (e) A superhydrophobic polystyrene film composed of microspheres and nanofibers.[14] (f) A porous, layered structure of alumina made via ice formation, imparting much greater mechanical strength to the material. Scale bar is 500 μm.[37]

1.1.5 Self-Healing Properties

Another source of recent interest has been the mimicry of the way organisms heal,[3,40] frequently via bleeding and clotting.[41] To mimic bleeding, a number of studies have contained repair components in hollow fibers[40,42] or microcapsules[43,44] so that upon rupture, the components release and repair the material. To mimic clotting, nanoparticles dispersed in polymer films have been used to deposit at the damage site.[41]

1.2 Convective Assembly

Convective assembly was first researched and developed as a deposition technique for two-dimensional colloidal crystals by Denkov, et al.[45] For a suspension of colloidal particles on a substrate with a vanishing contact angle, evaporation results in the pinning of the three-phase contact line. When this occurs, the particles begin to collect at the three-phase contact line and arrange into a close-packed, ordered structure, as shown in Figure 1.2.

The pinning of the three-phase contact line results in the thinning of the liquid film near the contact line as the liquid evaporates. The onset of the colloidal crystal formation occurs when the thickness of the liquid film becomes smaller than the diameter of the suspended particles.[45,46] At that point, the deformation of the menisci between particles results in attractive capillary forces between the particles that result in a close-packed structure.[46]

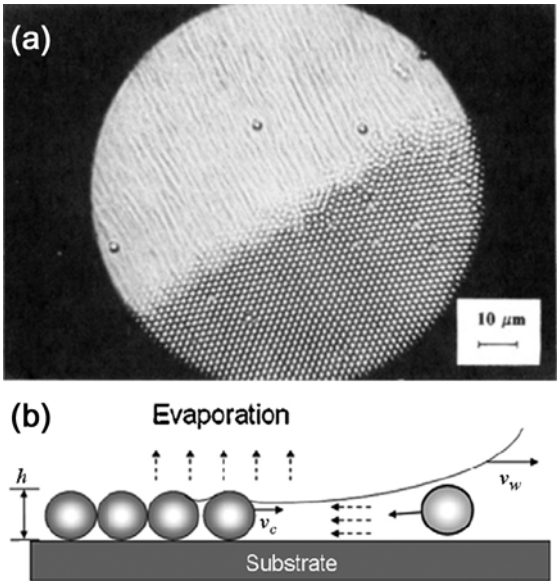

Figure 1.2. (a) Optical micrograph showing the hexagonal packing of the colloidal crystal and the transport of additional particles to the growing crystal front.[45] (b) Schematic showing the formation of a colloidal crystal in a thin film via convective assembly.[47]

Capillary forces are defined as the interactions between particle surfaces caused by fluid interfaces. Attractive immersion capillary forces occur when there is an overlap of the menisci around two similar particles that are partially immersed in a thin liquid film. The deformation of the liquid film caused by the particles protruding from the surface thus results in the attraction and eventual adhesion of the two particles.[48,49] The evaporation from the thin liquid film that causes the attractive capillary forces between the particles also engenders a flow of liquid toward the pinned contact line to compensate for the evaporated liquid. Suspended particles are pulled along with the liquid, thus convectively transporting them to the pinned contact line.[45,50] The flow of particles then allows for the crystal to grow as evaporation of the thin film continues.

This has been characterized by balancing the flux of solvent evaporating from the system and the flux of solvent transporting particles to the growing crystal:[51-53]

$$v_c = \frac{\beta l j_e \varphi}{h(1-\varepsilon)(1-\varphi)}$$

where v_c is the crystal growth rate, β is the coefficient of proportionality, l is the drying length, j_e is the evaporation flux, φ is the concentration of the suspension, h is the height of the crystal, and ε is the porosity of the crystal. The value of the coefficient of proportionality, β, is dependent upon the particle-particle and particle-substrate interactions; it varies between 0 and 1 and approaches 1 for weakly interacting systems.[52]

A variety of experimental setups have been used for convective assembly of particles onto substrates. Experiments were initially performed using a cell in which the particle suspension was placed on a horizontal hydrophilic substrate, resulting in the formation of a colloidal crystal.[45,46,50,53,54] More recently, a stationary substrate has been angled and had a droplet of suspension placed upon it.[51,55] In other studies, a substrate has been placed vertically in a vessel containing a particle suspension and left until evaporation has deposited a crystal on the substrate.[56-58] By vertically withdrawing a substrate from a particle suspension,[52,59] the deposition technique was developed into a continuous process.

Previous research in our group has improved upon this vertical withdrawal technique by trapping a droplet of a concentrated suspension between two plates. A linear

motor, as shown below in Figure 1.3, moves the top plate along the horizontal bottom substrate upon which the particles will be deposited. As with previous experiments involving convective assembly, the three-phase contact line pins, resulting in the nucleation of a colloidal crystal at that point. The meniscus was withdrawn at a constant rate by pushing the top plate with a linear motor. By using concentrated particle suspensions in addition to withdrawing the meniscus, cm-scale colloidal crystal were formed in minutes instead of hours or weeks.[47]

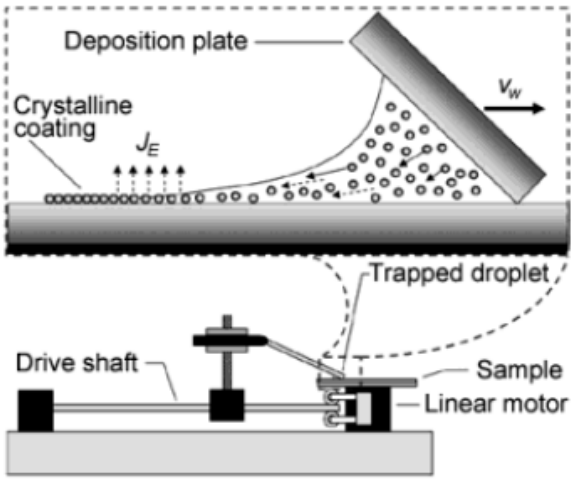

Figure 1.3. Schematic showing the rapid convective assembly apparatus, in which the top plate is moved along the substrate using a linear motor. The inset shows the evaporation of liquid from the growing colloidal crystal and the convective transport of liquid and particles to the growing crystal front.[47]

Control and understanding of the convective assembly process has increased as the effects of various parameters have been understood. The number of particle layers has been found to be affected by the slope of the meniscus,[56,60] the particle concentration,[47,59] and the withdrawal rate.[47,59,61] It has also been determined that

particle ordering is highly dependent on the temperature of the system.[55,62] While the relative humidity has been shown to have no effect on the deposited crystals,[47] increasing the evaporation rate does seem to improve the crystal quality.[58,60] Additionally, it has been shown that significant ordering is present only when the particles and the substrate have the same charge because of a higher particle mobility near the growing crystal front.[63]

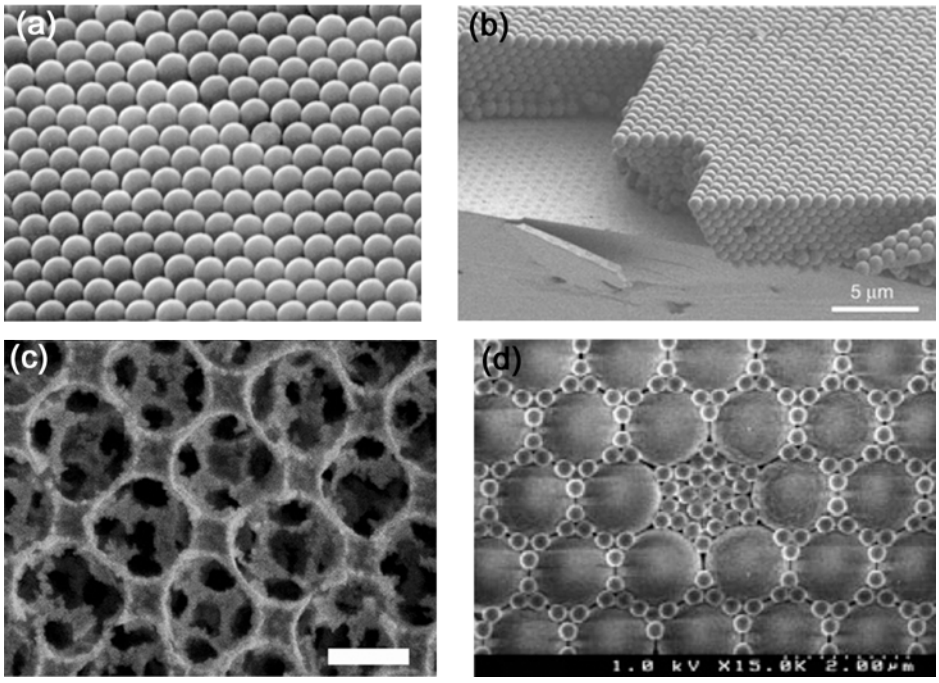

Figure 1.4. SEM images showing colloidal crystals formed via convective assembly. (a) Hexagonal packing of latex particles.[72] (b) Cross-section of a colloidal crystal.[74] (c) A square lattice of templated gold nanoparticles formed by the latex microspheres that were simultaneously deposited with the nanoparticles. Scale bar is 500 nm.[67] (d) Colloidal crystal showing the arrangement of two sizes of latex particles deposited simultaneously.[58]

The degree of control that can now be exerted over the process has allowed for the development of a number of intriguing uses for convective assembly. Colloidal

crystals have been used as templates for the deposition of other porous materials. The material of interest, if in particle form, can be deposited concurrently with the large colloidal particles or may be deposited following crystal deposition. The larger particles used as a template can then be removed, leaving a porous structure behind.[64-74] Multiple particle sizes have been deposited separately in successive layers[75] and also simultaneously.[58,67,76,77] As can be seen in Figure 1.4, the smaller particles are clustered around the bases of the larger particles; this phenomena is known as size-selective segregation.[77]

1.3 Convective Assembly of Biological Particles

Convective assembly has been used to deposit proteins, bacteria, and viruses by several different methods over the last 15 years with a variety of motivations for such arrays. Proteins have been deposited in two-dimensional arrays for the potential applications of the development of immunoassays,[78] sensors and biosensors,[78-80] electrical devices,[79,80] and catalytic materials,[80] in addition to structural analysis of the proteins.[78,80-82] Bacteria have been deposited in such arrays for use in surface enhanced Raman spectroscopy,[83] and anisotropic viruses, such as tobacco mosaic virus (TMV), have been assembled into arrays because of the unique optical and electrical properties engendered by the shape of the particles.[84]

A number of methods have been used to deposit proteins using convective assembly. As previously discussed, convective assembly takes place when evaporation

decreases the thickness of the thin liquid film until lateral capillary forces can pull the particles together. This thin liquid film can exist on either a solid substrate or on a liquid layer.[79,85] Initial research used liquid surfaces for the alignment of protein molecules,[54,77,86,87] and more recent work has led to the deposition of well-ordered protein arrays on solid substrates.[80,81]

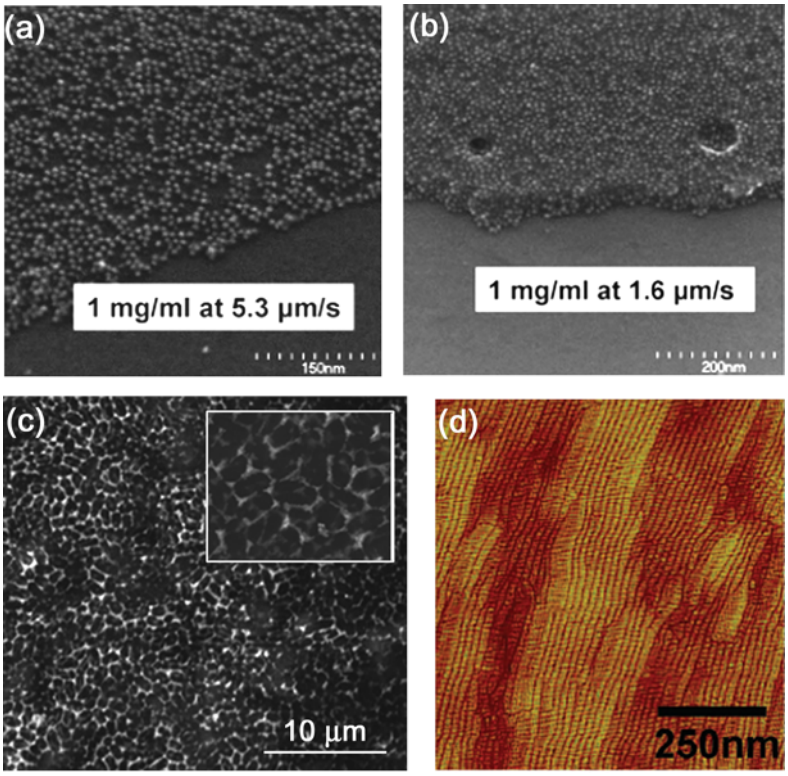

Figure 1.5. Biological particles deposited using rapid convective assembly. (a) & (b) Monolayer and multilayer of ferritin molecules.[80] (c) Multilayer of *E. coli* and silver nanoparticles.[83] (d) Film of TMV, oriented in the direction of deposition.[84]

1.3.1 Assembly on Liquid Surfaces

The first of the methods researched to deposit proteins in a two-dimensional array used a mercury trough. A droplet of ferritin solution was placed on a mercury surface.

The solution spread across the surface of the mercury, completely wetting it, to the walls of the trough.[77,87] As evaporation occurred, the thickness of the wetting film decreased, resulting in lateral capillary forces that pulled the protein molecules in a hexagonal array.[86] The dried array could then be transferred to a solid substrate for analysis. These studies resulted in the formation of close-packed, ordered arrays of particles, but they showed only the coating of very small areas (~1 μm^2). This technique was also used for the assembly of polio virus particles.[77]

Perfluorinated oil (F-oil) was also used as a liquid substrate for the assembly of arrays of protein molecules.[54] A Teflon ring was pressed against a glass plate, and a layer of F-oil was injected and then topped with a layer of ferritin solution. By then removing the majority of the oil layer, the evaporation rate of water from the solution was increased. After a couple of days, the water and oil evaporated completely, leaving behind groups of hexagonally packed ferritin molecules that lacked long-range ordering. Larger latex particles were also deposited using this technique, and observations confirmed that convective assembly was responsible for the alignment of particles.[54]

1.3.2 Assembly on Solid Substrates

In order to deposit proteins directly onto solid substrates in an ordered array, it was necessary to form stable films that were thinner than the protein diameter so that lateral capillary forces would align the protein molecules into an ordered array. By mechanically spreading the protein solution over the surface, a wetting film can be

formed with the necessary stability for convective assembly to occur.[81] This was accomplished by depositing the protein solution at the contact area between a horizontal silicon wafer and a vertical platinum plate. By moving the silicon wafer at a constant velocity, the contact line of the protein solution pinned and was dragged along the plate to form the thin, wetting film. The resultant ferritin arrays were hexagonally ordered but shown only for very small areas.[81]

More recently, the rapid convective assembly technique developed in our research group (Figure 1.3) has been used to deposit biological particles on silicon wafers and on glass. As discussed earlier, a droplet of concentrated suspension is trapped between a horizontal slide and an angled slide. By laterally moving the top slide, the contact line pins and forms a thin film in which convective assembly occurs.[47] Ferritin molecules were aligned into ordered monolayer and multilayer arrays by controlling the protein concentration and the withdrawal rate.[80] Bacterial cells (*E. coli* or *Staphylacoccus cohnii*) were deposited concurrently with silver nanoparticles to form very thick multilayers of cells and particles.[83] TMV, as well, has been deposited in thick, well-ordered films using this rapid convective assembly technique.[84]

1.4 Deposition of Linear Arrays

Using the same rapid convective assembly apparatus previously developed in our research group,[47] TMV was deposited onto glass substrates not only to form films,[84] but also to form aligned fibers.[88] The structure of the TMV films formed on the substrate

could be controlled by withdrawal rate of the meniscus and by the substrate contact angle. Lowering the meniscus withdrawal rate served to increase the thickness of the fibers and decrease the degree of branching. By using a hydrophobic substrate, the fibers formed were much more organized than those deposited on hydrophilic surfaces. On the hydrophobic substrates, dewetting of the thin liquid film resulted in fingering instabilities, where TMV was bundled into large fibers. By attaching gold nanoparticles to the surfaces of the virus particles and then using silver enhancement to deposit a layer of silver over the gold nanoparticles, the TMV fibers became electrically conductive wires.[88] This same technique has also been used to deposit lines of bacteriophage M13 as a surface upon which to culture mouse fibroblasts into patterned lines.[89]

In addition to depositing arrays of virus particles for use as templates for the deposition of metal or cells, a number of techniques have been used to deposit arrays of nanoparticle lines. Patterned self-assembled monolayers (SAMs), dip coating,[93-97] patterned polydimethylsiloxane (PDMS),[90,98,99] and droplet printing,[100,101] as well as lithography,[102,103] DNA templating,[104] and dielectrophoresis (DEP)[105] have all been used to deposit nanoparticle lines.

1.4.1 Patterning using SAMs

Several techniques have been developed that use SAMs to either encourage or discourage adhesion of particles in particular regions of the substrate. These regions were patterned such that the techniques resulted in the deposition of arrays of particle lines.

To encourage adhesion, microcontact printing[106] was used to deposit a SAM on a gold-coated silicon substrate in a pattern, and the remaining regions of the substrate were coated with an adhesion-resistant SAM. Polyelectrolyte layers were then deposited onto the stamped, adhesive regions, and upon exposure of the entire substrate to a suspension of latex microspheres, the particles adhered to the polyelectrolyte layers to form an array of microparticle lines.

By inking a PDMS stamp using solvents that dewetted on its surface, the ink solution was contained in the recesses of the stamp. After removing the excess solvent, the stamp was brought into contact with a glass slide and baked to transfer the pattern to the substrate. Silane SAMs were deposited using this method, and then CdSe nanoparticles were preferentially deposited on the silanes. Additionally, TiO_2 nanoparticles have been directly deposited using this technique.[90]

Using diffraction gratings, PDMS stamps were first molded and then were used to deposit hydrophobic, passivating siloxane molecules on a silicon substrate. By exposure to a metallization precursor and then an electroless plating solution, metal was deposited on the unstamped regions of the substrate. The resultant array of lines deposited was rough and of varying width.[91]

By using electric field induced oxidation[107,108] by atomic force microscopy (AFM) after the SAM was deposited onto a silicon wafer, the organic monolayers were removed and the silicon surface was changed to SiO_2. The AFM tip was used to pattern the substrate in a series of parallel lines. The patterned substrate was then exposed to a

silver nanoparticle suspension, and the particles deposited on the SiO_2 surfaces, forming an array of nanoparticle lines.[92]

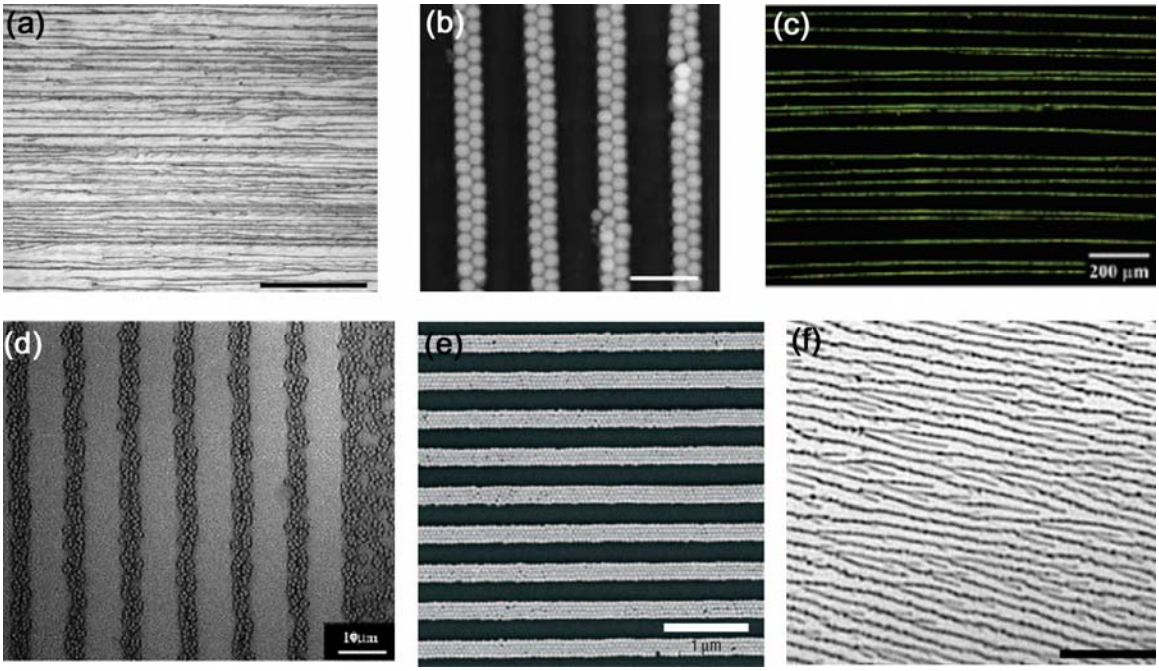

Figure 1.6. Arrays of nanowires and nanoparticle lines. (a) Parallel wires formed by silver enhancement of TMV fibers deposited via meniscus dewetting using the rapid convective assembly apparatus. Scale bar is 500 μm.[88] (b) Latex microsphere lines formed in the troughs of wrinkled polyelectrolyte films. Scale bar is 2 μm.[97] (c) Gold nanoparticle lines formed using slip-stick motion via dip coating.[95] (d) Lines of latex microspheres deposited on polyelectrolyte layers patterned on a substrate using SAMs. (e) Lines of gold nanoparticles formed by depositing the particles on a PDMS stamp and then transferring the dried particles to the substrate.[98] (f) Array of parallel gold microwires formed on the surface of a glass substrate using DEP. Scale bar 50 μm.[105]

1.4.2 Dip Coating

Dip coating has been used for many years to deposit films and particles onto substrates by withdrawing the substrate from a vessel containing the suspension to be deposited. As the substrate is withdrawn, a thin film becomes entrained on the

surface,[109] and as the withdrawal rate of the substrate increases, so does the thickness of the deposited film.[110,111] The early research on dip coating focused on understanding the procedure[112-116] and studying the deposited film structure;[112,114] recent work has used dip coating to deposit particles in patterns on a substrate. Using dip coating in conjunction with dewetting of the substrate,[94] patterning of the substrate,[97] or stick-slip motion[93,95,96] resulted in the formation of arrays of particle lines.

When substrates with contact angles from <10° to >60° were withdrawn from a vessel containing a dilute Langmuir-Blodgett film of nanoparticles, the particles were transferred onto the substrates. Fingering instabilities in the drying front, resulting from the presence of a water-soluble polymer, caused the nanoparticles to aggregate into more concentrated regions. As additional particles were transferred to the substrate, the dewetting continued, resulting in the formation of nanoparticle lines parallel to the direction of deposition.[94]

Multilayer polyelectrolyte films were carefully stretched and retracted, resulting in wrinkling of the film into parallel lines. These films were then drawn out of a particle suspension, with troughs of the wrinkled film parallel to the direction of substrate withdrawal. The particles deposited into the troughs, forming an array of nanoparticle lines.[97]

When a moderately hydrophobic substrate was pulled up out of a Langmuir-Blodgett monolayer of nanoparticles, a stick-slip motion was observed, resulting in the deposition of a series of lines parallel to the meniscus.[95] By withdrawing a substrate

with limited wettability from a dispersion of silver nanowires, parallel lines of nanowires were deposited via the stick-slip motion. These lines, also parallel to the meniscus, were electrically conductive.[96] Similarly, lines formed when gold-coated silicon wafers were withdrawn from a latex microsphere suspension. These lines were parallel to the meniscus and formed due to stick-slip motion.[93]

1.4.3 Patterning using PDMS

A number of techniques used PDMS to pattern nanoparticles onto a substrate. Several of these techniques deposited the particles onto the PDMS and then onto a substrate[90,98] or used the PDMS template as the substrate,[99] in addition to a number of techniques that deposited SAMs and then particles onto the substrate.

In order to deposit nanoparticles on a PDMS stamp, the meniscus of a colloidal suspension was withdrawn over the surface, resulting in the deposition of particles into the recesses of the stamp via convective assembly. The PDMS stamp was then brought into contact with the substrate, and the dried particles adhered to the substrate, resulting in the deposition of arrays of nanoparticle lines.[98]

Similarly, a meniscus was withdrawn over a patterned, hydrophobic PDMS template. The liquid meniscus pinned and deformed around the vertical structures of the template. Capillary forces and particle flow towards the contact line engendered by evaporation seemed to cause the deposition of particles around the vertical structures.

This resulted in patterns dependent upon the patterned template, including arrays of particle lines.[99]

1.4.4 Droplet Printing

Using ink jet technology[100] or modified drop-on-demand printing,[101] uniform microdroplets of gold nanoparticle suspension were deposited in continuous lines on a substrate. Using laser irradiation, the lines were cured to form continuous, conductive arrays of lines.[100,101]

1.4.5 Patterning using Lithography

A patterned substrate was prepared by photolithography and then chemical etching of a silicon substrate, resulting in stripes of SiO_2. A droplet containing silica nanoparticles was placed onto the substrate and allowed to dry. The particles were convectively transported to the regions between the SiO_2 stripes and were there assembled into close-packed structures via lateral capillary forces.[102]

Silanes were patterned onto a silicon substrate using lithography to form linear hydrophobic and hydrophilic regions. A nanoparticle suspension was quickly withdrawn from the container holding the substrate, and once the liquid level dropped lower than the substrate surface, the liquid dewetted from the hydrophobic regions. This resulted in the deposition of the nanoparticles onto the hydrophilic sections of the substrate, forming an array of lines.[103]

1.4.6 DNA Templating

Droplets of a DNA solution were placed on a glass substrate, and an air flow was used to drive the flow of fluid in one direction. Metallization of the DNA samples using electroless deposition resulted in the formation of palladium wires.[104]

1.4.7 Dielectrophoresis

A gold nanoparticle suspension was contained in an experimental cell containing two electrodes. When alternating current was applied, the particles began to aggregate and form microwires between the electrodes via positive DEP, in which the particles are attracted to the regions of high field intensity.[117] While the technique can also be used to form wires in the bulk of the suspension, arrays of microwires were deposited onto the glass substrate by using a higher frequency and decreasing the electric field as the wires grew.[105]

1.5 Deposition of Individual Lines

While there are numerous techniques to deposit arrays of nanoparticle lines, fewer techniques have been used to deposit single lines of nanoparticles on a substrate. The methods for deposition are quite varied, using SAMs,[118] micropipettes,[119,120] fountain pen nanolithography,[121,122] and electro-hydrodynamic printing.[123,124]

SAMs that were modified to form a pattern were used to deposit silica microparticle lines. The SAMs were deposited on silicon substrates that were then

modified with a diamond tip or an atomic force microscopy (AFM) probe to form a line of silanol groups. The patterned substrate was then immersed in a suspension containing the silica microparticles, which bound to the silanol regions of the substrate, forming single lines of particles.[118]

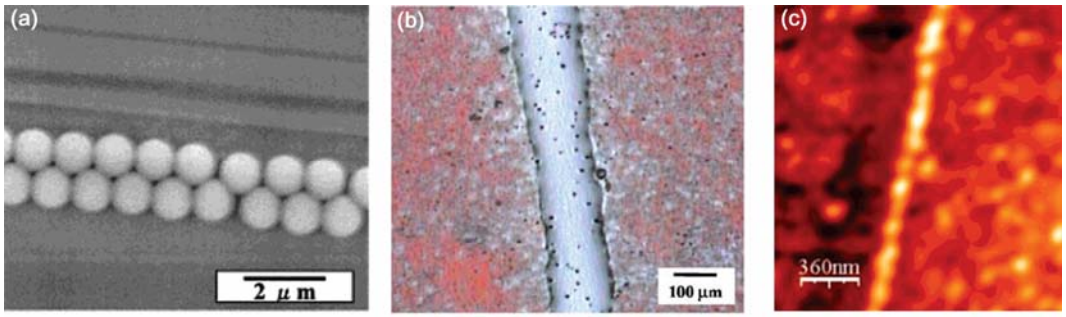

Figure 1.7. Single micro- and nanoparticle lines. (a) Silica microparticle line formed by modifying the SAM deposited on the substrate and then immersing the substrate in a particle suspension.[118] (b) Line of silver nanoparticles formed via electro-hydrodynamic printing.[123] (c) Gold nanoparticle line formed via fountain pen nanolithography. [122]

Gold nanoparticle lines have been deposited using a micropipette that was held vertically above the substrate, such that the nanoparticle suspension was able to wet the substrate. By moving the substrate laterally, a line of gold nanoparticles was drawn.[119] In one technique, a laser was used to sinter the nanoparticles following deposition, resulting in an electrically conductive line.[119] In another variation, following deposition of the nanoparticles, a droplet of deionized water was placed upon the line and then placed on a hotplate. Dewetting caused by thermocapillarity and convection resulted in the reduction of the line width.[120]

Fountain pen nanolithography[125] was also used to deposit lines of nanoparticles. A cantilevered micropipette was brought into contact with a substrate, and the

nanoparticle suspension flowed out of the tip. Once the suspending liquid evaporated, a line of nanoparticles was left on the substrate. Using this technique, lines of green fluorescent protein[121] and electrically conductive lines of gold nanoparticles[122] have been deposited.

Individual lines of silver nanoparticles[123] and alumina nanoparticles[124] were deposited on substrates using electro-hydrodynamic printing. The jet from which the nanoparticle suspension was ejected serves as the anode, and the suspension travels toward the nearest ground electrode, which in this case is a pin underneath the substrate. By laterally moving the substrate, a line of nanoparticles was deposited on the substrate. The silver nanoparticle lines were thermally cured and then found to be electrically conductive.[123]

1.6 Topical Layout of the Dissertation

As discussed in this introduction, many biomaterials have been developed to mimic the structure or functionality of natural materials, and many other materials have gone beyond this to create new structures using colloidal techniques to deposit biomaterials. Chapters 2 and 3 build upon these ideas, using rapid convective assembly to deposit live yeast cells. Chapter 2 discusses the development of a new technique, convective-sedimentation assembly, to uniformly deposit large particles and cells in close-packed arrays in the presence of sedimentation, and details a model of the process to understand the deposition phenomena. Chapter 3 uses this convective-sedimentation

assembly technique to deposit arrays of yeast cells and large latex particles and shows the proof-of-concept of a self-cleaning surface.

Chapters 4 and 5 discuss the development of two novel techniques for the deposition of single lines of gold nanoparticles. Chapter 4 covers the development of a technique using a capillary to draw lines of gold nanoparticles, and components of both convective assembly and dip coating are present the process. The lines have been characterized and found to be electrically conductive. Chapter 5 discusses a technique that uses a vertically placed wedge on a substrate as a template for the formation of a gold nanoparticle line from a droplet via convective assembly. The gold nanoparticles used to develop these techniques are a model system for peptide-capped gold nanoparticles.[126] These nanoparticles, which have an affinity for heavy metal ions,[127] when assembled in a line, could feasibly be used to develop a sensor.

1.7 References

[1] Niemeyer, C. M. "Nanoparticles, Proteins, and Nucleic Acids: Biotechnology Meets Materials Science." *Angew. Chem., Int. Ed.* **2001**, *40*, 4128-4158.

[2] Fratzl, P. "Biomimetic Materials Research: What Can We Really Learn from Nature's Structural Materials?" *J. R. Soc. Interface* **2007**, *4*, 637-642.

[3] Barthelat, F. "Biomimetics for Next Generation Materials." *Phil. Trans. R. Soc. A* **2007**, *365*, 2907-2919.

[4] Barthlott, W.; Neinhuis, C. "Purity of the Sacred Lotus, or Escape from Contamination in Biological Surfaces." *Planta* **1997**, *202*, 1-8.

[5] Blossey, R. "Self-Cleaning Surfaces – Virtual Realities." *Nat. Mater.* **2003**, *2*, 301-306.

[6] Guo, Z.; Liu, W. "Biomimic from the Superhydrophobic Plant Leaves in Nature: Binary Structure and Unitary Structure." *Plant Sci.* **2007**, *172*, 1103-1112.

[7] Ma, M.; Hill, R. M. "Superhydrophobic Surfaces." *Curr. Opin. Colloid Interface Sci.* **2006**, *11*, 193-202.

[8] Otten, A.; Herminghaus, S. "How Plants Keep Dry: A Physicist's Point of View." *Langmuir* **2004**, *20*, 2405-2408.

[9] Zhang, X.; Tan, S.; Zhao, N.; Gao, X.; Zhang, X.; Zhang, Y.; Xu, J. "Evaporation of Sessile Water Droplets on Superhydrophobic Natural Lotus and Biomimetic Polymer Surfaces." *ChemPhysChem* **2006**, *7*, 2067-2070.

[10] Feng, X.; Jiang, L. "Design and Creation of Superwetting/Antiwetting Surfaces." *Adv. Mater.* **2006**, *18*, 3063-3078.

[11] Neinhuis, C.; Barthlott, W. "Characterization and Distribution of Water-Repellent, Self-Cleaning Plant Surfaces." *Ann. Bot.* **1997**, *79*, 667-677.

[12] Feng, X.-Q.; Gao, X.; Wu, Z.; Jiang, L.; Zheng, Q.-S. "Superior Water Repellancy of Water Strider Legs with Hierarchical Structures: Experiments and Analysis." *Langmuir* **2007**, *23*, 4892-4896.

[13] Gao, X.; Jiang, L. "Water-Repellent Legs of Water Striders." *Nature* **2004**, *432*, 36.

[14] Sun, T.; Feng, L.; Gao, X.; Jiang, L. "Bioinspired Surfaces with Special Wettability." *Acc. Chem. Res.* **2005**, *38*, 644-652.

[15] Rijke, A. M. "The Water Repellency and Feather Structure of Cormorants, Phalacrocoracidae." *J. Exp. Biol.* **1968**, *48*, 185-189.

[16] Bormashenko, E.; Bormashenko, Y.; Stein, T.; Whyman, G.; Bormashenko, E. "Why Do Pigeon Feathers Repel Water? Hydrophobicity of Pennae, Cassie-Baxter Wetting Hypothesis and Cassie-Wenzel Capillarity-Induced Wetting Transition." *J. Colloid Interface Sci.* **2007**, *311*, 212-216.

[17] Zhai, L.; Berg, M. C.; Cebeci, F. C.; Kim, Y.; Milwid, J. M.; Rubner, M. F.; Cohen, R. E. "Patterned Superhydrophobic Surfaces: Toward a Synthetic Mimic of the Namib Desert Beetle." *Nano Lett.* **2006**, *6*, 1213-1217.

[18] Chen, W.; Fadeev, A. Y.; Hsieh, M. C.; Öner, D.; Youngblood, J.; McCarthy, T. J. "Ultrahydrophobic and Ultralyophobic Surfaces: Some Comments and Examples." *Langmuir* **1999**, *15*, 3395-3399.

[19] Genzer, J.; Efimenko, K. "Recent Developments in Superhydrophobic Surfaces and their Relevance to Marine Fouling: A Review." *Biofouling* **2006**, *22*, 339-360.

[20] Li, X.-M.; Reinhoudt, D.; Crego-Calama, M. "What Do We Need for a Superhydrophobic Surface? A Review on the Recent Progress in the Preparation of Superhydrophobic Surfaces." *Chem. Soc. Rev.* **2007**, *36*, 1350-1368.

[21] Öner, D.; McCarthy, T. J. "Ultrahydrophobic Surfaces. Effects of Topography Length Scales on Wettability." *Langmuir* **2000**, *16*, 7777-7782.

[22] Zhang, Y. X.; Zeng, H. C. "Template-Free Parallel One-Dimensional Assembly of Gold Nanoparticles." *J. Phys. Chem. B* **2006**, *110*, 16812-16815.

[23] Onda, T.; Shibuichi, S.; Satoh, N.; Tsujii, K. "Super-Water-Repellent Fractal Surfaces." *Langmuir* **1996**, *12*, 2125-2127.

[24] Vukusic, P.; Sambles, J. R. "Photonic Structures in Biology." *Nature* **2003**, *424*, 852-855.

[25] Parker, A. R.; Townley, H. E. "Biomimetics of Photonic Nanostructures." *Nat. Nanotechnol.* **2007**, *2*, 347-353.

[26] Vukusic, P.; Sambles, J. R.; Lawrence, C. R.; Wootton, R. J. "Quantified Interference and Diffraction in Single *Morpho* Butterfly Scales." *Proc. R. Soc. Lond. B* **1999**, *266*, 1403-1411.

[27] Kertesz, K.; Balint, Z.; Vertesy, Z.; Mark, G. I.; Lousse, V.; Vigneron, J.-P.; Biro, L. P. "Photonic Crystal Type Structures of Biological Origin: Structural and Spectral Characterization." *Curr. Appl. Phys.* **2006**, *6*, 252-258.

[28] Vukusic, P.; Sambles, J. R.; Lawrence, C. R. "Colour Mixing in Wing Scales of a Butterfly." *Nature* **2000**, *404*, 457.

[29] Aizenberg, J.; Weaver, J. C.; Thanawala, M. S.; Sundar, V. C.; Morse, D. E.; Fratzl, P. "Skeleton of *Euplectella* Sp.: Structural Hierarchy from the Nanoscale to the Macroscale." *Science* **2005**, *309*, 275-278.

[30] Li, C.; Kaplan, D. L. "Biomimetic Composites Via Molecular Self-Assembly and Biomineralization." *Curr. Opin. Solid State Mat. Sci.* **2003**, *7*, 265-271.

[31] Sundar, V. C.; Yablon, A. D.; Grazul, J. L.; Ilan, M.; Aizenberg, J. "Fibre-Optical Features of a Glass Sponge." *Nature* **2003**, *424*, 899-900.

[32] Aizenberg, J. "Crystallization in Patterns: A Bio-Inspired Approach." *Adv. Mater.* **2004**, *16*, 1295-1302.

[33] Brinker, C. J.; Lu, Y.; Sellinger, A.; Fan, H. "Evaporation-Induced Self-Assembly: Nanostructures Made Easy." *Adv. Mater.* **1999**, *11*, 579-585.

[34] Kaplan, D. L. "Mollusc Shell Structures: Novel Design Strategies for Synthetic Materials." *Curr. Opin. Solid State Mat. Sci.* **1998**, *3*, 232-236.

[35] Ballarini, R.; Heuer, A. H. "Secrets in the Shell." *Am. Scientist* **2007**, *95*, 422-429.

[36] Tang, Z.; Kotov, N. A.; Magonov, S.; Ozturk, B. "Nanostructured Artificial Nacre." *Nat. Mater.* **2003**, *2*, 413-418.

[37] Deville, S.; Saiz, E.; Nalla, R. K.; Tomsia, A. P. "Freezing as a Path to Build Complex Composites." *Science* **2006**, *311*, 515-518.

[38] Ge, L.; Sethi, S.; Ajayan, P. M.; Dhinojwala, A. "Carbon Nanotube-Based Synthetic Gecko Tapes." *Proc. Natl. Acad. Sci. U. S. A.* **2007**, *104*, 10792-10795.

[39] Lee, J.; Fearing, R. S. "Contact Self-Cleaning of Synthetic Gecko Adhesive from Polymer Microfibers." *Langmuir* **2008**, *24*, 10587-10591.

[40] Trask, R. S.; Williams, G. J.; Bond, I. P. "Biomimetic Self-Healing of Advanced Composite Structures Using Hollow Glass Fibres." *J. R. Soc. Interface* **2007**, *4*, 363-371.

[41] Trask, R. S.; Williams, H. R.; Bond, I. P. "Self-Healing Polymer Composites: Mimicking Nature to Enhance Performance." *Bioinsp. Biomim.* **2007**, *2*, P1-P9.

[42] Trask, R. S.; Bond, I. P. "Biomimetic Self-Healing of Advanced Composite Structures Using Hollow-Glass Fibres." *Smart Mater. Struct.* **2006**, *15*, 704-710.

[43] White, S. R.; Sottos, N. R.; Geubelle, P. H.; Moore, J. S.; Kessler, M. R.; Sriram, S. R.; Brown, E. N.; Viswanathan, S. "Autonomic Healing of Polymer Composites." *Nature* **2001**, *409*, 794-797.

[44] Wilson, G. O.; Moore, J. S.; White, S. R.; Sottos, N. R.; Andersson, H. M. "Autonomic Healing of Epoxy Vinyl Esters via Ring Opening Metathesis Polymerization." *Adv. Funct. Mater.* **2008**, *18*, 44-52.

[45] Denkov, N. D.; Velev, O. D.; Kralchevsky, P. A.; Ivanov, I. B.; Yoshimura, H.; Nagayama, K. "Mechanism of Formation of Two-Dimensional Crystals from Latex Particles on Substrates." *Langmuir* **1992**, *8*, 3183-3190.

[46] Dimitrov, A. S.; Dushkin, C. D.; Yoshimura, H.; Nagayama, K. "Observations of Latex Particle Two-Dimensional-Crystal Nucleation in Wetting Films on Mercury, Glass, and Mica." *Langmuir* **1994**, *10*, 432-440.

[47] Prevo, B. G.; Velev, O. D. "Controlled, Rapid Deposition of Structured Coatings from Micro- and Nanoparticle Suspensions." *Langmuir* **2004**, *20*, 2099-2107.

[48] Kralchevsky, P. A.; Nagayama, K. "Capillary Interactions between Particles Bound to Interfaces, Liquid Films and Biomembranes." *Adv. Colloid and Interface Sci.* **2000**, *85*, 145-192.

[49] Kralchevsky, P. A.; Denkov, N. D. "Capillary Forces and Structuring in Layers of Colloid Particles." *Curr. Opin. Colloid Interface Sci.* **2001**, *6*, 383-401.

[50] Denkov, N. D.; Velev, O. D.; Kralchevsky, P. A.; Ivanov, I. B.; Yoshimura, H.; Nagayama, K. "2-Dimensional Crystallization." *Nature* **1993**, *361*, 26.

[51] Dimitrov, A. S.; Nagayama, K. "Steady-State Unidirectional Convective Assembling of Fine Particles into 2-Dimensional Arrays." *Chem. Phys. Lett.* **1995**, *243*, 462-468.

[52] Dimitrov, A. S.; Nagayama, K. "Continuous Convective Assembly of Fine Particles into Two-Dimensional Arrays on Solid Surfaces." *Langmuir* **1996**, *12*, 1303-1311.

[53] Dushkin, C. D.; Yoshimura, H.; Nagayama, K. "Nucleation and Growth of 2-Dimensional Colloidal Crystals." *Chem. Phys. Lett.* **1993**, *204*, 455-460.

[54] Lazarov, G. S.; Denkov, N. D.; Velev, O. D.; Kralchevsky, P. A.; Nagayama, K. "Formation of Two-Dimensional Structures from Colloidal Particles on Fluorinated Oil Substrate." *J. Chem. Soc. Faraday Trans.* **1994**, *90*, 2077-2083.

[55] Rakers, S.; Chi, L. F.; Fuchs, H. "Influence of the Evaporation Rate on the Packing Order of Polydisperse Latex Monofilms." *Langmuir* **1997**, *13*, 7121-7124.

[56] Im, S. H.; Kim, M. H.; Park, O. O. "Thickness Control of Colloidal Crystals with a Substrate Dipped at a Tilted Angle into a Colloidal Suspension." *Chem. Mater.* **2003**, *15*, 1797-1802.

[57] Jiang, P.; Bertone, J. F.; Hwang, K. S.; Colvin, V. L. "Single-Crystal Colloidal Multilayers of Controlled Thickness." *Chem. Mater.* **1999**, *11*, 2132-2140.

[58] Kitaev, V.; Ozen, G. A. "Self-Assembly Surface Patterns of Binary Colloidal Crystals." *Adv. Mater.* **2003**, *15*, **75-78**.

[59] Gu, Z.-Z.; Fujishima, A.; Sato, O. "Fabrication of High-Quality Opal Films with Controllable Thickness." *Chem. Mater.* **2002**, *14*, 760-765.

[60] Dushkin, C. D.; Lazarov, G. S.; Kotsev, S. N.; Yoshimura, H.; Nagayama, K. "Effect of Growth Conditions on the Structure of Two-Dimensional Latex Crystals: Experiment." *Colloid Polym. Sci.* **1999**, *277*, 914-930.

[61] Prevo, B. G.; Fuller, J. C.; Velev, O. D. "Rapid Deposition of Gold Nanoparticle Films with Controlled Thickness and Structure by Convective Assembly." *Chem. Mater.* **2005**, *17*, 28-35.

[62] Im, S. H.; Park, O. O. "Effect of Evaporation Temperature on the Quality of Colloidal Crystals at the Air-Water Interface." *Langmuir* **2002**, *18*, 9642-9646.

[63] Yan, Q.; Gao, L.; Sharma, V.; hiang, Y.-M.; Wong, C. C. "Particle and Substrate Charge Effects on Colliodal Self-Assembly in a Sessile Drop." *Langmuir* **2008**, *24*, 11518-11522.

[64] Jiang, P.; Cizeron, J.; Bertone, J. F.; Colvin, V. L. "Preparation of Macroporous Metal Films from Colloidal Crystals." *J. Am. Chem. Soc.* **1999**, *121*, 7957-7958.

[65] Jiang, P.; Bertone, J. F.; Colvin, V. L. "A Lost-Wax Approach to Monodisperse Colloids and their Crystals." *Science* **2001**, *291*, 453-457.

[66] Kalkman, J.; de Bres, E.; Polman, A.; Jun, Y.; Norris, D. J.; 't Hart, D. C.; Hoogenboom, J. P.; van Blaaderen, A. "Selective Excitation of Erbium in Silicon-Infiltrated Silica Colloidal Photonic Crystals." *J. Appl. Phys.* **2004**, *95*, 2297-2302.

[67] Kuncicky, D. M.; Christesen, S. D.; Velev, O. D. "Role of the Micro- and Nanostructure in the Performance of Surface-Enhanced Raman Scattering Substrates Assembled from Gold Nanoparticles." *Appl. Spectrosc.* **2005**, *59*, 401-409.

[68] Norris, D. J.; Vlasov, Y. A. "Chemical Approaches to Three-Dimensional Semiconductor Photonic Crystals." *Adv. Mater.* **2001**, *13*, 371-376.

[69] Subramania, G.; Constant, K.; Biswas, R.; Sigalas, M. M.; Ho, K. M. "Optical Photonic Crystals Fabricated from Colloidal Systems." *Appl. Phys. Lett.* **1999**, *74*, 3933-3935.

[70] Turner, M. E.; Trentler, T. J.; Colvin, V. L. "Thin Films of Macroporous Metal Oxides." *Adv. Mater.* **2001**, *13*, 180-183.

[71] Velev, O. D.; Tessier, P. M.; Lenhoff, A. M.; Kaler, E. W. "A Class of Porous Metallic Nanostructures." *Nature* **1999**, *401*, 548.

[72] Velev, O. D.; Kaler, E. W. "Structured Porous Materials via Colloidal Crystal Templating: From Inorganic Oxides to Metals." *Adv. Mater.* **2000**, *12*, 531-534.

[73] Vlasov, Y. A.; Yao, N.; Norris, D. J. "Synthesis of Photonic Crystals for Optical Wavelengths from Semiconductor Quantum Dots." *Adv. Mater.* **1999**, *11*, 165-169.

[74] Vlasov, Y. A.; Bo, X.-Z.; Sturm, J. C.; Norris, D. J. "On-Chip Natural Assembly of Silicon Photonic Bandgap Crystals." *Nature* **2001**, *414*, 289-293.

[75] Prasad, T.; Rengarajan, R.; Mittleman, D. M.; Colvin, V. L. "Advanced Photonic Crystal Architectures from Colloidal Self-Assembly Techniques." *Opt. Mater.* **2005**, *27*, 1250-1254.

[76] Prevo, B. G.; Hwang, Y.; Velev, O. D. "Convective Assembly of Antireflective Silica Coatings with Controlled Thickness and Refractive Index." *Chem. Mater.* **2005**, *17*, 3642-3651.

[77] Yamaki, M.; Higo, J.; Nagayama, K. "Size-Dependent Separation of Colloidal Particles in Two-Dimensional Convective Self-Assembly." *Langmuir* **1995**, *11*, 2975-2978.

[78] Adachi, E.; Nagayama, K. "Assembly Process of 2D Protein Arrays in Wetting Films." *Adv. Biophys.* **1997**, *34*, 81-92.

[79] Nagayama, K. "Protein Arrays: Concepts and Subjects." *Adv. Biophys.* **1997**, *34*, 3-23.

[80] Yuan, Z.; Petsev, D. N.; Prevo, B. G.; Velev, O. D.; Atanassov, P. "Two-Dimensional Nanoparticle Arrays Derived from Ferritin Monolayers." *Langmuir* **2007**, *23*, 5498-5504.

[81] Adachi, E.; Nagayama, K. "Formation of Holoferritin Hexagonal Arrays in Secondary Films Due to Alder-Type Transition." *Langmuir* **1996**, *12*, 1836-1839.

[82] Denkov, N. D.; Kralchevsky, P. A.; Ivanov, I. B. "Lateral Capillary Forces and Two-Dimensional Arrays of Colloid Particles and Protein Molecules." *J. Dispersion Sci. Technol.* **1997**, *18*, 577-591.

[83] Kahraman, M.; Yazici, M. M.; Sahin, F.; Culha, M. "Convective Assembly of Bacteria for Surface-Enhanced Raman Scattering." *Langmuir* **2008**, *24*, 894-901.

[84] Wargacki, S. P.; Pate, B.; Vaia, R. A. "Fabrication of 2D Ordered Films of Tobacco Mosaic Virus (TMV): Processing Morphology Correlations for Convective Assembly." *Langmuir* **2008**, *24*, 5439-5444.

[85] Nagayama, K. "Two-Dimensional Self-Assembly of Colloids in Thin Liquid Films." *Colloids and Surfaces A: Physicochem. Eng. Aspects* **1996**, *109*, 363-374.

[86] Nagayama, K. "Fabrication of Protein Crystalline Films on Mercury." *Mater. Sci. Eng., C* **1994**, *1*, 87-94.

[87] Yamaki, M.; Matsubara, K.; Nagayama, K. "A Thin Liquid Layer on the Surface of Mercury as a Matrix of a Flow-Mediated Two-Dimensional Assembly of Proteins." *Langmuir* **1993**, *9*, 3154-3158.

[88] Kuncicky, D. M.; Naik, R. R.; Velev, O. D. "Rapid Deposition and Long-Range Alignment of Nanocoatings and Arrays of Electrically Conductive Wires from Tobacco Mosaic Virus." *Small* **2006**, *2*, 1462-1466.

[89] Rong, J.; Lee, L. A.; Li, K.; Harp, B.; Mello, C. M.; Niu, Z.; Wang, Q. "Oriented Cell Growth on Self-Assembled Bacteriophage M13 Thin Films." *Chem. Comm.* **2008**, 5185-5187.

[90] Cherniavskaya, O.; Adzic, A.; Knutson, C.; Gross, B. J.; Zang, L.; Liu, R.; Adams, D. M. "Edge Transfer Lithography of Molecular and Nanoparticle Materials." *Langmuir* **2002**, *18*, 7029-7034.

[91] Moran, C. E.; Radloff, C.; Halas, N. J. "Benchtop Fabrication of Submicrometer Metal Line and Island Arrays Using Passivative Microcontact Printing and Electroless Plating." *Adv. Mater.* **2003**, *15*, 804-807.

[92] Yonezawa, T.; Itoh, T.; Shirahata, N.; Masuda, Y.; Koumoto, K. "Positioning of Cationic Silver Nanoparticle by Using AFM Lithography and Electrostatic Interaction." *Appl. Surf. Sci.* **2007**, *254*, 621-626.

[93] Ghosh, M.; Fan, F.; Stebe, K. J. "Spontaneous Pattern Formation by Dip Coating of Colloidal Suspensions on Homogeneous Surfaces." *Langmuir* **2007**, *23*, 2180-2183.

[94] Huang, J.; Kim, F.; Tao, A. R.; Connor, S.; Yang, P. "Spontaneous Formation of Nanoparticle Stripe Patterns through Dewetting." *Nat. Mater.* **2005**, *4*, 896-900.

[95] Huang, J.; Tao, A. R.; Connor, S.; He, R.; Yang, P. "A General Method for Assembling Single Colloidal Particle Lines." *Nano Lett.* **2006**, *6*, 524-529.

[96] Huang, J.; Fan, R.; Connor, S.; Yang, P. "One-Step Patterning of Aligned Nanowire Arrays by Programmed Dip Coating." *Angew. Chem., Int. Ed.* **2007**, *46*, 2414-2417.

[97] Lu, C.; Mohwald, H.; Fery, A. "A Lithography-Free Method for Directed Colloidal Crystal Assembly Based on Wrinkling." *Soft Matter* **2007**, *3*, 1530-1536.

[98] Kraus, T.; Malaquin, L.; Schmid, H.; Riess, W.; Spencer, N. D.; Wolf, H. "Nanoparticle Printing with Single-Particle Resolution." *Nat. Nanotechnol.* **2007**, *2*, 570-576.

[99] Malaquin, L.; Kraus, T.; Schmid, H.; Delamarche, E.; Wolf, H. "Controlled Particle Placement through Convective and Capillary Assembly." *Langmuir* **2007**, *23*, 11513-11521.

[100] Bieri, N. R.; Chung, J.; Poulikakos, D.; Grigoropoulos, C. P. "Manufacturing of Nanoscale Thickness Gold Lines by Laser Curing of a Discretely Deposited Nanoparticle Suspension." *Superlattices Microstruct.* **2004**, *35*, 437-444.

[101] Chung, J.; Ko, S.; Bieri, N. R.; Grigoropoulos, C. P.; Poulikakos, D. "Conductor Microstructures by Laser Curing of Printed Gold Nanoparticle Ink." *Appl. Phys. Lett.* **2004**, *84*, 801-803.

[102] Bae, C.; Shin, H.; Moon, J. "Facile Route to Aligned One-Dimensional Arrays of Colloidal Nanoparticles." *Chem. Mater.* **2007**, *19*, 1531-1533.

[103] Yerushalmi, R.; Ho, J. C.; Jacobson, Z. A.; Javey, A. "Generic Nanomaterial Positioning by Carrier and Stationary Phase Design." *Nano Lett.* **2007**, *7*, 2764-2768.

[104] Deng, Z.; Mao, C. "DNA-Templated Fabrication of 1D Parallel and 2D Crossed Metallic Nanowire Arrays." *Nano Lett.* **2003**, *3*, 1545-1548.

[105] Bhatt, K. H.; Velev, O. D. "Control and Modeling of the Dielectrophoretic Assembly of On-Chip Nanoparticle Wires." *Langmuir* **2004**, *20*, 467-476.

[106] Singhvi, R.; Kumar, A.; Lopez, G. P.; Stephanopoulos, G. N.; Wang, D. I. C.; Whitesides, G. M.; Ingber, D. E. "Engineering Cell Shape and Function." *Science* **1994**, *264*, 696-698.

[107] Day, H. C.; Allee, D. R. "Selective Area Oxidation of Silicon with a Scanning Force Microscope." *Appl. Phys. Lett.* **1993**, *62*, 2691-2693.

[108] Yasutake, M.; Ejiri, Y.; Hattori, T. "Modification of Silicon Surface Using Atomic Force Microscope with Conducting Probe." *Jpn. J. Appl. Phys.* **1993**, *32*, L1021-L1023.

[109] Scriven, L. E. "Physics and Applications of Dip Coating and Spin Coating." In *Better Ceramics through Chemistry III*; Brinker, C. J.; Clark, D. E.; Ulrich, D. R., Eds.; Materials Research Society: Pittsburgh, 1988; pp. 717-729.

[110] Deryagin, B. M.; Levi, S. M. "Theory of Coating a Viscous Liquid on a Moving Support." In *Film Coating Theory: The Physical Chemistry of Coating Thin Layers on a Moving Support*; The Focal Press: London, 1964; pp. 25-48.

[111] Landau, L.; Levich, B. "Dragging of a Liquid by a Moving Plate." *Acta Physicochimica U.R.S.S.* **1942**, *17*, 42-54.

[112] Brinker, C. J.; Scherer, G. W. "Film Formation." In *Sol-Gel Science: The Physics and Chemistry of Sol-Gel Processing*; Academic Press, Inc.: San Diego, 1990; pp. 788-836.

[113] Hurd, A. J.; Brinker, C. J. "Sol-Gel Film Formation by Dip Coating." In *Better Ceramics through Chemistry IV*; Zelinski, B. J. J.; Brinker, C. J.; Clark, D. E.; Ulrich, D. R., Eds.; Materials Research Society: Pittsburgh, 1990; pp. 575-581.

[114] Schunk, P. R.; Hurd, A. J.; Brinker, C. J. "Free-Meniscus Coating Processes." In *Liquid Film Coating: Scientific Principles and their Technological Implications*; Kistler, S. F.; Schweizer, P. M., Eds.; Chapman & Hall: London, 1997; p. 67.

[115] Tallmadge, J. A. "A Theory of Entrainment for Angular Withdrawal of Flat Supports." *AIChE J.* **1971**, *17*, 243-246.

[116] White, D. A.; Tallmadge, J. A. "Theory of Drag out of Liquids on Flat Plates." *Chem. Eng. Sci.* **1965**, *20*, 33-37.

[117] Hermanson, K. D.; Lumsdon, S. O.; Williams, J. P.; Kaler, E. W.; Velev, O. D. "Dielectrophoretic Assembly of Electrically Functional Microwires from Nanoparticle Suspensions." *Science* **2001**, *294*, 1082-1086.

[118] Masuda, Y.; Itoh, M.; Yonezawa, T.; Koumoto, K. "Low-Dimensional Arrangement of SiO_2 Particles." *Langmuir* **2002**, *18*, 4155-4159.

[119] Choi, T. Y. P., D.; Grigoropoulos, C. "Fountain-Pen-Based Laser Microstructuring with Gold Nanoparticle Inks." *Appl. Phys. Lett.* **2004**, *85*, 13-15.

[120] Dockendorf, C. P. R.; Choi, T.-Y.; Poulikakos, D.; Stemmer, A. "Size Reduction of Nanoparticle Ink Patterns by Fluid-Assisted Dewetting." *Appl. Phys. Lett.* **2006**, *88*, 131903-1-3.

[121] Taha, H.; Marks, R. S.; Gheber, L. A.; Rousso, I.; Newman, J.; Sukenik, C.; Lewis, A. "Protein Printing with an Atomic Force Sensing Nanofountainpen." *Appl. Phys. Lett.* **2003**, *83*, 1041-1043.

[122] Taha, H.; Lewis, A.; Sukenik, C. "Controlled Deposition of Gold Nanowires on Semiconducting and Nonconducting Surfaces." *Nano Lett.* **2007**, *7*, 1883-1887.

[123] Lee, D. Y.; Hwang, E. S.; Yu, T. U.; Kim, Y. J.; Hwang, J. "Structuring of Micro Line Conductor Using Electro-Hydrodynamic Printing of a Silver Nanoparticle Suspension." *Appl. Phys. A: Mater. Sci. Process.* **2006**, *82*, 671-674.

[124] Lee, D.-Y.; Yu, J.-H.; Shin, Y.-S.; Park, D.; Yu, T.-U.; Hwang, J. "Formation of Ceramic Nanoparticle Patterns Using Electrohydrodynamic Jet Printing with Pin-to-Pin Electrodes." *Jpn. J. Appl. Phys.* **2008**, *47*, 1723-1725.

[125] Lewis, A.; Kheifetz, Y.; Shambrodt, E.; Radko, A.; Khatchatryan, E.; Sukenik, C. "Fountain Pen Nanochemistry: Atomic Force Control of Chrome Etching." *Appl. Phys. Lett.* **1999**, *75*, 2689-2691.

[126] Slocik, J. M.; Stone, M. O.; Naik, R. R. "Synthesis of Gold Nanoparticles Using Multifunctional Peptides." *Small* **2005**, *1*, 1048-1052.

[127] Slocik, J. M.; Naik, R. R. "Biologically Programmed Synthesis of Bimetallic Nanostructures." *Adv. Mater.* **2006**, *18*, 1988-1992.

Chapter 2. Deposition of Coatings from Live Yeast Cells and Large Particles by "Convective-Sedimentation" Assembly

2.1 Introduction

Close-packed and uniform films and coatings composed of colloidal particles have a wide variety of potential applications. One facile and simple process to organize and deposit the particles in a liquid film into crystalline and close-packed structures is convective assembly from drying menisci.[1,2] A wide variety of particle types have been deposited by this method, including colloidal latex,[1-6] gold nanoparticles,[7,8] anisometric zeolites,[9] and colloidal silica.[10,11] Many different applications for such coatings are being developed, including antireflective coatings,[11] SERS enhancement substrates for sensors,[7,12] materials for surface-assisted desorption/ionization mass spectrometry,[13] biosensors,[14] catalysis,[15] macroporous films,[7,16,17] and photonic crystals.[18-20]

Live microbial and animal cells present an interesting object for colloidal assembly as "particles of a kind."[21] A large number of cell deposition techniques have been investigated in recent years, and the resulting cell films represent interesting biomaterials. Most of the cell deposition techniques reported involve patterning, electrodes or templating. Such methods include the use of electroactive substrates,[22] dielectrophoresis between microelectrodes,[21] modulated magnetic fields,[23] inkjet and laser printing,[24,25] optical trapping,[26] biologically-friendly lithography,[27-29] covalent bonding to alkanethiols,[30] encapsulation with a polyelectrolyte,[31] laminar flow patterning[32] and droplet templating.[33] Several methods use polydimethylsiloxane

(PDMS) to pattern substrates for cell growth.[34-37] Recently, it has been demonstrated that the convective assembly method can be used for deposition of cells,[38] and the related "drawdown method" has been used to deposit cells and particles in unpatterned centimeter-scale patches on a substrate.[39]

The process of convective assembly of two-dimensional (2D) colloidal crystals begins when the contact line of a receding liquid surface pins and the thin liquid film becomes thinner than the diameter of the particles. The menisci formed around the particles give rise to attractive capillary forces, and as the liquid evaporates, the particles are pulled together to form two-dimensional crystal nuclei.[1,3] A flux of liquid from the bulk of the suspension to the drying front of the crystal compensates for the fluid loss due to evaporation, which results in convective transport of particles to the drying front, propagating the crystal growth.[1,2] A mass balance allows to correlate the crystal growth rate, v_c, to the evaporation rate and particle volume fraction:

$$v_c = \frac{\beta j_e l \phi}{h(1-\varepsilon)(1-\phi)}$$

where β is an interaction parameter, j_e is the rate of evaporation, l is the drying length, ϕ is the volume fraction of the particles in suspension, h is the height of the deposited colloidal crystal, and ε is the porosity of the crystal.[3,4]

Prevo and Velev reported a modified convective assembly method that allows rapid and controllable deposition of particulate coatings from miniscule volumes of suspension.[6] A small liquid body containing particles at high volume fraction is trapped between two plates, and a linear motor pushes the top plate along the long axis of the

bottom plate, thereby dragging the meniscus with it. Formation of the colloidal crystal occurs in a thin film on the bottom plate by conventional convective assembly. The use of a high volume fraction of particles serves to decrease drastically both the volume of the suspension and the time necessary for deposition of the colloidal crystal.[6]

We report here how a modification of the above method for convective assembly at a high volume fraction can be used to deposit rapidly close-packed yeast cell coatings on glass plates. The cells are much larger than the other types of particles deposited previously using this method, which affects the deposition process by the presence of sedimentation. The goals of this investigation are to investigate the fundamentals of the effect of cell size on the deposition process and develop means of controlling of the convective assembly procedure to obtain large uniform coatings. We first present a model simulating the cell deposition process that allows identifying the conditions that control the coating uniformity. We then investigate the effect of these parameters on the deposition of coatings from cells and mixed cells and particles.

2.2 Materials and Methods

2.2.1 Preparation and Characterization of Yeast Cell Suspension

A 10 wt% suspension of yeast cells was prepared by dispersing 0.5 g of Fleischmann's active dry baker's yeast, *Saccharomyces cerevisiae* (ACH Food Companies, Memphis, TN), in 4500 μL of deionized water obtained from an RiOs 16 reverse-osmosis water purification system (Millipore Corporation, Bedford, MA). The

yeast cells were sprinkled over the room temperature water and allowed to reside for 5 min. The vial was then manually agitated to suspend the yeast cells in the water and was allowed to sit for 30 min. Following the cell hydration, 0.25 g of anhydrous dextrose (Fisher Scientific Chemical Division, Fair Lawn, NJ) was added to the suspension.

The pH of the suspension was measured using a compact pH meter (HORIBA Instruments, Irvine, CA) and was adjusted to 8.0 using cell culture tested 1.0 N NaOH (Sigma-Aldrich, St. Louis, MO). The pH was then adjusted every 30 – 45 min for several hours using small aliquots of NaOH until it stabilized at 8.0. Immediately prior to deposition, the cell suspension was sonicated gently (Branson Ultrasonics Corporation, Danbury, CT) for 15 – 20 s to break up aggregates.

The cell dispersions showed some degree of aggregation as the cells resist changes in the pH of the suspension away from the isoelectric point of 4 because of the –COOH groups and the other protonated macromolecules on their surface. The aggregation state of the yeast cells in these suspensions was determined by optical microscopy. Following 20 s of sonication, samples of the suspensions were taken prior to and following pH adjustment (i.e., at a pH of ~4.3 and of ~8.2). 10 μL of the suspension were diluted in 500 μL of deionized water, mounted on microscope slides and digitally photographed using an Olympus BX61 optical microscope. The percentage of aggregated cells was decreased by both by the sonication and by repeatedly adjusting the pH of the suspension away from the isoelectric point, resulting in less than 25% of the cells being in aggregates.

2.2.2 Deposition of Cell Coatings

Fisherbrand 25 mm × 75 mm glass microscope slides (Fisher Scientific) were cleaned by overnight immersion in a NOCHROMIX solution (GODAX Laboratories, Cabin John, MD). The slides were carefully rinsed with deionized water and dried in an oven at 70°C for 45 min. Two clean glass slides were attached to the deposition device. It was important that the edge of the top slide lie flat on the bottom slide to ensure the formation of a uniform meniscus. A volume of 12 μL from the cell suspension was then injected between the two slides and spread to form a uniform meniscus. The linear motor pushing the top slide was operated at 21.1 μm/s while the cells were deposited onto the substrate in 15 – 45 min. The suspension was deposited at the ambient lab temperature of 22 ± 2.5°C, and an ambient relative humidity of the lab ranging from 30% to 60%.

2.2.3 Coating Characterization and Modeling

To determine the uniformity of an entire coating, images were taken using a low-magnification Olympus SZ61 microscope equipped with a digital camera. An Olympus BX61 microscope with a CCD camera and 5× to 50× objectives were used for collecting high-magnification images of the cell structure using bright field, phase contrast, or oblique lighting. Images of the coatings were analyzed using digital image processing. Adobe Photoshop 7.0.1 was used in to measure the surface fraction of the cell coverage and the uniformity of the layers. A Leica TCS SPI laser scanning confocal workstation attached to a Leica IMBE inverted microscope with a Hamamatsu cooled color CCD was

used to collect Z-stacks of images for three-dimensional rendering of the coatings. Active dried *S. cerevisiae* from MP Biomedicals (Solon, OH) was used for confocal imaging because the cells are fluorescent. A 488 nm Argon laser was used to view coatings with a 40x oil immersion objective. The various deposition mechanisms at work during convective-sedimentation assembly were modeled using Maple 9.00.

2.2.4 Deposition of Mixed Yeast Cell–Latex Coatings

The yeast cell suspension for mixed coatings was prepared as described above. Sulfate latex microspheres (10 μm) (Interfacial Dynamics Corporation, Eugene, OR) were washed and concentrated using a Fisher Marathon micro A microcentrifuge (2700 *g* for 5 min). The two suspensions were mixed in a proportion such that the number of cells in the suspension would approximately equal the number of particles. The combined suspension was sonicated to reduce cell aggregation before deposition. The suspension was injected between the slides and deposited with the device at a forward inclination of 30°. To confirm the viability of the yeast cells, FUN 1 cell stain (Molecular Probes, Eugene, OR) was incubated with the cells for 30 min in a final concentration of 20 μM. The cells were then viewed in the fluorescence microscopy mode of the BX61. The live, vital cells metabolized the dye, and thus were no longer uniformly fluorescent.

2.3 Results and Discussion

The process of assembly of cells by convective evaporation is different from the assembly processes of conventional colloid particles because the morphology of cells is variable, they can interact in dense suspensions, and the size of the cells used in this study was an order of magnitude or more larger than the particles previously deposited using this method (12 nm – 1 μm).[6-8,11] The greater tendency toward-sedimentation turned out to be a major factor affecting the process and specifically the uniformity of the coatings. In order to understand the effect of these factors and design processes where the cells can be deposited with maximal efficiency and uniform thickness we performed numerical evaluation of the parameters affecting the deposition process and their effect on the coating uniformity.

The sedimentation rate, V_s, of the large particles was estimated using the Stokes equation[40]

$$V_s = \frac{2 r_{cell}^2 \left(\rho_{cell} - \rho_{susp}\right) g}{9 \mu_{susp}}$$

where r_{cell} is the radius of a cell, ρ_{cell} is the density of a cell, ρ_{susp} is the density of the suspension media, g is gravitational acceleration, and μ_{susp} is the viscosity of the suspension. The major assumption in the Stokes equation is that the particles are noninteracting hard spheres in a diluted suspension. The concentration of yeast cells in the suspensions being deposited in our experiments, however, is relatively high at 10 wt%. The viscosity of the suspension was adjusted to account for the high concentration

of particles by using literature data for the relative viscosity vs. concentration of yeast cells[41] (the relative viscosity of our suspension was 1.4). The sedimentation rate of the cells in the suspension may also differ from the Stokes rate because of cell-cell interactions; at the experimental pH, the cell surfaces are negatively charged due to the presence of carboxyl and phosphate groups, so, electrostatic repulsion forces predominate.[42,43]

The sedimentation rate of the cells estimated from the Stokes equation was 1.16 μm/s. This is nearly 10% of the withdrawal speed, which was maintained at 21.1 μm/s for all experiments, while depositing a coating of length from 10 mm to 25 mm. Clearly, a significant amount of the cells in the liquid meniscus will sediment on the bottom slide during coating deposition. Thus, we define "convective-sedimentation assembly" as the process of depositing large particles or cells by evaporative convective assembly in the presence of sedimentation (Figure 2.1). The process involves a combination of multiple effects and complex particle transfer and deposition mechanisms. We developed a computational procedure that takes into account the effects involved and simulates the deposition process. The procedure and the results of the calculations are described below.

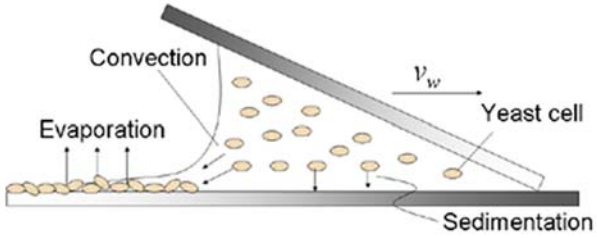

Figure 2.1. Schematic of the convective-sedimentation assembly process. The bottom slide remains in place while the top slide is translated to the right by a linear motor at a rate, v_w. Sedimentation, evaporation, and convection act on the cells during the deposition process.

2.3.1 Convective-Sedimentation Deposition Model

2.3.1.1 System Geometry

The deposition takes place at the edge of a long meniscus of water trapped between two plates. The geometry is translationally invariable in the meniscus direction and there is no redistribution of material parallel to the meniscus edge. Neglecting the effects of the two sides, which only slightly affect the deposition at the edges of the plates, we consider a slice with a width of a single cell diameter perpendicular to the edge. Because the plates in the experiments are hydrophilized, the water-glass contact angle was assumed ≈ 0°. The meniscus of the entrained liquid was assumed cylindrical[44] and tangent to both plates (Figure 2.2a). To test the validity of this assumption, we calculated the Bond number, which is the ratio of gravitational forces to surface tension:

$$Bo = \frac{\rho g r^2}{\sigma}$$

where ρ is the density of the suspension media, g is gravitational acceleration, r is the characteristic length, and σ is the surface tension. The characteristic length could be either the radius or the diameter of the meniscus. Thus, the estimated Bond number is between 0.2 and 0.3, indicating that surface tension predominates,[45] so the assumption that the meniscus is cylindrical is reasonable. The meniscus geometry is then described by a system of four equations, the parameters in which are defined in Figure 2.2b.

$$y_1 = -\sqrt{r^2 - (x - a_x)^2} + a_y$$

$$x_2 = d_x$$

$$y_3 = (c_x - x)\tan(\phi + \theta)$$

$$y_4 = -x\ \tan\theta + e_y$$

The experimentally variable parameters are the angle between the two plates, ϕ, and the angle of the bottom plate with the horizontal, θ. These two angles, together with the volume of the liquid body, defined the geometry of the system (Figure 2.2b). To calculate the values of all parameters, an initial estimate of the radius of the meniscus was made based on the known physical parameters of the system. This radius was used to determine the initial locations of points A, B, C, D, E, and P, as well as the lines y_1, x_2, y_3, and y_4. The set of simplified equations ignores the unshaded area in Figure 2.2b, but this small volume may not significantly affect the results.

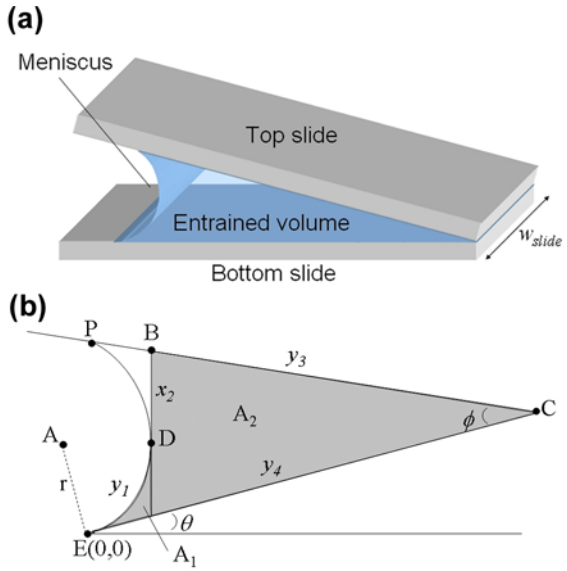

Figure 2.2. (a) Three-dimensional drawing of the physical system, with the position and shape of the meniscus. (b) Definition of the geometrical parameters used in the deposition model.

The target function in the iterative procedure for calculating the exact radius of curvature and meniscus shape was the side area of the slice, A_{sys}. It was determined independently by dividing entrained volume by the width of the slide w_{slide}. The surface area was also calculated by integration over the shaded areas A_1 and A_2 in Figure 2.2b: $A_1 = \int_0^{D_x} \left(y_1(x) - y_4(x)\right)dx$ and $A_2 = \int_{D_x}^{C_x} \left(y_3(x) - y_4(x)\right)dx$. The value of the radius, r, was varied until $(A_1 + A_2)$ became equal to A_{sys}.

2.3.1.2 Model Components and Assumptions

Several assumptions were made to simplify the calculations. The cells were assumed to be spherical and well dispersed particles of uniform density. The evaporation

rate was assumed constant over the entire deposition time span and over the surface of the meniscus, while the evaporation from the exposed sides of the entrained volume was neglected.

The process included three distinct mechanisms for cell redistribution: convection, sedimentation, and evaporation. The convection and evaporation components of the model describe the action of convective assembly, where the cells were pulled forward and then deposited at the front of the meniscus. In order to account for the sedimentation component, we also had to consider the effect of the liquid flow mixing and recirculation opposing the sedimentation, which would otherwise lead to a permanent vertical gradient in cell concentration. When we simulated cell deposition without any mixing in the liquid bulk, we obtained significant deviations from the experimental results. Further, simulations of the fluid flow in the liquid body demonstrated that a significant degree of fluid mixing and recirculation within the entrained volume was present as a result of the mechanical withdrawal of the meniscus and the convection of fluid caused by evaporation. To evaluate the impact of the circulation, basic modeling of the flows in the system was completed using FEMLAB. The simulation took into account the evaporation of the liquid and the movement of the bottom plate with regard to the meniscus but without cells in the entrained volume.

The streamlines of the simulated flow plotted in Figure 2.3 demonstrate that mixing occurs within the entrained volume, with the highest rates at the meniscus. The velocity vectors in the inset show a large vortex near the meniscus and decreasing

velocity away from the meniscus. When the sedimentation rate was compared to the value of the velocity field at a height of 10 μm along the length of the entrained volume, the sedimentation rate exceeded the velocity field for 28% of the entrained volume. Thus, the velocity of the fluid appears high enough to keep the cells well mixed in most of the fluid volume. Only the particles within two cell diameters of the surface were affected by sedimentation; the cells in the bulk of the entrained volume were well mixed at all times. Thus, in the further modeling, the concentration of cells within the entrained volume was kept uniform at all times.

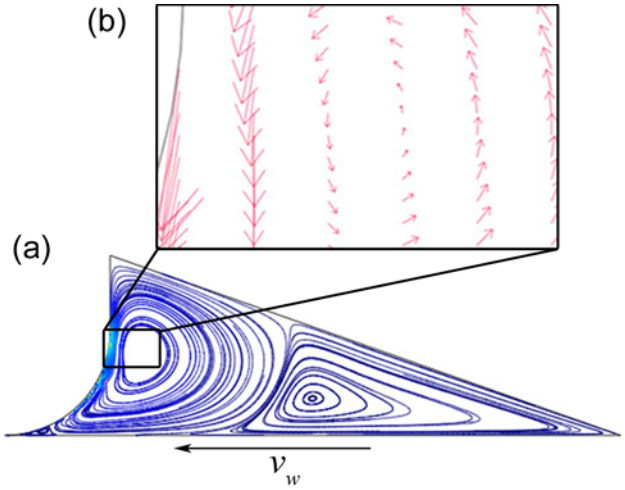

Figure 2.3. FEMLAB simulation of the fluid flow within the entrained volume. (a) Streamlines of the flow. (b) Velocity vectors showing circulation near the meniscus. Size of the arrows indicates relative magnitude of the vectors.

2.3.1.3 Algorithm of the Simulation

The simulation algorithm calculated the number of cells deposited at any given moment on the bottom slide below the moving meniscus. The bottom surface is split into an array of "bins" into which the cells are deposited (Figure 2.4a & d). Each bin in the

array has a width equal to one cell diameter. The meniscus motion is modeled by moving at each time interval the bottom surface, with the array's bins, relative to the entrained volume. The array was shifted to the left at time intervals, t, based on the withdrawal speed, v_w, and the bin width: $t = \frac{2 r_{cell}}{v_w}$. The movement of the bottom slide served to simplify the calculations and was physically equivalent to the motion of the top slide with the attached meniscus in the experiments. Since the system is well mixed, the total number of cells in the entrained volume was decreased by the number of cells deposited in the bins at each time increment following the algorithms describing the three deposition mechanisms (see below). The time then advanced one unit, and the array index increased by one. Before the next step, the entrained volume was decreased proportionally to the evaporation rate, and the geometry of the entrained volume was recalculated. The entire procedure continued iteratively until either no cells remained or the entrained volume had been entirely evaporated (Figure 2.4).

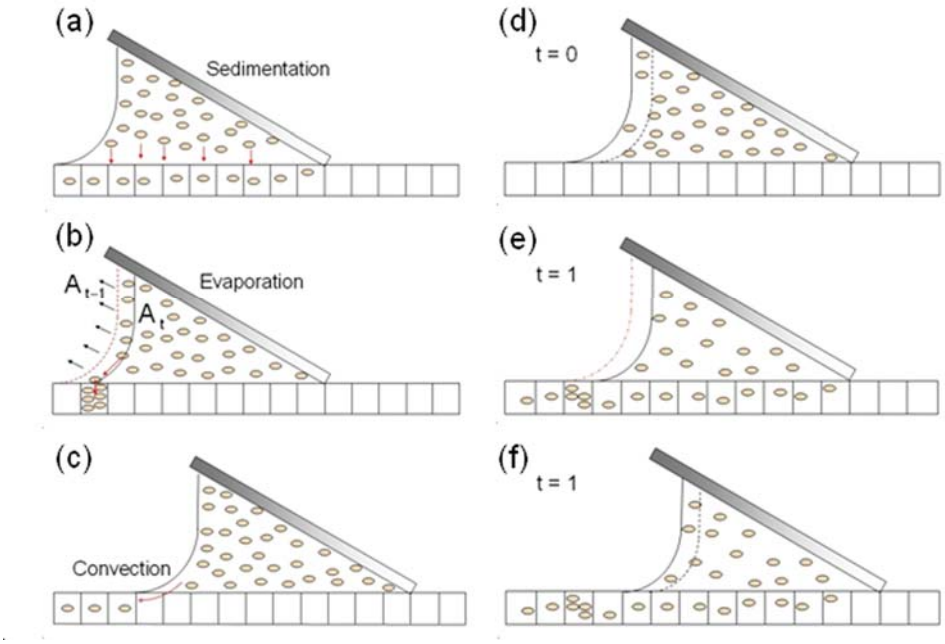

Figure 2.4. (a) – (c) Illustration of the algorithms taking into account the three deposition mechanisms: (a) *Sedimentation*, in which the cells drop straight down onto the plate. (b) *Evaporation*, during which the cells in the evaporating portion of the entrained volume, $A_{t-1} - A_t$, are deposited in the bin directly under the meniscus. (c) *Convection*, in which cells are pulled into the thin film in front of the meniscus and are deposited there. (d) – (f) Schematic sequence of the algorithm of the combined three-mechanism model: (d) Initial condition of the entrained volume and the array representing the bottom plate. The decreased meniscus volume following evaporation is indicated by the dashed line. (e) Time has increased by a single interval, evaporation has occurred, and cells have been deposited. (f) The bottom array has advanced, corresponding to the moving of the top slide and thus the meniscus. The bin width in all frames has been increased for ease of visualization.

2.3.1.4 Sedimentation Algorithm

The FEMLAB modeling of fluid velocity points out that the particles remain uniformly distributed in the bulk of the entrained volume until they approach the substrate. The height from which cells will sediment onto the substrate was calculated

using the Stokes sedimentation rate as $h = V_s t$. All cells contained in the boundary layer of height *h* will be deposited onto the substrate (Figure 2.4a). The number of cells landing into each bin in a time interval, *t*, can then be determined as the deposition flux:

$$n_{sediment,\ bin} = \frac{n\, h\, l_{volume}}{A_{int}\, z_{sediment}}$$

where *n* is the number of cells in the bulk, l_{volume} is the length of the entrained volume, and z_{sediment} is the number of bins under the entrained volume. The cells that had sedimented were divided evenly among the bins currently under the entrained volume. The primary parameters used in the numerical evaluation of the sedimentation are listed in Table 2.1.

2.3.1.5 Evaporation Algorithm

The evaporation rate was assumed constant for the entire deposition process and over the entire meniscus. As the liquid evaporated, the entrained volume decreased, and thus its geometry had to be recalculated. The numerical relationship between the radius of curvature, *r*, and the entrained volume, *V*, plotted in Figure 2.5, could be approximated well by $r = a\ V^{0.5}$, where *a* varies from 0.06 to 0.14, depending on the values of θ and ϕ. Keeping in mind that the entrained volume is the area, A_{int}, multiplied by the width of the slide, it is reasonable that *V* would decrease with r^2. This relationship was used to determine *r* at each volume instead of recalculating it using the iterative procedure described above.

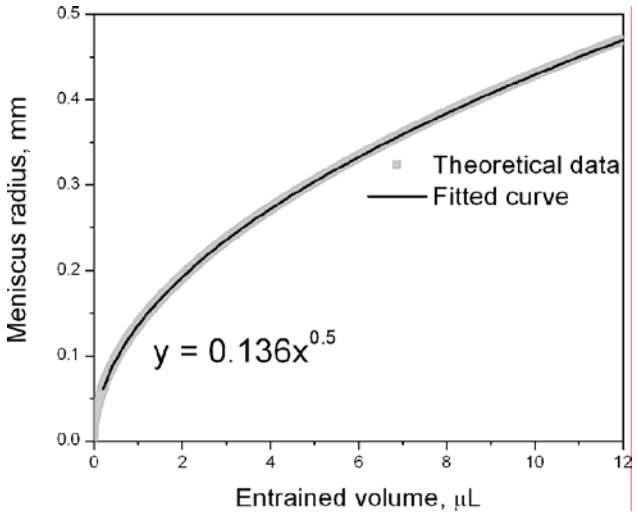

Figure 2.5. Relationship between the meniscus radius and the entrained volume as evaporation progresses. The fitting equation and parameters are included in the plot.

In addition to decreasing the entrained volume, evaporation also results in the collection and deposition of the cells in the vicinity of the meniscus. To simulate this effect, the cells collected at the air-water meniscus are deposited into the bin directly below it (Figure 2.4b). The number of cells deposited by evaporation is calculated by the change in the area of the (single slice of the) entrained volume. The deposition flux at a given time, t, is: $n_{evap} = n \frac{A_{t-1} - A_t}{A_{t-1}}$, where the parameters used are defined in Table 2.1.

Table 2.1. Summary of the primary parameters used in the calculations.

Symbol	Equation	Denoted Parameter
Sedimentation		
V_s	$V_s = \frac{2 r_{cell}^2 (\rho_{cell} - \rho_{susp}) g}{9 \mu_{susp}}$	Sedimentation rate
T	$t = \frac{2 r_{cell}}{v_w}$	Time step for progression of the array
H	$h = V_s t$	Height from which sedimentation occurs
$z_{sediment}$	$z_{sediment} = \frac{l_{volume}}{d_{cell}}$	Number of bins under entrained volume into which sedimentation occurs
$n_{sediment,\ bin}$	$n_{sediment,\ bin} = \frac{n h l_{volume}}{A_{int} z_{sediment}}$	Deposition flux due to sedimentation
Evaporation		
J_e	–	Evaporation flux
n_{evap}	$n_{evap} = n \frac{A_{t-1} - A_t}{A_{t-1}}$	Deposition flux due to evaporation
Convection		
L_{film}	$L_{film} = \frac{v_w d_{cell} (1-\varepsilon)(1-c_i)}{\beta j_e c_i}$	Length of the thin film in which convection occurs
N_{film}	$N_{film} = \frac{v_w d_{cell}^2 (1-\varepsilon)}{V_{cell} w_{slide}}$	Number of cells deposited by convection at a given time
z_{conv}	if $z_{conv} < 200$, $z_{conv} = \frac{L_{film}}{d_{cell}}$ else $z_{conv} = 200$	Number of bins in the thin film
n_{conv}	$n_{conv} = \frac{N_{film} t}{z}$	Deposition flux due to convection

2.3.1.6 Convection Algorithm

Convection, which drags the cells inside the film to the end of the meniscus for deposition in a close-packed layer, has a significant effect on the structure of the coating. This is modeled by distributing the cells deposited by convection into the bins at the edge of the meniscus where a thin liquid film is formed in the actual system (Figure 2.4c).

The material flux balance first derived by Dimitrov and Nagayama,[4] modified for the cell system, defines the length of the thin film in which deposition by convection occurs:

$$L_{film} = \frac{v_w \, d_{cell} \, (1-\varepsilon)(1-c_i)}{\beta \, j_e \, c_i}$$

where ε is the porosity of the cell layer, c_i is the concentration of the bulk suspension at that particular time, β is the coefficient of proportionality that depends on particle-particle and particle-substrate interactions (varies from 0 to 1 being highest for noninteracting particles in dilute suspensions), and j_e is the evaporation flux. The value of ε was determined from the initial layer thickness measured from experimental data where sedimentation did not yet affect the coating. The value of the coefficient of proportionality, β was chosen empirically as 0.5, reflecting that the large yeast cells have high friction with the substrate and that the suspension was highly concentrated.

The particle flux is described by two equations: $h_f \, j_p = v_c \, h(1-\varepsilon)$ and $j_p = N_p \, V_p \, v_p$, where h_f is the liquid film thickness, j_p is the particle flux, v_c is the rate of crystal growth, h is the height of the particle layer, N_p is the number of particles per unit

volume, V_p is the volume of one particle, and v_p is the macroscopic mean velocity of the suspended particles.[4] By combining these two equations we obtain:

$$h_f \, N_p \, v_p = \frac{v_c \, h(1-\varepsilon)}{V_p}$$

It is difficult to determine v_p experimentally, so a new variable, N_{film}, was defined as the total number of particles deposited in the thin film per unit of time:

$$\frac{N_{film}}{h^2} = N_p \, v_p$$

Since the deposition process occurs at steady state, $v_c = v_w$, it is also reasonable to assume that $h_f \approx h$. The thickness of the layer, h, for this situation is the diameter of one cell. Combining all above, we arrive at the following equation for the balance in a one cell thick slice of the meniscus:

$$N_{film} = \frac{v_w \, d_{cell}^2 (1-\varepsilon)}{V_{cell} \, w_{slide}}$$

The value of N_{film} remains constant for the entire deposition process, but the value of L_{film} changes with the concentration, c_i. The number of bins that L_{film} consists of, z_{conv}, is calculated by dividing L_{film} by the cell diameter. Thus, the deposition flux was calculated as follows:

$$n_{conv} = \frac{N_{film} \, t}{z_{conv}}$$

The number of bins, z_{conv}, increases rapidly as the concentration decreases, as the balance points out that the length of the film is inversely related to the particle

concentration. Extremely high values for the film length are not physically realistic as too long films will break and dewet. A value of z_{conv} = 200 was set as the maximum number of bins, allowing a maximum drying length of 1000 μm, a reasonable value considering reported values of 1400 – 2600 μm for latex particles.[6] For z_{conv} < 200, the calculated number of cells, n_{conv}, is placed into z_{conv} bins directly in front of the meniscus. For z_{conv} > 200, n_{conv} is placed into only the first 200 bins in front of the meniscus. The parameters used to calculate the convection are listed in Table 2.1.

2.3.1.7 Model Component Analysis

The convection, evaporation, and sedimentation mechanisms affect the deposition process and the uniformity of the coating in different ways. To evaluate how the interplay of the deposition mechanisms affects the uniformity of the coating, the effect of each mechanism on a profile was evaluated individually. The results of this analysis are plotted in Figure 2.6.

When convection is the primary deposition mechanism, the coating thickness is nearly constant, which is exactly the case for all our earlier studies with microparticles[6] and nanoparticles.[8,11] Decreasing the rate of convection does not significantly change the coating profile because a small number of cells is spread thinly over a uniform number of bins for the majority of the coating. When sedimentation is the primary effect, the peak is very high, and the profile has a very steep slope. However, if the effect of sedimentation is decreased while still keeping it the primary component, the curve levels out and the

peak drops down significantly because a larger number of cells are deposited into a non-uniform number of bins at each time.

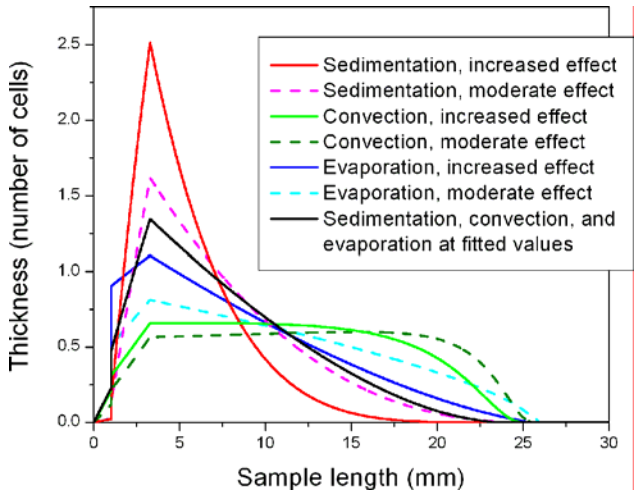

Figure 2.6. Simulated effect of the processes taking place during the deposition on the coating. When sedimentation is the leading effect, a sharp peak is seen in the profile; as the effect of sedimentation is decreased, the peak shortens, improving the coating uniformity. When convection is the primary effect, the coating is relatively flat and uniform, and as the effect is decreased, a small peak appears at the end side of the coating. For evaporation as the primary effect, a small peak is present, and as the effect is decreased, the peak shortens, improving the coating uniformity. A fit of a real experimental profile is included in black for comparison.

When the deposition flux due to evaporation is the primary effect, a lower peak results, leading to a coating that closely resembles the profile fitted to the experimental data. When the effect of evaporation on the deposition flux is decreased to a moderate value, the height of the peak drops, and the direction of curvature of the profile changes. The uniformity of the coating thereby improves. For large spheres, coating quality has been found to increase with an increase in the evaporation rate.[46] However, in Figure 2.6, evaporation refers only to the deposition flux due to evaporation; the evaporation rate

itself is not changed. From our analysis, we can see that a lower sedimentation rate and fewer cells deposited by evaporation would result in a more uniform coating, which could be accomplished by changing the suspending media and increasing the deposition rate to increase the effect of the vortex.

2.3.2 Convective-Sedimentation Deposition

The experimental deposition of large-scale cell layers matched the expectations of the simulation. The cell coatings were near single layer and uniform throughout most of their middle section. An example of a coating from cells deposited by convective-sedimentation assembly is shown in Figure 2.7a. A three-dimensional rendering of a coating structure observed by confocal microscopy is presented in Figure 2.7b. The images collected in the Z-stacks showed that the majority of the cells were within 5 μm of the surface, and the remainder were within 10 μm of the surface, indicating that the cell coating is packed mostly into a single layer. Dispersed islands of cells in a second layer are seen in several locations as bright spots.

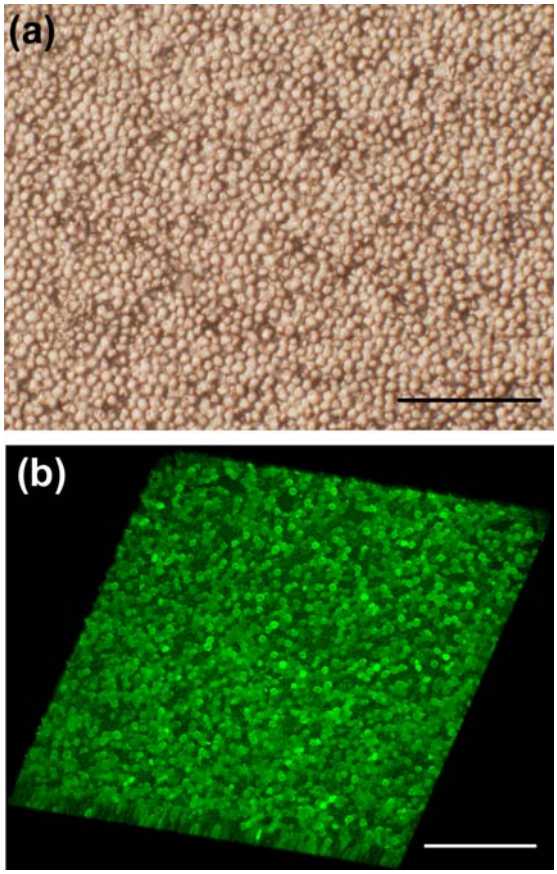

Figure 2.7. (a) Optical micrograph of a nearly complete monolayer of yeast cells. (b) Three-dimensional rendering of a dense yeast cell coating using confocal microscopy. A few cells deposited in a second layer are observed. Both scale bars are 50 μm.

The sedimentation process concurrent to the convective assembly was likely resulting in thickening of the layer of deposited cells. It appears that sedimentation causes the coatings deposited to be of nonuniform density overall because more cells have sedimented onto the layer at the back end of the coating than at the front edge. The change in the thickness of the layer becomes observable partway along the length of the coating (Figure 2.8d – f).

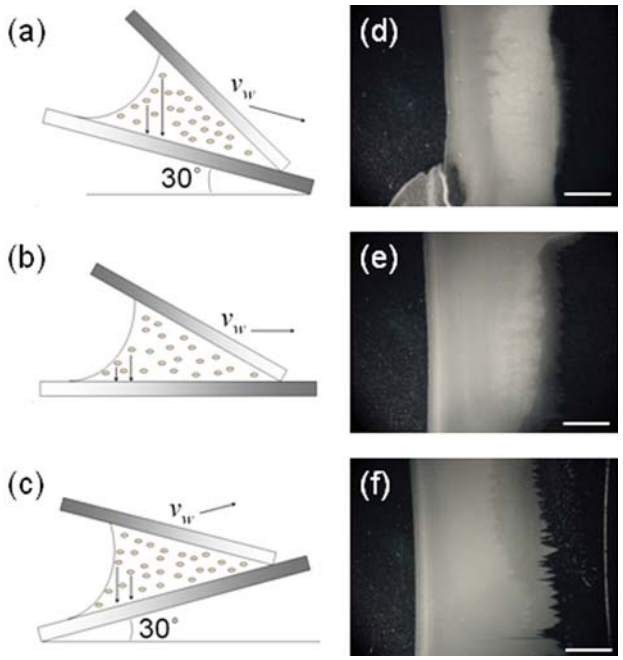

Figure 2.8. Examples of the effect of device inclination on the coating uniformity. (a) – (c) Schematics of device alignment at (a) backward inclination, (b) no inclination, and (c) forward inclination. (d) – (f) Micrographs of coatings deposited at the corresponding inclinations. All scale bars are 5 mm.

One way to affect the sedimentation and potentially to improve the uniformity of the coating is to incline the deposition set-up and thus change the trajectories of the settling cells. Inclining the entire device should change the point at which the coating thickness changes, assuming that mixing within the meniscus does not significantly change the direction of sedimentation from the vertical. By moving that point of thickness change to the front of the coating, the uniformity of the coating should improve, while moving this point backward should decrease the uniformity. To test this hypothesis, the effect of sedimentation direction and of inclination of the deposition device on the coating uniformity was investigated. The device was inclined backward (Figure 2.8a), in

which case the cells sediment farther down the coating, and thus away from the meniscus, and forward (Figure 2.8c), in which case the cells sediment toward the meniscus. The device was angled 0°, 10°, 20°, 30°, 45° and 59° in both forward and backward inclinations and the resulting coatings were examined by microscopy.

In Figure 2.8d – f, the coating begins on the left, with thinner layers being darker. The coatings thicken as deposition progresses. The transition from thinner to thicker coatings is abrupt, defining the point at which the sedimentation begins to contribute strongly to the thickness. This abrupt thickness change was confirmed using higher magnification optical microscopy. The inclination has a significant effect on uniformity. The coating deposited with backward inclination (Figure 2.8d) has a small, uniformly thin area followed by a larger, uniformly thick area. The coating deposited at no inclination (Figure 2.8e) has a small, uniformly thin area where deposition was initiated; it then thickens, but the thickness varies over the length of the sample, as shown by the color variations. The coating deposited at forward inclination (Figure 2.8f) has a very small thin area, followed by a large, uniform thick area that thins as the liquid meniscus runs out of material. As expected, depositing the coating by inclining the device forward improved its uniformity, because the thickness increased at an earlier point on the coating. Backward inclination, which causes thickening at a point farther along the deposit, decreased the uniformity of the coating. The effect of the inclination angle on the uniformity of the cell films is modeled and analyzed quantitatively in the next sections.

2.3.3 Parametric Experiments and Model Evaluation

It is difficult to suppress the cell sedimentation, so two additional experimental parameters were varied independently to optimize the convective-sedimentation deposition process and to assess the predictive capability of the model. These parameters were θ, the angle of the entire device, and ϕ, the angle between the two slides. As in the first experiments, a 10 wt% suspension of live yeast cells, adjusted to a pH of 8, was deposited at ambient temperature and relative humidity. Initially, θ was varied, and the results were used to fit the model to the data. The angles that coatings were deposited at were 59°, 45°, 20°, and 10°, both forward and backward, in addition to no inclination. For this experiment, ϕ was held constant at 19°.

The experiments in which ϕ was varied while θ was held constant were performed at both forward and backward inclinations of 20°. The angles of ϕ at which coatings were deposited were 11°, 17°, 23°, and 29°. This set of experiments was then used to determine how well the model fits the data from the ϕ variation based on the parameters from the θ fit. To reconstruct the profiles of the actual cell coatings, images of the plates with deposited layers were acquired and analyzed to determine the cell coverage and the uniformity of the layers. A grid pattern was used to obtain images over the entirety of the sample. At each position along the length of the substrate, three images were taken across the width of the sample. The nonuniform side edges of the deposited layer were not imaged, but the front and back ends of the deposited layer were imaged.

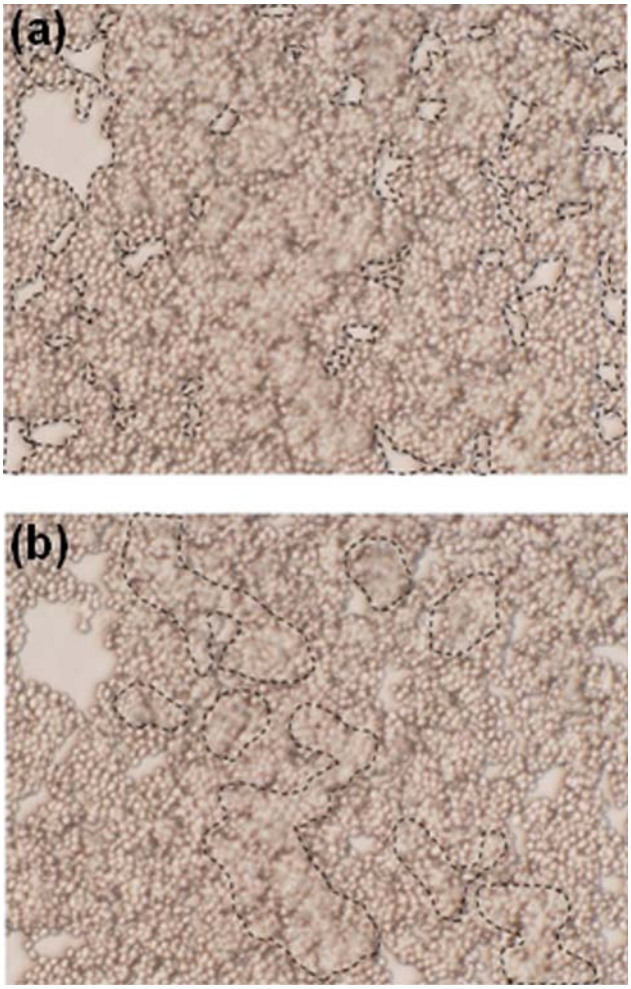

Figure 2.9. Illustration of the image analysis of a cell coating for development of a thickness profile. (a) Selection of areas (dotted lines) of the image without cells. (b) Selection of areas of the image with two layers of cells.

The images collected were analyzed as follows. First, all of the areas in an image without cells were selected at one time (see Figure 2.9a), and the number of pixels was counted. Then, all the areas that were two cell layers thick were selected (see Figure 2.9b), and again the number of pixels was counted. The fraction of the area covered was determined from the total number of pixels in the image as follows:

$$Fraction\ Covered = \frac{N_{Total} - N_{Empty} + N_{2-Layer}}{N_{Total}}$$

where N is the number of pixels for the given condition. The coatings were no more than two cell layers thick. The fraction covered can be interpreted as the average thickness of the coating at that position. Thus, a fractional coverage of less than 1.0 would indicate an incomplete layer, and a value greater than 1.0 would indicate that a portion of the layer is two cells thick. These data were then used to plot the thickness of the coating as a function of the distance from the beginning.

2.3.4 Fitting and Model Accuracy

The results of the θ variation experiment were used to fit the model to the experimental data. The first fitting parameter was the evaporation flux. The fitted value of $J_e = 0.014$ μm/s is $\approx 40\%$ of the flux estimated in the earlier experiments with monodisperse latex particles.[6] This is a reasonable value for a parameter that is otherwise hard to measure, as we expect evaporation from a thick dense layer of hydrated cells containing some proteins and buffers to be slowed with regards to the one from latex spheres in pure water. The second fitting parameter was the deposition flux, n_{evap}. We assumed in the model development that all cells at the vicinity of the meniscus would be carried by the flux in the drying film and deposited into the first bin under the meniscus. After fitting, we obtain that only 37.5% of the cells are deposited in the first bin, and the remainder are redispersed in the meniscus bulk. The redispersion can be correlated to the FEMLAB calculations that show a vortex near the meniscus, which

would likely redistribute many of the cells entrained in the meniscus, decreasing the flux (Figure 2.3). The last fitting parameter was the sedimentation rate, V_s. This parameter needs fitting as the sedimentation of the cells in the thin boundary layer towards the substrate is likely slowed down by the proximity of the surface. The sedimentation rate was found to best match the experimental data at a fitted rate of 0.35 μm/s, which is ~1/3 of the calculated bulk value of 1.16 μm/s. This value agrees well with the literature. Since we are examining sedimentation close to a solid plane the Stokes rate should be corrected for the additional dissipation in the thin liquid layer between the sphere and the surface. For yeast cells that should reach the surface in 1 s, based on the calculated rate of 1.16 μm/s, the center of the particle is 3.66 μm from the surface. Since the ratio of particle radius to distance of the particle center from the surface is 0.68, earlier theoretical studies point out that the rate should be decreased by a factor of ~3.036,[47] in excellent agreement with our fitted value.

Most of the lengths and thicknesses of the coatings calculated from the model are in good agreement with the experimentally determined profiles (Figure 2.10a). All θ variation profiles show that device inclination leads to more uniform coatings (Figure 2.11a – b). The data have higher variability than the model; however, the experiments show a greater dependence on θ than does the model. The experiments showed that forward inclination at high angles results in more uniform coatings. Additionally, the experiments showed that at backward inclination, the peak that results from sedimentation moves further back along the sample length. The model indicates that

backward inclination leads to marginally more uniform coatings; however, these differences fall within the experimental error for the profiles.

At both forward and backward inclinations for ϕ variation, both data and model indicated that the coating length decreases and the coating thickness changes more rapidly as ϕ increases (Figure 2.11c – f). When the forward-inclined coatings are compared to the backward-inclined coatings, both model and experiment agree that the forward-inclined coatings are longer. At both inclination directions for 23° and 29°, the length and height of the coatings calculated using the model matches the experimental values. Additionally, the lengths of the backward-inclined coatings at 11° and 17° from the model match those from experiment, although their heights do not. For forward inclination, both the lengths and heights differ significantly. Even though the model does not fit well at low ϕ, we can draw the conclusion that for each inclination direction, $\phi = 11°$ with forward inclination yields the most uniform coatings.

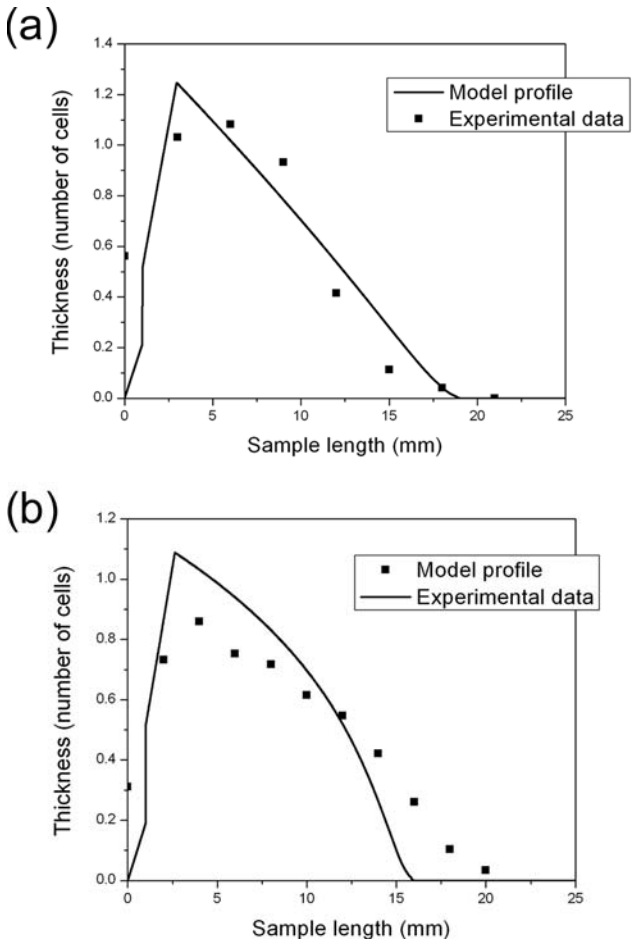

Figure 2.10. Comparison of simulated profiles with experimental data illustrating the accuracy of the model. (a) Experimental data from a θ variation experiment, where $\theta = 0°$. (b) Experimental data from a ϕ variation experiment, where $\phi = 29°$, with a forward inclination of 20°.

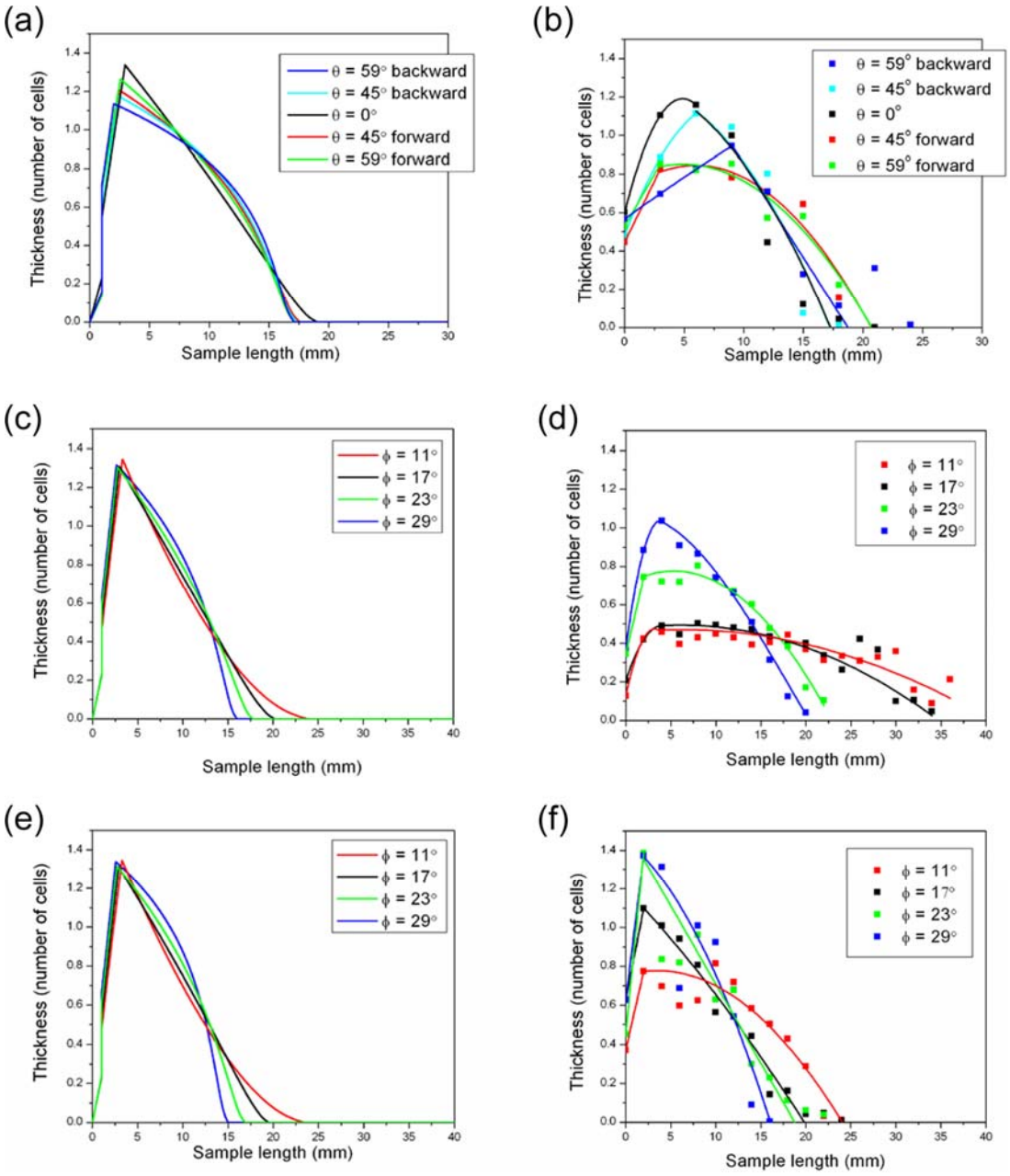

Figure 2.11. Coating thickness profiles from model and experimental data. (a) Model, and (b) Experiment profiles showing the effect of variation of θ. (c) Model, and (d) Experiment profiles showing the effect of variation of ϕ at a forward inclination of 20°. (e) Model, and (f) Experiment profiles showing the effect of variation of ϕ at a backward inclination of 20°. Lines in all experiment plots are to guide the eye.

In summary, the model captures the key trends found in the experimental data but fails to predict quantitatively some of the profiles of the deposited coatings. Because the experiments were performed using a concentrated cell suspension, there are numerous parameters such as the interactions between the cells and their partial aggregation that are hard to control and could affect the profiles of some of the coatings deposited. However, the results clearly point out how the deposition conditions during the convective-sedimentation assembly can be adjusted so that live cell coatings can be deposited uniformly. Both the model and the experiments showed that increasing the angle θ results in more uniform coatings. The experimental data show that the coatings deposited at a forward inclination of 45° and 59° were the most uniform. Both the model and the experimental profiles indicated that decreasing the angle ϕ between the plates in both inclination directions improved the uniformity of the coating, with ϕ = 11° at forward inclination resulting in the most uniform coatings.

2.3.5 Co-Deposition of Yeast Cells and Large Particles

Cell coatings have a wide variety of potential applications, including bioreactor surface coatings, biosensors, gradient bioassays, cell signaling studies, toxicity studies, implant coatings, self-cleaning "artificial skin" and others. One of the specific advantages of the convective assembly is that it can be used to deposit any type of particles suspended in liquid,[48] which may include potentially a wide number of cell types in suspension. A potential problem of such coatings could be the low mechanical stability

and poor abrasion resistance of the cell layers. One simple solution to this problem is to co-deposit the cells together with a protective layer of particles.[49] A rudimentary system of this type was demonstrated by co-depositing with the convective-sedimentation process mixed monolayers of yeast cells and large latex particles (10 μm). The large latex particles were used to create a porous covering that would provide protection from external perturbations for the yeast cells. Thus, the cells would be protected while still having access to nutrients and being able to proliferate through the coating of latex particles. The latex particles and yeast cells were mixed together prior to deposition. The amounts of the yeast cell suspension and the latex suspension that were used for the deposition were determined such that the number of yeast cells would be approximately equal to the number of latex particles. An example of such a composite coating is shown in Figure 2.12a.

During the deposition process, the yeast cells collected around the larger latex particles. This can best be seen in the thin section at the front of the sample in Figure 2.12b,c. The clustering of yeast cells around the bottom parts of the latex particle also occurs with multimodal colloidal particles and is known as *size-selective segregation*. The meniscus around the larger latex particles draws the smaller yeast cells closer via capillary forces.[50,51] When the sample thickens due to sedimentation, a complete monolayer of latex particles deposits on the top of the coating with yeast cells collected around the bases of the latex particles (Figure 2.12d,e).

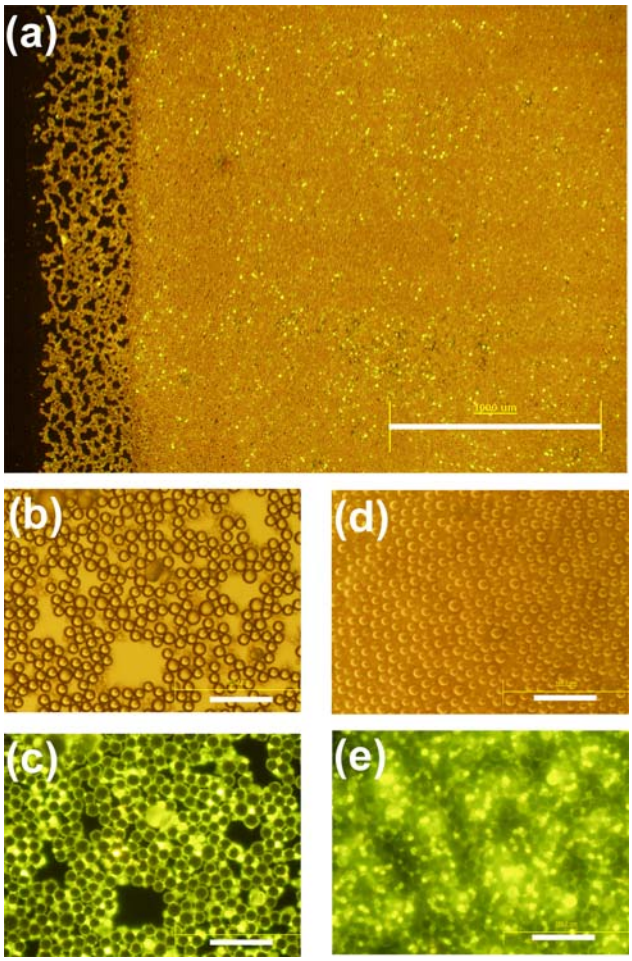

Figure 2.12. (a) Micrographs of a composite coating of particles and yeast cells. The cells are stained and fluoresce. (b) & (c) Submonolayer coating of yeast cells and particles. (c) Yeast cells cluster around the latex particles. (d) & (e) Complete monolayer coating of latex particles. Image (e) is taken from the bottom up and shows the collection of the yeast cells around the bottom part of the latex particles. The scale bar is 1000 μm for (a) and 50 μm for (b) – (e).

To confirm the viability of the deposited cells, FUN® 1 cell stain was added to a cell coating, which was then viewed to determine whether the dye had been metabolized. The presence of nonuniform fluorescence within the cells, where the dye was collected in the center of cell, confirmed that the cells were able to metabolize. Such coatings

immersed in media where the cells could grow and divide may function as an "artificial skin," where debris and contaminants collected on the top layer of cells are sloughed off by external flows. As the bottom layer of cells is protected by the large latex particles, it may remain in place for regeneration of the top cell layer of the coating. By changing the type of cell used, additional functionality (e.g., contaminant digestion, antibacterial secretion) could be added to such coatings.

2.4 Conclusions

We investigated the deposition of live cells and large particles using convective assembly. Sedimentation was found to alter significantly the uniformity of the coatings. A "convective-sedimentation" assembly method was developed for the rapid deposition of uniform, close-packed coatings of yeast cells. This method could also be used for the deposition of other suspensions of robust cells and large particles. A computational model of the deposition process helped in understanding the various mechanisms involved in the convective-sedimentation deposition process. Parametric experiments served the dual purpose of optimizing the deposition process and evaluating the computational model.

Several conclusions are clear from the investigation of the experimental and model profiles. The model approximates the experimental trends reasonably well at most conditions for variation of the angle of the deposition device, θ, and the angle between the two plates, ϕ. Both experiment and model indicated that large forward inclination, θ,

along with small ϕ yield more uniform coatings. The monolayer composite coatings of cells and particles have potential applications including bioreactor surface coatings, biosensors, gradient bioassays, cell signaling and toxicity studies, implant coatings, self-cleaning "artificial skin" and others.

2.5 Acknowledgments

This study was supported by NCSU/NIH MBTP and by an NSF CAREER grant. We are grateful to Suk Tai Chang for his assistance with the FEMLAB modeling, to Nina Allen and Eva Johannes for the use of the Leica confocal microscope in the Cellular and Molecular Imaging Facility, and to Julian Willoughby for his assistance in performing the theta variation experiments.

2.6 References

[1] Denkov, N. D.; Velev, O. D.; Kralchevsky, P. A.; Ivanov, I. B.; Yoshimura, H.; Nagayama, K. "Mechanism of Formation of Two-Dimensional Crystals from Latex Particles on Substrates." *Langmuir* **1992**, *8*, 3183-3190.

[2] Denkov, N. D.; Velev, O. D.; Kralchevsky, P. A.; Ivanov, I. B.; Yoshimura, H.; Nagayama, K. "2-Dimensional Crystallization." *Nature* **1993**, *361*, 26.

[3] Dimitrov, A. S.; Nagayama, K. "Steady-State Unidirectional Convective Assembling of Fine Particles into 2-Dimensional Arrays." *Chem. Phys. Lett.* **1995**, *243*, 462-468.

[4] Dimitrov, A. S.; Nagayama, K. "Continuous Convective Assembly of Fine Particles into Two-Dimensional Arrays on Solid Surfaces." *Langmuir* **1996**, *12*, 1303-1311.

[5] Dushkin, C. D.; Yoshimura, H.; Nagayama, K. "Nucleation and Growth of 2-Dimensional Colloidal Crystals." *Chem. Phys. Lett.* **1993**, *204*, 455-460.

[6] Prevo, B. G.; Velev, O. D. "Controlled, Rapid Deposition of Structured Coatings from Micro- and Nanoparticle Suspensions." *Langmuir* **2004**, *20*, 2099-2107.

[7] Kuncicky, D. M.; Christesen, S. D.; Velev, O. D. "Role of the Micro- and Nanostructure in the Performance of Surface-Enhanced Raman Scattering Substrates Assembled from Gold Nanoparticles." *Appl. Spectrosc.* **2005**, *59*, 401-409.

[8] Prevo, B. G.; Fuller, J. C.; Velev, O. D. "Rapid Deposition of Gold Nanoparticle Films with Controlled Thickness and Structure by Convective Assembly." *Chem. Mater.* **2005**, *17*, 28-35.

[9] Lee, J. A.; Meng, L. L.; Norris, D. J.; Scriven, L. E.; Tsapatsis, M. "Colloidal Crystal Layers of Hexagonal Nanoplates by Convective Assembly." *Langmuir* **2006**, *22*, 5217-5219.

[10] Jiang, P.; Bertone, J. F.; Hwang, K. S.; Colvin, V. L. "Single-Crystal Colloidal Multilayers of Controlled Thickness." *Chem. Mater.* **1999**, *11*, 2132-2140.

[11] Prevo, B. G.; Hwang, Y.; Velev, O. D. "Convective Assembly of Antireflective Silica Coatings with Controlled Thickness and Refractive Index." *Chem. Mater.* **2005**, *17*, 3642-3651.

[12] Freeman, R. G.; Grabar, K. C.; Allison, K. J.; Bright, R. M.; Davis, J. A.; Guthrie, A. P.; Hommer, M. B.; Jackson, M. A.; Smith, P. C.; Walter, D. G.; Natan, M. J. "Self-Assembled Metal Colloid Monolayers – An Approach to SERS Substrates." *Science* **1995**, *267*, 1629-1632.

[13] Finkel, N. H.; Prevo, B. G.; Velev, O. D.; He, L. "Ordered Silicon Nanocavity Arrays in Surface-Assisted Desorption/Ionization Mass Spectrometry." *Anal. Chem.* **2005**, *77*, 1088-1095.

[14] Wang, K.; Xu, J. J.; Chen, H. Y. "Biocomposite of Cobalt Phthalocyanine and Lactate Oxidase for Lactate Biosensing with MnO_2 Nanoparticles as an Eliminator of Ascorbic Acid Interference." *Sens. Actuators, B* **2006**, *114*, 1052-1058.

[15] Yagi, M.; Tomita, E.; Sakita, S.; Kuwabara, T.; Nagai, K. "Self-Assembly of Active IrO_2 Colloid Catalyst on an Ito Electrode for Efficient Electrochemical Water Oxidation." *J. Phys. Chem. B* **2005**, *109*, 21489-21491.

[16] Jiang, P.; Cizeron, J.; Bertone, J. F.; Colvin, V. L. "Preparation of Macroporous Metal Films from Colloidal Crystals." *J. Am. Chem. Soc.* **1999**, *121*, 7957-7958.

[17] Turner, M. E.; Trentler, T. J.; Colvin, V. L. "Thin Films of Macroporous Metal Oxides." *Adv. Mater.* **2001**, *13*, 180-183.

[18] Kalkman, J.; de Bres, E.; Polman, A.; Jun, Y.; Norris, D. J.; 't Hart, D. C.; Hoogenboom, J. P.; van Blaaderen, A. "Selective Excitation of Erbium in Silicon-Infiltrated Silica Colloidal Photonic Crystals." *J. Appl. Phys.* **2004**, *95*, 2297-2302.

[19] Norris, D. J.; Vlasov, Y. A. "Chemical Approaches to Three-Dimensional Semiconductor Photonic Crystals." *Adv. Mater.* **2001**, *13*, 371-376.

[20] Subramania, G.; Constant, K.; Biswas, R.; Sigalas, M. M.; Ho, K. M. "Optical Photonic Crystals Fabricated from Colloidal Systems." *Appl. Phys. Lett.* **1999**, *74*, 3933-3935.

[21] Gupta, S.; Alargova, R. G.; Kilpatrick, P. K.; Velev, O. D. "On-Chip Electric Field Driven Assembly of Biocomposites of Live Cells and Functionalized Particles." *Soft Matter* **2008**, *4*, 726-730.

[22] Yousaf, M. N.; Houseman, B. T.; Mrksich, M. "Using Electroactive Substrates to Pattern the Attachment of Two Different Cell Populations." *Proc. Natl. Acad. Sci. U. S. A.* **2001**, *98*, 5992-5996.

[23] Kimura, T.; Sato, Y.; Kimura, F.; Iwasaka, M.; Ueno, S. "Micropatterning of Cells Using Modulated Magnetic Fields." *Langmuir* **2005**, *21*, 830-832.

[24] Barron, J. A.; Spargo, B. J.; Ringeisen, B. R. "Biological Laser Printing of Three Dimensional Cellular Structures." *Appl. Phys. A: Mater. Sci. Process.* **2004**, *79*, 1027-1030.

[25] Roth, E. A.; Xu, T.; Das, M.; Gregory, C.; Hickman, J. J.; Boland, T. "Inkjet Printing for High-Throughput Cell Patterning." *Biomaterials* **2004**, *25*, 3707-3715.

[26] Odde, D. J.; Renn, M. J. "Laser-Guided Direct Writing of Living Cells." *Biotechnol. Bioeng.* **2000**, *67*, 312-318.

[27] Irimia, D.; Karlsson, J. O. M. "Development of a Cell Patterning Technique Using poly(ethylene glycol) disilane." *Biomed. Microdevices* **2003**, *5*, 185-194.

[28] Karp, J. M.; Yeo, Y.; Geng, W.; Cannizarro, C.; Yan, K.; Kohane, D. S.; Vunjak-Novakovic, G.; Langer, R. S.; Radisic, M. "A Photolithographic Method to Create Cellular Micropatterns." *Biomaterials* **2006**, *27*, 4755-4764.

[29] Suh, K. Y.; Seong, J.; Khademhosseini, A.; Laibinis, P. E.; Langer, R. "A Simple Soft Lithographic Route to Fabrication of poly(ethylene glycol) Microstructures for Protein and Cell Patterning." *Biomaterials* **2004**, *25*, 557-563.

[30] Veiseh, M.; Wickes, B. T.; Castner, D. G.; Zhang, M. "Guided Cell Patterning on Gold–Silicon Dioxide Substrates by Surface." *Biomaterials* **2004**, *25*, 3315-3324.

[31] Krol, S.; Nolte, M.; Diaspro, A.; Mazza, D.; Magrassi, R.; Gliozzi, A.; Fery, A. "Encapsulated Living Cells on Microstructured Surfaces." *Langmuir* **2005**, *21*, 705-709.

[32] Takayama, S.; McDonald, J. C.; Ostuni, E.; Liang, M. N.; Kenis, P. J. A.; Ismagilov, R. F.; Whitesides, G. M. "Patterning Cells and Their Environments Using Multiple Laminar Fluid Flows in Capillary Networks." *Proc. Natl. Acad. Sci. U. S. A.* **1999**, *96*, 5545-5548.

[33] Nellimoottil, T. T.; Rao, P. N.; Ghosh, S. S.; Chattopadhyay, A. "Evaporation-Induced Patterns from Droplets Containing Motile and Nonmotile Bacteria." *Langmuir* **2007**, *23*, 8655-8658.

[34] Chen, C. S.; Mrksich, M.; Huang, S.; Whitesides, G. M.; Ingber, D. E. "Geometric Control of Cell Life and Death." *Science* **1997**, *276*, 1425-1428.

[35] Folch, A.; Toner, M. "Cellular Micropatterns on Biocompatible Materials." *Biotechnol. Prog.* **1998**, *14*, 388-392.

[36] Ostuni, E.; Kane, R.; Chen, C. S.; Ingber, D. E.; Whitesides, G. M. "Patterning Mammalian Cells Using Elastomeric Membranes." *Langmuir* **2000**, *16*, 7811-7819.

[37] Singhvi, R.; Kumar, A.; Lopez, G. P.; Stephanopoulos, G. N.; Wang, D. I. C.; Whitesides, G. M.; Ingber, D. E. "Engineering Cell Shape and Function." *Science* **1994**, *264*, 696-698.

[38] Kahraman, M.; Yazici, M. M.; Sahin, F.; Culha, M. "Convective Assembly of Bacteria for Surface-Enhanced Raman Scattering." *Langmuir* **2008**, *24*, 894-901.

[39] Lyngberg, O. K.; Thiagarajan, V.; Stemke, D. J.; Schottel, J. L.; Scriven, L. E.; Flickinger, M. C. "A Patch Coating Method for Preparing Biocatalytic Films of *Escherichia Coli*." *Biotechnol. Bioeng.* **1999**, *62*, 44-55.

[40] Russel, W. B.; Saville, D. A.; Schowalter, W. R. *Colloidal Dispersions*, Cambridge UP: Cambridge, 1989.

[41] Aiba, S.; Kitai, S.; Ishida, N. "Density of Yeast Cell and Viscosity of its Suspension." *J. Gen. Appl. Microbiol.* **1962**, *8*, 103-108.

[42] Ahimou, F.; Denis, F. A.; Touhami, A.; Dufrene, Y. F. "Probing Microbial Cell Surface Charges by Atomic Force Microscopy." *Langmuir* **2002**, *18*, 9937-9941.

[43] Tazhibaeva, S. M.; Musabekov, K. B.; Orazymbetova, A. B.; Zhubanova, A. A. "Surface Properties of Yeast Cells." *Colloid J.* **2003**, *65*, 132-135.

[44] Hunter, R. J. *Foundations of Colloid Science*, Clarendon Press: Oxford, 1987.

[45] Princen, H. M. "The Equilibrium Shape of Interfaces, Drops, and Bubbles. Rigid and Deformable Particles at Interfaces." In *Surface and Colloid Science*; Matijevic, E., Ed. Wiley-Interscience: New York, 1969;

[46] Kitaev, V.; Ozen, G. A. "Self-Assembly Surface Patterns of Binary Colloidal Crystals." *Adv. Mater.* **2003**, *15*, **75-78**.

[47] Brenner, H. "The Slow Motion of a Sphere through a Viscous Fluid Towards a Plane Surface." *Chem. Eng. Sci.* **1961**, *16*, 242-251.

[48] Prevo, B. G.; Kuncicky, D. M.; Velev, O. D. "Engineered Deposition of Coatings from Nano- and Micro-Particles: A Brief Review of Convective Assembly at High Volume Fraction." *Colloids and Surfaces A: Physicochem. Eng. Aspects* **2007**, *311*, 2-10.

[49] Flickinger, M. C.; Schottel, J. L.; Bond, D. R.; Aksan, A.; Scriven, L. E. “Painting and Printing Living Bacteria: Engineering Nanoporous Biocatalytic Coatings to Preserve Microbial Viability and Intensify Reactivity.” *Biotechnol. Prog.* **2007**, *23*, 2-17.

[50] Kralchevsky, P. A.; Denkov, N. D. "Capillary Forces and Structuring in Layers of Colloid Particles." *Curr. Opin. Colloid Interface Sci.* **2001**, *6*, 383-401.

[51] Yamaki, M.; Higo, J.; Nagayama, K. "Size-Dependent Separation of Colloidal Particles in Two-Dimensional Convective Self-Assembly." *Langmuir* **1995**, *11*, 2975-2978.

Chapter 3. Self-Cleaning Composite Coatings of Yeast Cells and Latex Particles

3.1 Introduction

The idea of self-cleaning coatings was inspired by the lotus leaf; water droplets roll off of the superhydrophobic leaves, carrying contaminants with them.[1,2] Much research has gone into studying the superhydrophobicity of a wide variety of plant surfaces,[1-8] insects,[3,9-12] and feathers.[13,14] The vast majority of these natural surfaces have structures on multiple length scales, in addition to non-wetting surface chemistry.[2]

Most of the self-cleaning coatings developed to date mimic the super-hydrophobic structures of the aforementioned natural surfaces.[1,2,7] Water droplets deposited onto these surfaces immediately roll down, removing dust and dirt particles. Some coatings have roughened[15-20] surfaces, which serves to increase the contact angle on an already hydrophobic surface. Other surfaces possess highly structured topographies of posts of various shapes, sizes, and spacing.[7,8,16,21-27] Electrospinning of hydrophobic polymers has been used to create superhydrophobic mats of fibers.[28-32] Polyelectrolyte multilayers have been deposited with nanoparticles to create roughened surfaces.[33-35] Textiles,[36,37] as well as polymer films[38] and crystalline calcium phosphate layers,[39] have been prepared to be superhydrophobic.

Another approach in the development of self-cleaning surfaces has been the use of a coating of titania (TiO_2) nanoparticles, which have photocatalytic properties and

chemically decompose organic molecules.[40,41] Prevention of biofouling, as well, is another approach to self-cleaning surfaces. These surfaces are chemically modified to minimize bacterial and spore adhesion. [42-45]

Natural skin functions "as a protective barrier against the environment,"[46] which suggests the development of coatings in which the continually regenerating top layer of cells sloughs off, much as skin functions. Engineering methods for depositing uniform close-packed cell layers is a first step in a long road to developing skin-mimicking bioinspired surfaces. The use of rapid convective assembly for the deposition of live cell coatings with self-cleaning capabilities has not been discussed in the literature, even though surfaces that repel water, dirt, and chemical and biological species are of intense practical interest.

3.2 Materials and Methods

3.2.1 Preparation of Yeast Cell and Latex Suspensions

A 10 wt% suspension of yeast cells was prepared by dispersing 0.5 g of Fleischmann's active dry baker's yeast, *Saccharomyces cerevisiae* (ACH Food Companies, Memphis, TN), in 4500 μL of deionized water obtained from an RiOs 16 reverse-osmosis water purification system (Millipore Corporation, Bedford, MA). The yeast cells were sprinkled over the room temperature water and allowed to rest for 5 min, after which the vial was then manually agitated to suspend the yeast cells in the water. The cells were allowed to hydrate for 30 min, and then 0.25 g of anhydrous dextrose

(Fisher Scientific, Waltham, MA) was added to the suspension. The pH was measured using a compact pH meter (HORIBA Instruments, Irvine, CA) and was adjusted to 8.0 using cell culture tested 1.0 N NaOH (Sigma-Aldrich, St. Louis, MO). The pH was then adjusted every 30–45 min for several hours until it stabilized at ~8.0.

Sulfate latex microspheres (10 μm) (Interfacial Dynamics Corporation, Eugene, OR) were washed by centrifugation using a Fisher Marathon micro A microcentrifuge (2700 g for 5 min) and replacing the supernatant with deionized water and then were concentrated using the microcentrifuge at the same settings. The latex and yeast cell suspensions were mixed in a proportion such that the number of cells in the suspension would approximately equal the number of particles. Immediately prior to mixing, the cell suspension was sonicated gently (Branson Ultrasonics Corporation, Danbury, CT) for 15–20 s to break up aggregates. The combined suspension was also sonicated immediately prior to deposition to reduce cell aggregation.

3.2.2 Deposition of Mixed Yeast Cell–Latex Coatings

Fisherbrand 25 mm × 75 mm glass microscope slides were immersed overnight in a NOCHROMIX solution (GODAX Laboratories, Cabin John, MD). The slides were carefully rinsed with deionized water and dried in an oven at 70°C for 45 min. Two clean glass slides were attached to the rapid convective assembly deposition device discussed in Chapter 2, forward inclined at 30°, such that the edge of the top slide lay flat on the bottom slide to ensure the formation of a uniform meniscus (Figure 2.8c). A volume of

12 μL of the yeast cell-latex suspension was then injected between the two slides and spread to form a uniform meniscus. The linear motor pushing the top slide was operated at 21.1 μm/s while the cells and particles were deposited onto the substrate in 15 – 45 min. The suspension was deposited at the ambient lab temperature of 22 ± 2.5°C, and an ambient relative humidity of the lab ranging from 30% to 60%.

3.3 Results and Discussion

3.3.1 Yeast Cell Proliferation

Following deposition of the composite coating, a silicone perfusion chamber, open from the top, was sealed onto the slide around the coating, and growth medium (malt extract broth) was added to the chamber. The coating was imaged using a 40x water-immersion objective at several locations (micrograph and schematics shown in Figure 3.1a). The coating was covered and was left at room temperature for 24 – 48 hrs. After incubation, which allowed for significant proliferation of the yeast cells, the points previously imaged were relocated and imaged again (Figure 3.1b).

3.3.2 Self-Cleaning of Contaminants from the Coating

To simulate the arrival of debris or contaminants, 1 μm fluorescent latex particles were introduced to the surface of the cell coating. A 20 μL volume of this fluorescent latex suspension was added dropwise over the surface of the coating and was allowed to sit for 10–20 min to allow the particles to settle. Longer settling times allowed particle

aggregation to take place. After the settling period, the coatings were imaged again in both bright field and with fluorescence at the points previously used (Figure 3.1c). The coating was then exposed to a spray of growth medium from a syringe until most of the loose cells and particles had been removed from the coating. Both fluorescent and bright field imaging were again performed on the previously imaged points (Figure 3.1d).

Most of the cells and fluorescent particles (“contaminants”) have been removed from the coating (Figure 3.1d). At the same time, the bottom layer of yeast cells, along with the large, protective latex particles, remains attached to the surface. Thus, the coating functions broadly similar to skin, in that the top layer of cells catches contaminants and debris and then can be shed. When the coating was re-exposed to growth medium, the cells proliferated again and completely covered the surface, the same way as the cells had proliferated previously.

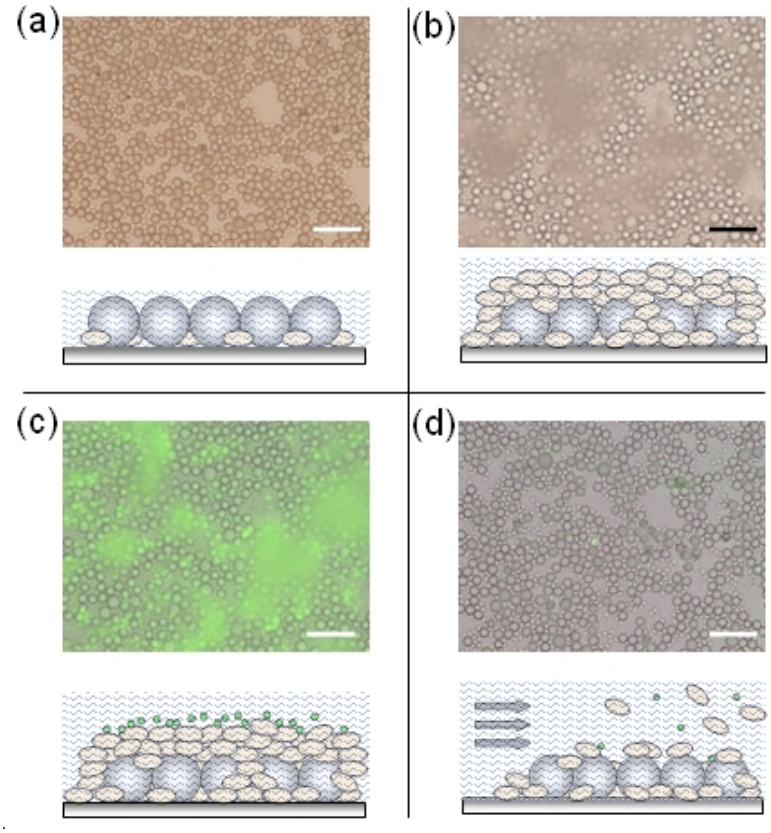

Figure 3.1. Images and schematics of cell-particle coatings with rudimentary self-cleaning properties. (a) Initial coating. (b) Coating after exposure to growth medium for 24 hours, allowing for significant cell proliferation. (c) Coating with fluorescent latex "contaminant." (d) Coating following contaminant and cell removal with a stream of growth medium. All scale bars are 50 μm.

3.4 Conclusions

We have demonstrated that the cell-particle composite makes a "self-cleaning" coating that regenerates itself. This concept could be expanded to include other cell types able to survive dehydration, either for specific application to a particular environment, or

for an additional functionality of the cell that could enhance the self-cleaning ability of the coating.

3.5 Acknowledgements

This study was supported by NCSU/NIH MBTP and by an NSF CAREER grant.

3.6 References

[1] Barthlott, W.; Neinhuis, C. "Purity of the Sacred Lotus, or Escape from Contamination in Biological Surfaces." *Planta* **1997**, *202*, 1-8.

[2] Blossey, R. "Self-Cleaning Surfaces – Virtual Realities." *Nat. Mater.* **2003**, *2*, 301-306.

[3] Feng, X.; Jiang, L. "Design and Creation of Superwetting/Antiwetting Surfaces." *Adv. Mater.* **2006**, *18*, 3063-3078.

[4] Guo, Z.; Liu, W. "Biomimic from the Superhydrophobic Plant Leaves in Nature: Binary Structure and Unitary Structure." *Plant Sci.* **2007**, *172*, 1103-1112.

[5] Ma, M.; Hill, R. M. "Superhydrophobic Surfaces." *Curr. Opin. Colloid Interface Sci.* **2006**, *11*, 193-202.

[6] Neinhuis, C.; Barthlott, W. "Characterization and Distribution of Water-Repellent, Self-Cleaning Plant Surfaces." *Ann. Bot.* **1997**, *79*, 667-677.

[7] Otten, A.; Herminghaus, S. "How Plants Keep Dry: A Physicist's Point of View." *Langmuir* **2004**, *20*, 2405-2408.

[8] Zhang, X.; Tan, S.; Zhao, N.; Gao, X.; Zhang, X.; Zhang, Y.; Xu, J. "Evaporation of Sessile Water Droplets on Superhydrophobic Natural Lotus and Biomimetic Polymer Surfaces." *ChemPhysChem* **2006**, *7*, 2067-2070.

[9] Feng, X.-Q.; Gao, X.; Wu, Z.; Jiang, L.; Zheng, Q.-S. "Superior Water Repellancy of Water Strider Legs with Hierarchical Structures: Experiments and Analysis." *Langmuir* **2007**, *23*, 4892-4896.

[10] Gao, X.; Jiang, L. "Water-Repellent Legs of Water Striders." *Nature* **2004**, *432*, 36.

[11] Sun, T.; Feng, L.; Gao, X.; Jiang, L. "Bioinspired Surfaces with Special Wettability." *Acc. Chem. Res.* **2005**, *38*, 644-652.

[12] Zhai, L.; Berg, M. C.; Cebeci, F. C.; Kim, Y.; Milwid, J. M.; Rubner, M. F.; Cohen, R. E. "Patterned Superhydrophobic Surfaces: Toward a Synthetic Mimic of the Namib Desert Beetle." *Nano Lett.* **2006**, *6*, 1213-1217.

[13] Bormashenko, E.; Bormashenko, Y.; Stein, T.; Whyman, G.; Bormashenko, E. "Why Do Pigeon Feathers Repel Water? Hydrophobicity of Pennae, Cassie-Baxter Wetting Hypothesis and Cassie-Wenzel Capillarity-Induced Wetting Transition." *J. Colloid Interface Sci.* **2007**, *311*, 212-216.

[14] Rijke, A. M. "The Water Repellency and Feather Structure of Cormorants, Phalacrocoracidae." *J. Exp. Biol.* **1968**, *48*, 185-189.

[15] Erbil, H. Y.; Demirel, A. L.; Avci, Y.; Mert, O. "Transformation of a Simple Plastic into a Superhydrophobic Surface." *Science* **2003**, *299*, 1377-1380.

[16] Li, X.-M.; Reinhoudt, D.; Crego-Calama, M. "What Do We Need for a Superhydrophobic Surface? A Review on the Recent Progress in the Preparation of Superhydrophobic Surfaces." *Chem. Soc. Rev.* **2007**, *36*, 1350-1368.

[17] Onda, T.; Shibuichi, S.; Satoh, N.; Tsujii, K. "Super-Water-Repellent Fractal Surfaces." *Langmuir* **1996**, *12*, 2125-2127.

[18] Shibuichi, S.; Yamamoto, T.; Onda, T.; Tsujii, K. "Super Water- and Oil-Repellent Surfaces Resulting from Fractal Structure." *J. Colloid Interface Sci.* **1998**, *208*, 287-294.

[19] Woodward, I.; Schofield, W. C. E.; Roucoules, V.; Badyal, J. P. S. "Super-Hydrophobic Surfaces Produced by Plasma Fluorination of Polybutadiene Films." *Langmuir* **2003**, *19*, 3432-3438.

[20] Youngblood, J. P.; McCarthy, T. J. "Ultrahydrophobic Polymer Surfaces Prepared by Simultaneous Ablation of Polypropylene and Sputtering of Poly(Tetrafluoroethylene) Using Radio Frequency Plasma." *Macromolecules* **1999**, *32*, 6800-6806.

[21] Ahuja, A.; Taylor, J. A.; Lifton, V.; Sidorenko, A. A.; Salamon, T. R.; Lobaton, E. J.; Kolodner, P.; Krupenkin, T. N. "Nanonails: A Simple Geometric Approach to Electrically Tunable Superhydrophobic Surfaces." *Langmuir* **2008**, *24*, 9-14.

[22] Chen, W.; Fadeev, A. Y.; Hsieh, M. C.; Öner, D.; Youngblood, J.; McCarthy, T. J. "Ultrahydrophobic and Ultralyophobic Surfaces: Some Comments and Examples." *Langmuir* **1999**, *15*, 3395-3399.

[23] Furstner, R.; Barthlott, W.; Neinhuis, C.; Walzel, P. "Wetting and Self-Cleaning Properties of Artificial Superhydrophobic Surfaces." *Langmuir* **2005**, *21*, 956-961.

[24] Gao, X.; Yao, X.; Jiang, L. "Effects of Rugged Nanoprotrusions on the Surface Hydrophobicity and Water Adhesion of Anisotropic Micropatterns." *Langmuir* **2007**, *23*, 4886-4891.

[25] Öner, D.; McCarthy, T. J. "Ultrahydrophobic Surfaces. Effects of Topography Length Scales on Wettability." *Langmuir* **2000**, *16*, 7777-7782.

[26] Yoshimitsu, Z.; Nakajima, A.; Watanabe, T.; Hashimoto, K. "Effects of Surface Structure on the Hydrophobicity and Sliding Behavior of Water Droplets." *Langmuir* **2002**, *18*, 5818-5822.

[27] Zhang, L.; Zhou, Z.; Cheng, B.; DeSimone, J. M.; Samulski, E. T. "Superhydrophobic Behavior of a Perfluoropolyether Lotus-Leaf-Like Topography." *Langmuir* **2006**, *22*, 8576-8580.

[28] Agarwal, S.; Horst, S.; Bognitzki, M. "Electrospinning of Fluorinated Polymers: Formation of Superhydrophobic Surfaces." *Macromol. Mater. Eng.* **2006**, *291*, 592-601.

[29] Ma, M.; Gupta, M.; Li, Z.; Zhai, L.; Gleason, K. K.; Cohen, R. E.; Rubner, M. F.; Rutledge, G. C. "Decorated Electrospun Fibers Exhibiting Superhydrophobicity." *Adv. Mater.* **2007**, *19*, 255-259.

[30] Ma, M.; Hill, R. M.; Lowery, J. L.; Fridrikh, S. V.; Rutledge, G. C. "Electrospun Poly(Styrene-*block*-dimethylsiloxane) Block Copolymer Fibers Exhibiting Superhydrophobicity." *Langmuir* **2005**, *21*, 5549-5554.

[31] Ma, M.; Mao, Y.; Gupta, M.; Gleason, K. K.; Rutledge, G. C. "Superhydrophobic Fabrics Produced by Electrospinning and Chemical Vapor Deposition." *Macromolecules* **2005**, *38*, 9742-9748.

[32] Zhu, Y.; Zhang, J.; Zheng, Y.; Huang, Z.; Feng, L.; Jiang, L. "Stable, Superhydrophobic, and Conductive Polyaniline/Polystyrene Films for Corrosive Environments." *Adv. Funct. Mater.* **2006**, *16*, 568-574.

[33] Jisr, R. M.; Rmaile, H. H.; Schlenoff, J. B. "Hydrophobic and Ultrahydrophobic Multilayer Thin Films from Perfluorinated Polyelectrolytes." *Angew. Chem., Int. Ed.* **2005**, *44*, 782-785.

[34] Zhai, L.; Cebeci, F. C.; Cohen, R. E.; Rubner, M. F. "Stable Superhydrophobic Coatings from Polyelectrolyte Multilayers." *Nano Lett.* **2004**, *4*, 1349-1353.

[35] Zhao, N.; Shi, F.; Wang, Z.; Zhang, X. "Combining Layer-by-Layer Assembly with Electrodeposition of Silver Aggregates for Fabricating Superhydrophobic Surfaces." *Langmuir* **2005**, *21*, 4713-4716.

[36] Gao, L.; McCarthy, T. J. ""Artificial Lotus Leaf" Prepared Using a 1945 Patent and a Commercial Textile." *Langmuir* **2006**, *22*, 5998-6000.

[37] Schuyten, H. A.; Reid, J. D.; Weaver, J. W.; Frick, J., J. G. "Imparting Water-Repellency to Textiles by Chemical Methods: A Review of the Literature." *Text. Res. J.* **1948**, *18*, 396-415, 490-503.

[38] Coulson, S. R.; Woodward, I. S.; Badyal, J. P. S. "Ultralow Surface Energy Plasma Polymer Films." *Chem. Mater.* **2000**, *12*, 2031-2038.

[39] Jarn, M.; Heikkila, M.; Linden, M. "Bioinspired Synthesis of Superhydrophobic Coatings." *Langmuir* **2008**, *24*, 10625-10628.

[40] Nakajima, A.; Hashimoto, K.; Watanabe, T. "Transparent Superhydrophobic Thin Films with Self-Cleaning Properties." *Langmuir* **2000**, *16*, 7044-7047.

[41] Wang, R.; Hashimoto, K.; Fujishima, A. "Light-Induced Amphiphilic Surfaces." *Nature* **1997**, *388*, 431-432.

[42] Cheng, G.; Zhang, Z.; Chen, S.; Bryers, J. D. J., S. "Inhibition of Bacterial Adhesion and Biofilm Formation on Zwitterionic Surfaces." *Biomaterials* **2007**, *28*, 4192-4199.

[43] Genzer, J.; Efimenko, K. "Recent Developments in Superhydrophobic Surfaces and Their Relevance to Marine Fouling: A Review." *Biofouling* **2006**, *22*, 339-360.

[44] Gudipati, C. S.; Finlay, J. A.; Callow, J. A.; Callow, M. E.; Wooley, K. L. "The Antifouling and Fouling-Release Performance of Hyperbranched Fluoropolymer (HBFP)-Poly(ethylene glycol) (PEG) Composite Coatings Evaluated by Adsorption of Biomacromolecules and the Green Fouling Alga *Ulva*." *Langmuir* **2005**, *21*, 3044-3053.

[45] Martinelli, E.; Agostini, S.; Galli, G.; Chiellini, E.; Glisenti, A.; Pettitt, M. E.; Callow, M. E.; Callow, J. A.; Graf, K.; Bartels, F. W. "Nanostructured Films of Amphiphilic Fluorinated Block Copolymers for Fouling Release Application." *Langmuir* **2008**, *24*, 13138-13147.

[46] Singer, A. J.; Clark, R. A. F. "Cutaneous Wound Healing." *N. Engl. J. Med.* **1999**, *341*, 738-746.

Chapter 4. Capillary-Guided Deposition of Linear Assemblies of Nanoparticles and Microparticles

4.1 Introduction

The deposition and assembly of micro- and nanoparticles into lines has received much interest in recent years and has resulted in the development of a variety of assembly techniques. A number of these techniques result in the deposition of a micro- or nanoparticle line on a substrate. These include dip coating,[1-5] droplet templating,[2,4] convective assembly,[6,7] meniscus withdrawal from a substrate,[8-10] other methods of evaporation driven assembly,[7,11] the use of Marangoni flow,[12] patterning using PDMS,[13-16] fountain pen nanolithography,[17] dielectrophoresis,[18] biomolecule templating,[8,19,20] and particle attachment to self assembled monolayers.[21] A handful of these techniques result in the formation of a nanoparticle line or wire in solution, including spontaneous formation of particle chains in suspension,[22-26] particle crosslinking,[24,27] optical trapping,[28] alignment in a magnetic field,[22,29] dielectrophoresis,[18,30] and biomolecule templating.[31] Other methods break materials down into lines of nanoparticles,[32-34] use printing methods to deposit lines of particles,[35-37] and melt nanoparticles into nanowires.[35,36] The electrical properties of the nanoparticle lines and wires deposited via several of the techniques above have also been studied.[8,14,17]

We report a technique that combines both convective assembly at high volume fraction and dip coating to deposit linear assemblies of gold nanoparticles and latex microspheres on flat substrates with vanishing contact angles. The goals of this investigation were to characterize the process depositing the lines and to understand the phenomena resulting in the deposited structures. Additionally, we characterized the electrical properties of the gold nanoparticle lines, which may potentially aid in developing deposition techniques for nanoparticle lines that can find applications in sensors.

4.1.1 Convective Assembly

Convective assembly has gotten a significant amount of attention in recent years as a method for depositing two-dimensional colloidal crystals on a substrate. The process begins with the pinning of the contact line of a receding liquid surface. As evaporation proceeds and the menisci between the particles become small enough, capillary pressure compacts the particles into a close-packed structure.[38,39] In order to compensate for evaporation, suspending liquid from the bulk is transported to the drying front, carrying particles with it and continuing the crystal growth.[40] A mass balance correlates the crystal growth rate to the evaporation rate and the particle volume fraction:

$$v_c = \frac{\beta j_e l \phi}{h(1-\varepsilon)(1-\phi)}$$

where v_c is the crystal growth rate, β is an interaction parameter, j_e is the evaporation rate, l is the drying length, ϕ is the volume fraction of the particles in suspension, h is the

height of the deposited crystal, and ε is the crystal porosity.[39,41] We have reported a modified technique that uses small volumes of suspension at high volume fraction. The suspension is trapped between two plates and is withdrawn using a linear motor, dragging the meniscus behind it.[42-44]

4.1.2 Dip Coating

Dip coating is an alternative method for depositing particle films on a substrate that has been studied for a number of years. The process involves withdrawing a substrate from a vessel containing the suspension to be deposited. As the substrate is withdrawn, a thin film of the suspension is entrained on the substrate.[45] The film thickness of a coating at low flow rates on a vertical substrate was first calculated by Landau and Levich:[46]

$$h_0 = 0.944 \frac{(\mu v_w)^{2/3}}{\sigma^{1/6} (\rho g)^{1/2}}$$

where h_0 is the film thickness, μ is the viscosity, v_w is the withdrawal rate, σ is the surface tension, ρ is the density, and g is gravitational acceleration. Additional research has provided corrections to several early assumptions,[47-50] solutions for angular withdrawal of the substrate,[48,51] and solutions for coating at higher flow rates.[49] Experiments, as well, have confirmed the results of these various models[48,50] and have given additional information regarding the film structure of sols and colloids during and following evaporation of the suspending liquid.[47,49]

In this study, we confine the meniscus by using a capillary that is withdrawn at a constant rate, resulting the assembly of micro- or nanoparticles into lines. Our goals were to understand and optimize the deposition process, correlate the effects of the particle concentration and withdrawal rate on the structure of the deposited lines, and characterize the electrical properties of the gold nanoparticle lines.

4.2 Materials and Methods

4.2.1 Substrate Preparation

Fisherbrand 25 mm × 75 mm glass microscope slides (Fisher Scientific, Waltham, MA) were immersed overnight in a Nochromix solution (GODAX Laboratories, Cabin John, MD) and then rinsed with deionized water from an RiOs 16 water purification system (Millipore Corporation, Bedford, MA) to thoroughly clean the substrates and give them vanishing contact angles. The slides were then air-dried.

For the experiments requiring higher substrate contact angles, a variety of methods were used. By washing the slides with Sparkleen detergent (Fisher Scientific) and then drying in an oven at 70°C for 8 hours, a contact angle of 19° was achieved. Microscope slides with a contact angle of 29° were prepared by overnight immersion in Nochromix, rinsing with deionized water, and drying in a 70°C oven for 8 hours. Higher contact angles were achieved by first preparing microscope slides with Nochromix as described in the previous paragraph, exposing the slide to a silane mixture for 10 min, washing copiously with deionized water, sonicating for 10 s (Branson Ultrasonics

Corporation, Danbury, CT), and then rinsing again with deionized water, prior to air drying. The 73° contact angle was achieved using chlorodimethylsilane (Acros Organics, NJ), and the 78° contact angle was achieved using a 13:2 ratio of chlorodimethylsilane and dichlorodimethylsilane (Sigma-Aldrich, St. Louis, MO). The contact angles were all determined using a goniometer.

4.2.2 Particle Preparation

The latex particles used were 0.91 μm surfactant-free sulfate latex (Interfacial Dynamics Corporation, Portland, OR). These were washed and concentrated to 11 – 25 vol% using a Fisher Marathon micro A microcentrifuge (2700 *g* for 5 min). The 15 nm gold nanoparticles used were synthesized by $HAuCl_4$ reduction in the presence of sodium citrate and tannic acid.[52] The particles were washed by centrifuging in Centricon Plus-20 centrifuge filters (Millipore) at 1500 *g* for 10 min, removing the supernatant, and replacing with deionized water. The suspension was then centrifuged again at 1500 *g* for 10 min. Following inversion of the filter, the concentrated suspension was collected by centrifugation at 750*g* for 5 min. The particles were then further concentrated to 2 – 7 wt% using the microcentrifuge at 9500 *g* for 15 min. The concentrations were determined via UV/Vis spectrophotometry, which also showed that the absorption peak remained constant at 524 ± 1 nm, indicating that the nanoparticles did not aggregate.

4.2.3 Capillary Preparation

Fisherbrand glass Pasteur pipets were heated in the flame of a butane burner and drawn out into capillaries with an outer diameter of 100 – 150 μm[53]. The capillary was broken, such that 5 – 8 cm of the capillary remained attached to the pipet, and all but 1 cm of the undrawn portion of the Pasteur pipet was cut away using a diamond file, leaving only the capillary.

4.2.4 Imaging

The deposited lines were optically imaged with an Olympus BX61 microscope with a CCD camera and 4× to 40× objectives in bright field lighting. To record the deposition process, an Olympus CKX41 inverted microscope with 10× to 40× objectives was used with a digital camera while the capillary was drawn by hand across the microscope slide. SEM imaging was performed with a Philips XL series scanning electron microscope with an accelerating voltage of 2 – 5 kV.

4.2.5 Electrical Characterization

Substrates with parallel gold lines were immersed in deionized water for 10 min, changing the water 4 times. Two electrodes were prepared by attaching two pieces of copper tape, spaced 5 mm apart, to a microscope slide. This slide could then be placed on top of a segment of the line. An Agilent 5 ½ digit multimeter (Santa Clara, CA) and a DC

regulated power supply (Extech Instruments, Waltham, MA) were used to apply a DC voltage and measure the resulting current.

4.3 Results and Discussion

The drawn glass capillary was filled with a concentrated suspension of gold nanoparticles or latex microspheres. For each capillary, it was necessary to rotate and angle the capillary tip to find the position at which it would release the particle suspension onto the substrate. Using a linear motor, the capillary was then dragged across a glass substrate at a constant rate, leaving a film of particle suspension on the substrate (Figure 4.1).

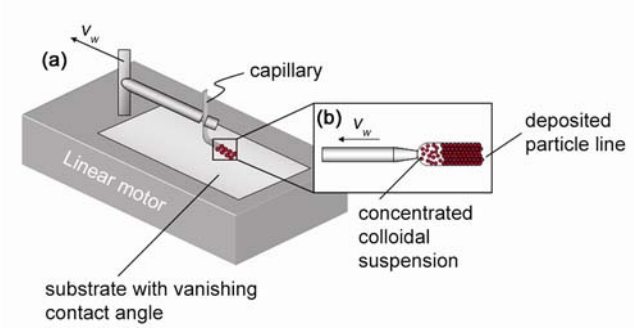

Figure 4.1. Schematic showing the capillary-guided deposition process. (a) The capillary filled with the concentrated particle suspension is withdrawn along a substrate. (b) The contact lines of the suspension pin upon exiting the capillary, resulting in the ordering of the particles.

4.3.1 Contact Angle Assessment

The use of capillary deposition at contact angles of 78°, 73°, 29°, 19°, and vanishing was explored by varying the preparation of the glass substrate. We found that the suspension contacting the substrate while still in the capillary had to pin on the

substrate in order for any of the suspension to exit the capillary. At nonvanishing substrate contact angles, we were able to induce pinning in order to get a flow of suspension, but the resultant structure on the substrate was a disconnected series of droplets. Thus, pinning of the suspension must occur not only at the initial point of contact to allow flow, but also along the edges of the deposited line of suspension in order for the suspension to dry into a continuous structure. A vanishing contact angle, therefore, is necessary to allow the particle suspension to pin and form a line of particles.

4.3.2 Line Structure

We found that the structure of the deposited line depends on the withdrawal rate. At low rates (≤0.5 mm/s), the line is comprised of a series of arcs (Figure 4.2). As demonstrated in Figure 4.3a – c, there is very little rearrangement of the particles from their initial positions during the drying process. This is due to the small volume of the suspending liquid being released with the particles, affording minimal time for rearrangement during evaporation.

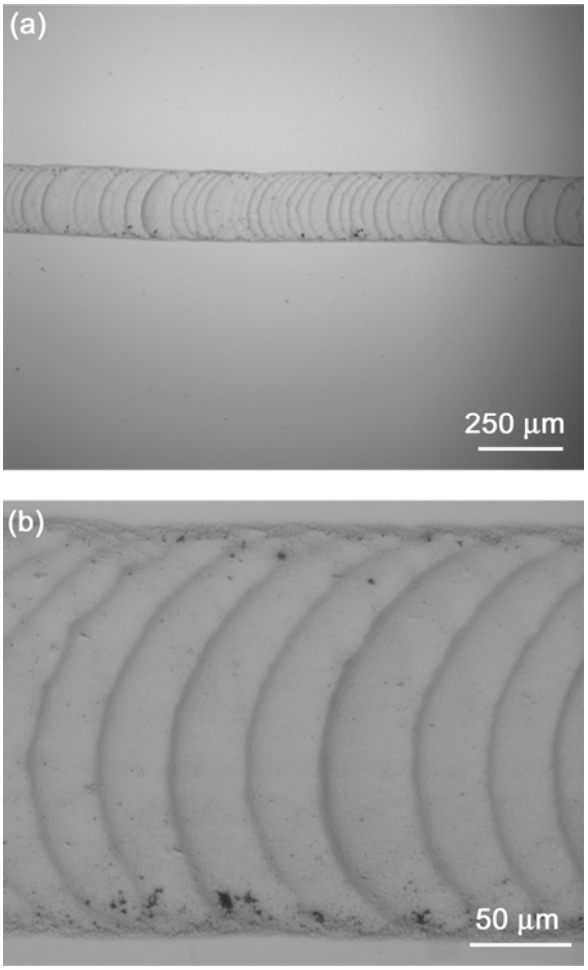

Figure 4.2. Optical micrographs of a 0.8 wt% gold nanoparticle suspension deposited at 0.5 mm/s showing a series of connected arcs. Deposition direction is from left to right.

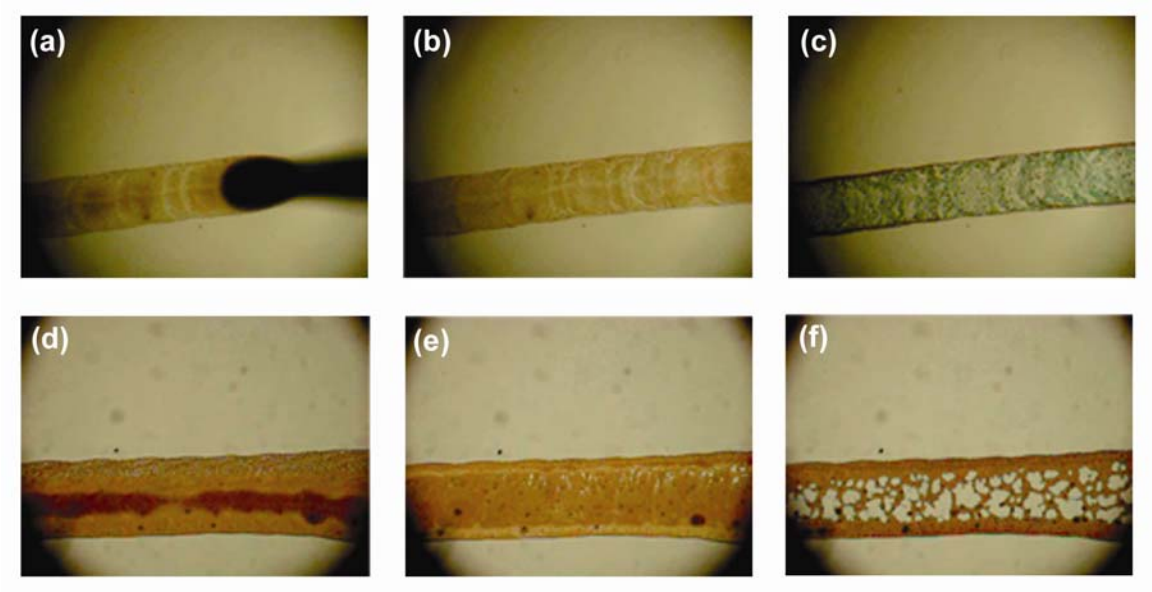

Figure 4.3. Time-lapsed images showing drying process of 0.91 μm latex particle suspensions withdrawn by hand. Deposition direction is from left to right. (a) – (c) 8.2 vol% suspension withdrawn at a low rate of ~4 mm/s. (a) Particle arrangement as initially deposited. (b) Minor rearrangement of particles occurred during first 0.8 s after withdrawal of the capillary. (c) Evaporation was complete after 1.7 s. (d) – (f) High withdrawal rate of ~21 mm/s of a 25 vol% particle suspension. (d) Initial arrangement of particles. (e) Significant rearrangement of the particles took 1.3 s. (f) Complete evaporation took 1.9 s. As the capillaries were withdrawn by hand, the withdrawal rates are inexact.

At high withdrawal rates (≥10 mm/s), the deposited structure morphs into two heavy, parallel lines with a thin section between them (Figures 4.3d – f, 4.4a). As can be seen in Figure 4.3d – f, there is significant rearrangement of the particles from their initial positions. This is because significantly more suspending liquid is released, affording the particles the time necessary for rearrangement. As can be seen from Figure 4.4b – c, the line at the edges of the capillary path is heavy and highly interconnected.

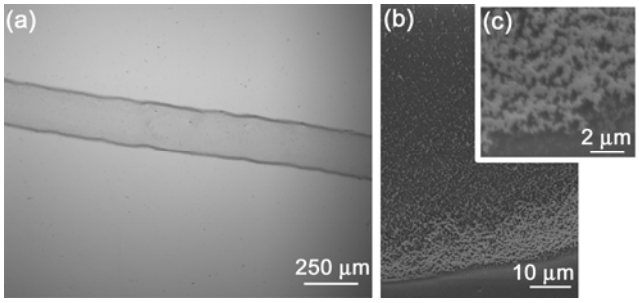

Figure 4.4. (a) Parallel lines of gold nanoparticles deposited at 30 mm/s. (b) & (c) SEM micrographs showing parallel line of gold nanoparticles, which is highly interconnected.

4.3.3 Particle Alignment

The amount of the particle suspension being released at a given time increases with increasing withdrawal rate of the capillary, which can be explained by dip coating. Since there is no slip at the surface, as the withdrawal rate of the capillary increases, the thickness of the liquid layer withdrawn will increase as well. Landau and Levich,[46] as well as Deryagin and Levi,[54] studied the problem of the relation of withdrawal rate to film thickness during dip coating. In deriving a solution, Landau and Levich assumed that the shape of the film was determined by the surface tension of the liquid. To determine if this condition had been met, we calculated the Capillary number,[49] *Ca*, which is the ratio of viscous forces to surface tension:

$$Ca = \frac{\mu v_w}{\sigma}$$

where μ is the viscosity, v_w is the withdrawal rate, and σ is the surface tension. For the derived solution to be valid,[46] Ca should be smaller than 10^{-2}; for our system, *Ca* does not exceed 3×10^{-3} for all possible conditions. Since the geometry of the system for

which the equations were derived varies significantly from the geometry of our system, we have chosen to use a correlation for the dimensionless film thickness,[50] T_0:

$$T_0 = 0.944\left(Ca\right)^{1/6}.$$

When we introduced our parameters into the correlation, we found that the dimensionless film thickness varied from 0.14 to 0.36, increasing with the withdrawal rate. Thus, the thickness of the liquid film increases proportionally with the withdrawal rate of the substrate, indicating that it is reasonable to attribute the variations in the film thickness to viscous flow.[45]

The thickness of the liquid film withdrawn from the capillary onto the substrate dictates the structure of the line. Particle rearrangement during the evaporation of the suspending liquid is due to convective assembly, resulting in collection of particles at the pinned three-phase contact line. The evaporation of the suspending liquid from the pinned contact line results in the transport of particles to that contact line, and capillary forces pull the particles into close contact.

At low withdrawal rates, very little suspending liquid is released, resulting in the pinning of the semi-circular periphery of the menisci formed by the fluid in the capillary, as shown in Figure 4.5a – b. The particles are transported to the pinned contact line, where they are assembled into a close-packed structure (Figure 4.5c). As the capillary is withdrawn along the substrate, this process occurs repeatedly. The resultant structure is therefore a connected series of arcs of particles along the path of the capillary, since there

are not enough particles deposited for each meniscus to make a solid structure before the capillary moves.

At high withdrawal rates, significantly more suspending liquid is released, resulting in the formation of a thick liquid film along the path of the capillary. The three-phase contact lines pin along the outer parallel edges of the liquid film (see Figure 4.5d – e). As evaporation occurs, the flow of fluid to the three-phase contact lines also transports the particles. Once the particles reach the outer edges of the film, they are assembled into a close-packed linear structure (Figure 4.5f). The resultant structure has thick, parallel lines with a region in between that has a much thinner covering of particles. As the deposited liquid film is thick and continuous, the deposited structure is also continuous.

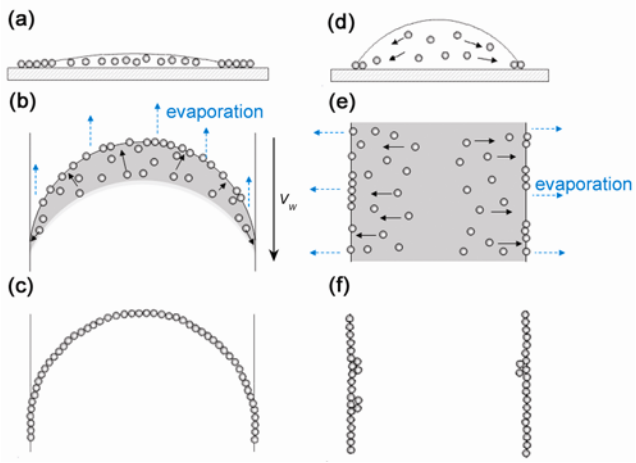

Figure 4.5. Schematics showing particle alignment for (a) – (c) low and (d) – (f) high withdrawal rates. (a) & (d) show side views of the film. (b) & (e) show top-down views of the film during evaporation. (c) & (f) show the final structure of the line.

4.3.4 Effect of Withdrawal Rate and Particle Concentration on Line Structure

The effect of the range of withdrawal rates and of the particle concentration on the structure of the lines deposited was investigated so that we could engineer the process to deposit uniform lines. The full range of the linear motor was explored, from 0.5 mm/s to 60 mm/s. A range of gold nanoparticle concentrations from 0.5 to 7.3 wt% were examined as well. The combined results of the experiments examining the range of velocities and particle concentrations are shown in Figure 4.6. As also explained in the previous paragraph, we found that at low withdrawal rates, arcs were deposited for all concentrations. At high withdrawal rates and high particle concentrations, two parallel lines were deposited. A variety of structures were deposited in between these two extremes, which we have classified in Figure 4.6 as “patchy lines” because they tended to have a moderately uniform but highly incomplete covering of particles. These “patchy lines” formed because the intermediate combinations of withdrawal rate and gold nanoparticle concentration result in the release of too much liquid for the pinning of the semi-circular menisci required for the deposition of arcs, yet not enough particles and liquid are released for the formation of the thick liquid film necessary for the deposition of parallel lines.

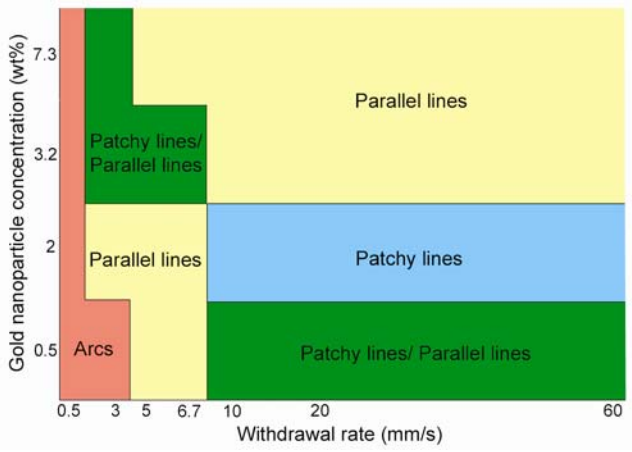

Figure 4.6. Operational diagram showing the structures deposited at the gold nanoparticle concentrations and withdrawal velocities used. For each combination of parameters, three lines were each sampled at three points along their lengths.

Based upon the results displayed in Figure 4.6, we believe that solid lines of gold nanoparticles with a uniform coverage could be deposited at withdrawal rates between 0.5 mm/s and 5 mm/s at higher gold nanoparticle concentrations than we were able to achieve. Under the conditions that result in parallel lines, the flow of fluid to the outer edges will prevent uniform coverage of particles. Both the arcs and the patchy lines are limited in substrate coverage by the number of particles exiting the capillary at a given time. Thus, at higher concentrations, it is possible that instead of forming patchy lines or arcs, solid, uniform lines could form.

4.3.5 Electrical Characterization

The ability of the parallel lines of gold nanoparticles to conduct current was also explored. The lines used were deposited from 7.3 wt% gold nanoparticle suspension at 60 mm/s and were then examined using an optical microscope to ensure that the parallel lines were unbroken. The gold nanoparticle lines were immersed in deionized water for 10 min to remove contaminants preventing good contact between the particles and the electrodes prior to electrical measurements. As can be seen in current-voltage plot in Figure 4.7, the linear response indicates an Ohmic behavior, with a resistance of 0.29 kΩ. Experiments showed that the current travels through the thick parallel lines; when only the thin layer in between is present, no current can be measured. Thus, the thick, interconnected lines are necessary for electrical conductance.

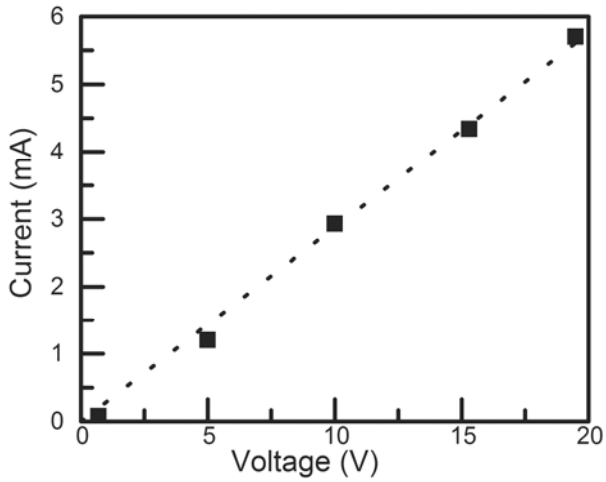

Figure 4.7. Current-voltage plot for a deposited gold nanoparticle parallel line structure.

4.4 Conclusions

We developed and characterized a capillary-guided technique for deposition of concentrated suspensions of nanoparticles and microparticles. By controlling the particle concentration and withdrawal rate of the capillary, we were able to control the structure of the line deposited. Due to viscous flow, commonly discussed in relation to dip coating, the amount of the suspension deposited varied with the withdrawal rate. This in turn determined the particle alignment scheme via convective assembly, resulting in either connected arcs or heavy parallel lines. We determined that the heavy parallel lines, due to the interconnected nature of the line structure, were conductive. This introduces the possibility that the lines could be constructed of functionalized nanoparticles for use as sensors.

4.5 Acknowledgements

This study was supported by the Air Force Research Laboratory. We are grateful to Laura Sowards for her assistance with the scanning electron microscope, to Caryn Heldt for her assistance with the inverted microscope, and to Suk Tai Chang for his assistance with the electrical measurements.

4.6 References

[1] Ghosh, M.; Fan, F.; Stebe, K. J. "Spontaneous Pattern Formation by Dip Coating of Colloidal Suspensions on Homogeneous Surfaces." *Langmuir* **2007**, *23*, 2180-2183.

[2] Huang, J.; Kim, F.; Tao, A. R.; Connor, S.; Yang, P. "Spontaneous Formation of Nanoparticle Stripe Patterns through Dewetting." *Nat. Mater.* **2005**, *4*, 896-900.

[3] Huang, J.; Tao, A. R.; Connor, S.; He, R.; Yang, P. "A General Method for Assembling Single Colloidal Particle Lines." *Nano Lett.* **2006**, *6*, 524-529.

[4] Huang, J.; Fan, R.; Connor, S.; Yang, P. "One-Step Patterning of Aligned Nanowire Arrays by Programmed Dip Coating." *Angew. Chem., Int. Ed.* **2007**, *46*, 2414-2417.

[5] Lu, C.; Mohwald, H.; Fery, A. "A Lithography-Free Method for Directed Colloidal Crystal Assembly Based on Wrinkling." *Soft Matter* **2007**, *3*, 1530-1536.

[6] Bae, C.; Shin, H.; Moon, J. "Facile Route to Aligned One-Dimensional Arrays of Colloidal Nanoparticles." *Chem. Mater.* **2007**, *19*, 1531-1533.

[7] Malaquin, L.; Kraus, T.; Schmid, H.; Delamarche, E.; Wolf, H. "Controlled Particle Placement through Convective and Capillary Assembly." *Langmuir* **2007**, *23*, 11513-11521.

[8] Kuncicky, D. M.; Naik, R. R.; Velev, O. D. "Rapid Deposition and Long-Range Alignment of Nanocoatings and Arrays of Electrically Conductive Wires from Tobacco Mosaic Virus." *Small* **2006**, *2*, 1462-1466.

[9] Yarin, A. L.; Szczech, J. B.; Megaridis, C. M.; Zhang, J.; Gamota, D. R. "Lines of Dense Nanoparticle Colloidal Suspensions Evaporating on a Flat Surface: Formation of Non-Uniform Dried Deposits." *J. Colloid Interface Sci.* **2006**, *294*, 343-354.

[10] Yerushalmi, R.; Ho, J. C.; Jacobson, Z. A.; Javey, A. "Generic Nanomaterial Positioning by Carrier and Stationary Phase Design." *Nano Lett.* **2007**, *7*, 2764-2768.

[11] Dockendorf, C. P. R.; Choi, T.-Y.; Poulikakos, D.; Stemmer, A. "Size Reduction of Nanoparticle Ink Patterns by Fluid-Assisted Dewetting." *Appl. Phys. Lett.* **2006**, *88*, 131903-1-3.

[12] Cai, Y.; Newby, B.-m. Z. "Marangoni Flow-Induced Self-Assembly of Hexagonal and Stripelike Nanoparticle Patterns." *J. Am. Chem. Soc.* **2008**, *130*, 6076-6077.

[13] Cherniavskaya, O.; Adzic, A.; Knutson, C.; Gross, B. J.; Zang, L.; Liu, R.; Adams, D. M. "Edge Transfer Lithography of Molecular and Nanoparticle Materials." *Langmuir* **2002**, *18*, 7029-7034.

[14] Huang, Y.; Duan, X.; Wei, Q.; Lieber, C. M. "Directed Assembly of One-Dimensional Nanostructures into Functional Networks." *Science* **2001**, *291*, 630-633.

[15] Kraus, T.; Malaquin, L.; Schmid, H.; Riess, W.; Spencer, N. D.; Wolf, H. "Nanoparticle Printing with Single-Particle Resolution." *Nat. Nanotechnol.* **2007**, *2*, 570-576.

[16] Moran, C. E.; Radloff, C.; Halas, N. J. "Benchtop Fabrication of Submicrometer Metal Line and Island Arrays Using Passivative Microcontact Printing and Electroless Plating." *Adv. Mater.* **2003**, *15*, 804-807.

[17] Taha, H.; Lewis, A.; Sukenik, C. "Controlled Deposition of Gold Nanowires on Semiconducting and Nonconducting Surfaces." *Nano Lett.* **2007**, *7*, 1883-1887.

[18] Bhatt, K. H.; Velev, O. D. "Control and Modeling of the Dielectrophoretic Assembly of On-Chip Nanoparticle Wires." *Langmuir* **2004**, *20*, 467-476.

[19] Aldaye, F. A.; Palmer, A. L.; Sleiman, H. F. "Assembling Materials with DNA as the Guide." *Science* **2008**, *321*, 1795-1799.

[20] Deng, Z.; Mao, C. "DNA-Templated Fabrication of 1D Parallel and 2D Crossed Metallic Nanowire Arrays." *Nano Lett.* **2003**, *3*, 1545-1548.

[21] Yonezawa, T.; Itoh, T.; Shirahata, N.; Masuda, Y.; Koumoto, K. "Positioning of Cationic Silver Nanoparticle by Using AFM Lithography and Electrostatic Interaction." *Appl. Surf. Sci.* **2007**, *254*, 621-626.

[22] Butter, K.; Bomans, P. H. H.; Frederik, P. M.; Vroege, G. J.; Philipse, A. "Direct Observation of Dipolar Chains in Iron Ferrofluids by Cryogenic Electron Microscopy." *Nat. Mater.* **2003**, *2*, 88-91.

[23] Liao, J.; Zhang, Y.; Yu, W.; Xu, L.; Ge, C.; Liu, J.; Gu, N. "Linear Aggregation of Gold Nanoparticles in Ethanol." *Colloids and Surfaces A: Physicochem. Eng. Aspects* **2003**, *223*, 177-183.

[24] Polavarapu, L.; Xu, Q.-H. "Water-Soluble Conjugated Polymer-Induced Self-Assembly of Gold Nanoparticles and its Application to SERS." *Langmuir* **2008**, *24*, 10608-10611.

[25] Zhang, Y. X.; Zeng, H. C. "Template-Free Parallel One-Dimensional Assembly of Gold Nanoparticles." *J. Phys. Chem. B* **2006**, *110*, 16812-16815.

[26] Zhang, Y. X.; Zeng, H. C. "Surfactant-Mediated Self-Assembly of Au Nanoparticles and their Related Conversion to Complex Mesoporous Structures." *Langmuir* **2008**, *24*, 3740-3746.

[27] Sardar, R.; Shumaker-Parry, J. S. "Asymmetrically Functionalized Gold Nanoparticles Organized in One-Dimensional Chains." *Nano Lett.* **2008**, *8*, 731-736.

[28] Terray, A.; Oakey, J.; Marr, D. W. M. "Fabrication of Linear Colloidal Structures for Microfluidic Applications." *Appl. Phys. Lett.* **2002**, *81*, 1555-1557.

[29] Furst, E. M.; Suzuki, C.; Fermigier, M.; Gast, A. P. "Permanently Linked Monodisperse Paramagnetic Chains." *Langmuir* **1998**, *14*, 7334-7336.

[30] Hermanson, K. D.; Lumsdon, S. O.; Williams, J. P.; Kaler, E. W.; Velev, O. D. "Dielectrophoretic Assembly of Electrically Functional Microwires from Nanoparticle Suspensions." *Science* **2001**, *294*, 1082-1086.

[31] Dreyfus, R.; Baudry, J.; Roper, M. L.; Fermigier, M.; Stone, H. A.; Bibette, J. "Microscopic Artificial Swimmers." *Nature* **2005**, *437*, 862-865.

[32] Fowlkes, J. D.; Pedraza, A. J.; Blom, D. A.; Meyer III, H. M. "Surface Microstructuring and Long-Range Ordering of Silicon Nanoparticles." *Appl. Phys. Lett.* **2002**, *80*, 3799-3801.

[33] Nishijo, J.; Oishi, O.; Judai, K.; Nishi, N. "Facile and Mass-Producible Fabrication of One-Dimensional Ag Nanoparticle Arrays." *Chem. Mater.* **2007**, *19*, 4627-4629.

[34] Qin, Y.; Liu, L.; Yang, R.; Gosele, U.; Knez, M. "General Assembly Method for Linear Metal Nanoparticle Chains Embedded in Nanotubes." *Nano Lett.* **2008**, *8*, 3221-3225.

[35] Bieri, N. R.; Chung, J.; Poulikakos, D.; Grigoropoulos, C. P. "Manufacturing of Nanoscale Thickness Gold Lines by Laser Curing of a Discretely Deposited Nanoparticle Suspension." *Superlattices Microstruct.* **2004**, *35*, 437-444.

[36] Chung, J.; Ko, S.; Bieri, N. R.; Grigoropoulos, C. P.; Poulikakos, D. "Conductor Microstructures by Laser Curing of Printed Gold Nanoparticle Ink." *Appl. Phys. Lett.* **2004**, *84*, 801-803.

[37] Lee, D. Y.; Hwang, E. S.; Yu, T. U.; Kim, Y. J.; Hwang, J. "Structuring of Micro Line Conductor Using Electro-Hydrodynamic Printing of a Silver Nanoparticle Suspension." *Appl. Phys. A* **2006**, *82*, 671-674.

[38] Denkov, N. D.; Velev, O. D.; Kralchevsky, P. A.; Ivanov, I. B.; Yoshimura, H.; Nagayama, K. "Mechanism of Formation of Two-Dimensional Crystals from Latex Particles on Substrates." *Langmuir* **1992**, *8*, 3183-3190.

[39] Dimitrov, A. S.; Nagayama, K. "Steady-State Unidirectional Convective Assembling of Fine Particles into 2-Dimensional Arrays." *Chem. Phys. Lett.* **1995**, *243*, 462-468.

[40] Denkov, N. D.; Velev, O. D.; Kralchevsky, P. A.; Ivanov, I. B.; Yoshimura, H.; Nagayama, K. "2-Dimensional Crystallization." *Nature* **1993**, *361*, 26.

[41] Dimitrov, A. S.; Nagayama, K. "Continuous Convective Assembly of Fine Particles into Two-Dimensional Arrays on Solid Surfaces." *Langmuir* **1996**, *12*, 1303-1311.

[42] Prevo, B. G.; Velev, O. D. "Controlled, Rapid Deposition of Structured Coatings from Micro- and Nanoparticle Suspensions." *Langmuir* **2004**, *20*, 2099-2107.

[43] Prevo, B. G.; Fuller, J. C.; Velev, O. D. "Rapid Deposition of Gold Nanoparticle Films with Controlled Thickness and Structure by Convective Assembly." *Chem. Mater.* **2005**, *17*, 28-35.

[44] Prevo, B. G.; Hwang, Y.; Velev, O. D. "Convective Assembly of Antireflective Silica Coatings with Controlled Thickness and Refractive Index." *Chem. Mater.* **2005**, *17*, 3642-3651.

[45] Scriven, L. E. "Physics and Applications of Dip Coating and Spin Coating." In *Better Ceramics through Chemistry III*; Brinker, C. J.; Clark, D. E.; Ulrich, D. R., Eds.; Materials Research Society: Pittsburgh, 1988; pp. 717-729.

[46] Landau, L.; Levich, B. "Dragging of a Liquid by a Moving Plate." *Acta Physicochimica U.R.S.S.* **1942**, *17*, 42-54.

[47] Brinker, C. J.; Scherer, G. W. "Film Formation." In *Sol-Gel Science: The Physics and Chemistry of Sol-Gel Processing*; Academic Press, Inc.: San Diego, 1990; pp. 788-836.

[48] Hurd, A. J.; Brinker, C. J. "Sol-Gel Film Formation by Dip Coating." In *Better Ceramics through Chemistry Iv*; Zelinski, B. J. J.; Brinker, C. J.; Clark, D. E.; Ulrich, D. R., Eds.; Materials Research Society: Pittsburgh, 1990; pp. 575-581.

[49] Schunk, P. R.; Hurd, A. J.; Brinker, C. J. "Free-Meniscus Coating Processes." In *Liquid Film Coating: Scientific Principles and Their Technological Implications*; Kistler, S. F.; Schweizer, P. M., Eds.; Chapman & Hall: London, 1997; p. 67.

[50] White, D. A.; Tallmadge, J. A. "Theory of Drag out of Liquids on Flat Plates." *Chem. Eng. Sci.* **1965**, *20*, 33-37.

[51] Tallmadge, J. A. "A Theory of Entrainment for Angular Withdrawal of Flat Supports." *AIChE J.* **1971**, *17*, 243-246.

[52] Slot, J. W.; Geuze, H. J. "A New Method of Preparing Gold Probes for Multiple-Labeling Cytochemistry." *Euro. J. Cell Biol.* **1985**, *38*, 87-93.

[53] Nagy, A.; Gertenstein, M. J.; Vintersten, K.; Behringer, R. *CSH Protocols* **2006**, doi:10.1101/pdb.prot4354.

[54] Deryagin, B. M.; Levi, S. M. "Theory of Coating a Viscous Liquid on a Moving Support." In *Film Coating Theory: The Physical Chemistry of Coating Thin Layers on a Moving Support*; The Focal Press: London, 1964; pp. 25-48.

Chapter 5. Wedge-Templated Deposition of Linear Assemblies of Microparticles and Nanoparticles

5.1 Introduction

In recent years, there has been significant interest in the deposition of nanoparticles into linear assemblies. A variety of techniques have been used to this effect, including dip coating,[1-5] convective assembly,[6,7] and other forms of meniscus withdrawal,[8-11] resulting in the formation of arrays of lines on a substrate. Lines have formed in a bulk suspension spontaneously,[12-17] using dielectrophoresis,[18,19] and using optical trapping.[20] Arrays of lines have been formed on a substrate using dielectrophoresis,[18] biomolecule templating,[9,21] Marangoni flow,[22] PDMS to directly deposit nanoparticles into patterns,[7,23,24] and laser curing printed lines of nanoparticles.[25,26] Electrohydrodynamic printing,[27,28] fountain pen nanolithography,[29,30] and meniscus withdrawal[8,31] have all been utilized deposit individual nanoparticle lines.

One example of meniscus-guided deposition is the formation of rings of particles during the evaporation of a sessile droplet containing a particle suspension.[4,22,32-35] Variations on the method have resulted in the assembly of spoke patterns,[2] aligned nanowires,[4] size-selective segregation of particles in the deposited structure,[36] and micropatches.[37] The deposition of DNA microarrays[38-40] is one example of an application that is making use of droplet patterning research.

A theoretical interpretation of ring formation from evaporating sessile droplets of particle suspensions was first reported by Deegan et al.[33] Their research showed that when the contact line of a sessile droplet becomes pinned, minimization of the free surface area results in the transport of fluid and particles to the pinned contact line.[41] This explanation of ring formation has improved upon to include other effects.[42-45] When the contact line of an evaporating sessile droplet does not pin, however, the contact angle remains constant for a large part of the evaporation process.[46-48] When this occurs, a particle patch, instead of a ring, forms.[37,49] It is the constant contact angle mode of sessile droplet evaporation that our technique uses.

We report here a novel technique for deposition of linear assemblies of micro- or nanoparticles from a sessile drop along a wedge template on a moderately hydrophobic substrate. The goals of this study were to understand the mechanism of the process by which the lines were deposited and to optimize the technique for the deposition of continuous gold nanoparticle lines. These deposited structures were also characterized.

5.2 Materials and Methods

5.2.1 Substrate Preparation

Fisherbrand 25 mm × 75 mm glass microscope slides (Fisher Scientific, Waltham, MA) were immersed overnight in a Nochromix solution (GODAX Laboratories, Cabin John, MD) and then cleaned with deionized water from an RiOs 16 water purification system (Millipore Corporation, Bedford, MA) and then air-dried. The slides were

exposed to a mixture of chlorodimethylsilane (Acros Organics, NJ) and dichlorodimethylsilane (Sigma-Aldrich, St. Louis, MO) for 10 min. After washing copiously, the slides were sonicated (Branson Ultrasonics Corporation, Danbury, CT) in deionized water for 10 s. Following a final rinse with deionized water, the slides were air-dried. Contact angle was measured using a goniometer.

A single-edged razor blade with a thickness of 0.2 mm was used as the wedge. For each experiment, a new blade was washed with Sparkleen 2 detergent (Fisher Scientific) and air dried.

5.2.2 Particle Preparation

The latex particles used were surfactant-free sulfate latex with a diameter of 0.30 μm (Interfacial Dynamics Corporation, Portland, OR) and Polybead microspheres with a diameter of 2.93 μm (Polysciences, Warrington, PA). These spheres were washed using a Fisher Marathon micro A microcentrifuge at 10800 *g* for 20 min and 2700 *g* for 5 min, respectively. The particle suspensions were then diluted with deionized water to concentrations of 0.002 vol% – 0.2 vol%. Tween 20 (Acros Organics, NJ) was added to the latex suspensions in concentrations of 0.001 wt% to 0.01 wt%.

The 15 nm gold nanoparticles used in this study were synthesized by reducing $HAuCl_4$ in the presence of sodium citrate and tannic acid.[50] The particles were prepared by centrifugation in Centricon Plus-20 centrifuge filters (Millipore) at 1500 *g* for 10 min, replacing the filtered liquid with deionized water, and then centrifuging again at 1500 *g*

for 10 min. Following inversion of the filter, centrifugation at 750 *g* for 5 min was used to concentrate the suspension. The microcentrifuge was run at 9500 *g* for 15 min to further concentrate the nanoparticle suspension to ~2 wt%. UV/Vis spectrophotometry was used to determine the suspension concentration and also showed that the absorption peak remained constant at 524 ± 1 nm, indicating that there was no nanoparticle aggregation.

5.2.3 Imaging

The deposited lines were imaged with an Olympus BX61 microscope with a CCD camera and 4× to 40× objectives in bright field lighting. To record the deposition process, an Olympus CKX41 inverted microscope with 10× to 40× objectives was used with a digital camera. SEM imaging was performed with a Philips XL series SEM apparatus at an accelerating voltage of 2 kV.

5.3 Results and Discussion

In order to deposit lines, a wedge, to be used as a template, is placed vertically on a glass substrate with controlled wettability. Dilute suspensions of gold nanoparticles or latex microspheres were used for the deposition process. A droplet of the particle suspension was placed on the substrate at the intersection with the wedge, as shown in Figure 5.1. The droplet was allowed to completely evaporate, and the wedge was lifted vertically off of the substrate. By controlling the wettability of the substrate, we were able

to inhibit pinning of the three-phase contact line and thus prevent the formation of a particle ring in the shape of the initial droplet.

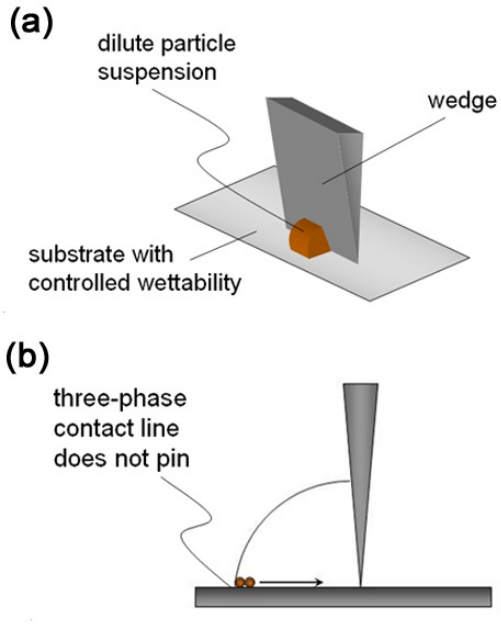

Figure 5.1. Schematics demonstrating alignment of particles via wedge-templated deposition.

5.3.1 Wettability Regimes

The wettability of the glass substrate was varied by exposing it to a mixture of chlorodimethylsilane and dichlorodimethylsilane. We found that by altering the ratio of the two silanes, the advancing contact angle could be controlled from 73° ± 2° to 89° ± 2°, resulting in three regimes of wettability.

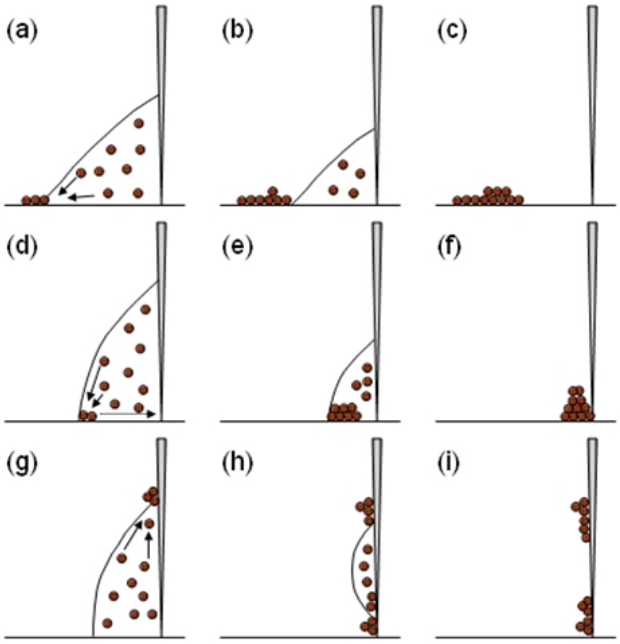

Figure 5.2. Schematics showing effect of surface contact angle. The droplet shape for each condition was drawn using images of a droplet positioned against a wedge on a substrate for each wetting regime. (a) – (c) Regime 1. Contact angle is too low, resulting in deposition of a ring. (d) – (f) Regime 2. Contact angle is such that the particle line moves with the meniscus, resulting in the deposition of a line. (g) – (i) Regime 3. Contact angle is too high, resulting in deposition of the particles on the wedge.

Regime 1 occurs when only chlorodimethylsilane was deposited, which resulted in an advancing contact angle of 73° and led to pinning of the three-phase contact line. Thus, the evaporation of the suspending liquid at the three-phase contact line led to the movement of particles towards it, resulting in the formation of a coffee ring structure (Figure 5.2a – c). Regime 3 is found by depositing only dichlorodimethylsilane, resulting in an advancing contact angle of 89°. The three-phase contact line pinned on the side of the wedge, and this resulted in the deposition of the particles on the wedge, leaving nothing on the substrate (Figure 5.2g – i). However, in Regime 2, at a contact angle of

78° ± 1.5°, we found that the formation of a line can occur because the three-phase contact line does not pin on either surface. The contact line on the glass substrate moves freely, resulting in the deposition of a line without a coffee ring structure being deposited (Figure 5.2d – f).

5.3.2 Deposition Mechanism

As a line of particles without a coffee ring structure was deposited in Regime 2, that was the focus of the remainder of this study. Once the droplet has been deposited at the edge of the wedge, the particles move to the three-phase contact line and form an ordered structure at the meniscus (Figure 5.3a). This occurs via convective assembly engendered by the evaporation of liquid[51-53] from the droplet at the three-phase contact line. Since the meniscus recedes freely on the substrate, the particles at the three-phase contact line also freely move inward toward the wedge as evaporation occurs (Figure 5.3b – c). The only place where the contact line does not move freely is at the wedge-substrate interface, where the liquid recedes in a stick-slip manner. Eventually, the droplet completely evaporates, leaving the structure aligned by the wedge (Figure 5.3d). Once the wedge has been removed from the substrate, a continuous line of particles remains.

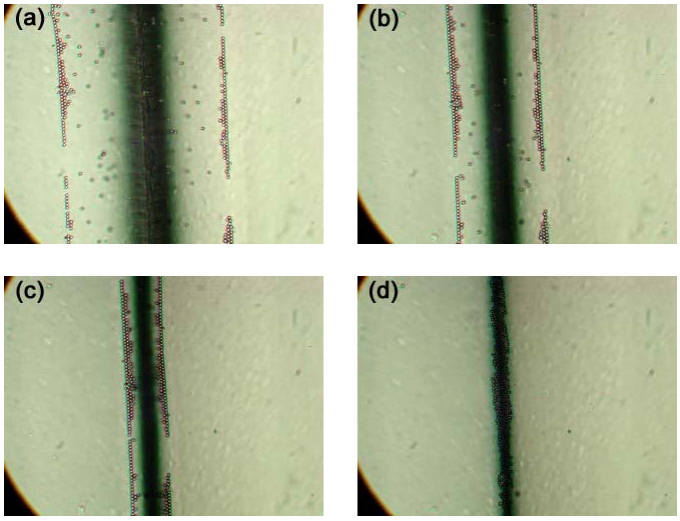

Figure 5.3. Time-lapsed bottom-up images showing the particle rearrangement within the droplet during evaporation. (a) – (c) Particles align at meniscus, which moves toward the wedge (central black line) as liquid evaporates. (d) Final structure is aligned against the wedge.

Lines of latex microspheres, as well as lines of gold nanoparticles, were deposited via this wedge-templating technique. Figure 5.4a – c shows an example of a three-dimensional, close-packed structure of latex microspheres, forming a continuous line. An example of a continuous line of gold nanoparticles is shown in Figure 5.4d – e.

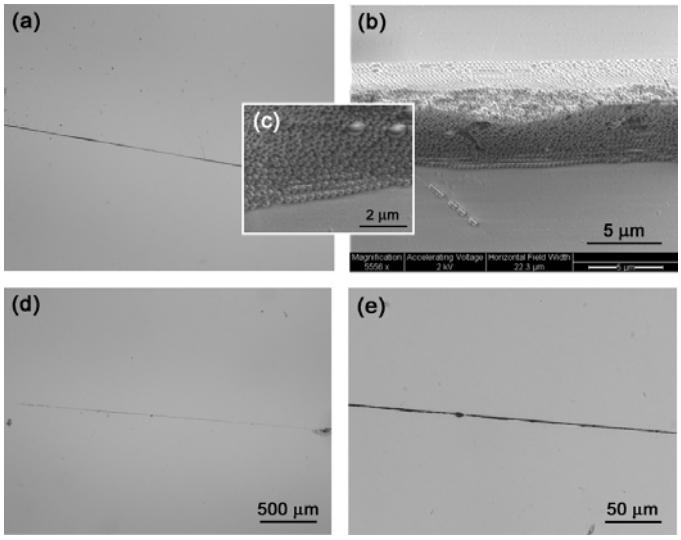

Figure 5.4. (a) & (b) SEM micrographs showing line of 0.30 µm latex particles. (c) & (d) Optical micrographs showing line of 15 nm gold nanoparticles.

5.3.3 Effect of Particle and Surfactant Concentrations on Line Structure

We evaluated the effect of particle concentration and surfactant concentration on the deposited structure. The concentration of the gold nanoparticle suspension was varied from 0.002 – 0.2 wt%, and the concentration of Tween 20 was varied from 0 – 0.1 wt%. In order to quantify the continuous part of the line, we determined the percentage of the line length consisting of a solid line. Increasing the concentration of the gold nanoparticle suspension resulted in an increase in the continuous part of the deposited line, a decrease in the line length, and an increase in line thickness (Figure 5.5). We were unable to conclusively determine the effect of Tween 20 on the deposited structure.

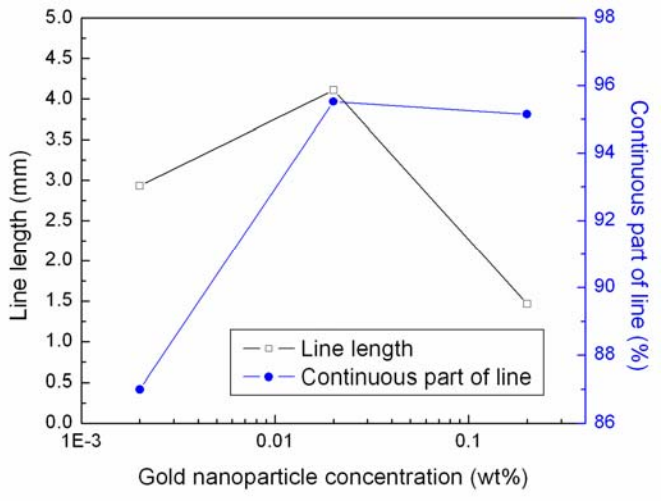

Figure 5.5. Plot showing the effect of gold nanoparticle concentration on the length and continuity of the deposited line. The Tween 20 concentration was held constant at 0.0001 wt%.

5.4 Conclusions

We have developed a novel, inexpensive, and simple technique requiring no special equipment for the deposition of dilute suspensions of nanoparticles and microparticles. We were able to convectively assemble particles at the freely moving three-phase contact line so that an ordered line of particles was deposited along the wedge. By controlling the substrate wettability and the particle concentration, we were able to deposit continuous, ordered linear structures that could potentially be used in the development of sensors.

5.5 Acknowledgements

This study was supported by the Air Force Research Laboratory. We are grateful to Laura Sowards for her assistance with the scanning electron microscope and to Caryn Heldt for her assistance with the inverted microscope.

5.6 References

[1] Ghosh, M.; Fan, F.; Stebe, K. J. "Spontaneous Pattern Formation by Dip Coating of Colloidal Suspensions on Homogeneous Surfaces." *Langmuir* 2007, *23*, 2180-2183.

[2] Huang, J.; Kim, F.; Tao, A. R.; Connor, S.; Yang, P. "Spontaneous Formation of Nanoparticle Stripe Patterns through Dewetting." *Nat. Mater.* 2005, *4*, 896-900.

[3] Huang, J.; Tao, A. R.; Connor, S.; He, R.; Yang, P. "A General Method for Assembling Single Colloidal Particle Lines." *Nano Lett.* 2006, *6*, 524-529.

[4] Huang, J.; Fan, R.; Connor, S.; Yang, P. "One-Step Patterning of Aligned Nanowire Arrays by Programmed Dip Coating." *Angew. Chem., Int. Ed.* 2007, *46*, 2414-2417.

[5] Lu, C.; Mohwald, H.; Fery, A. "A Lithography-Free Method for Directed Colloidal Crystal Assembly Based on Wrinkling." *Soft Matter* 2007, *3*, 1530-1536.

[6] Bae, C.; Shin, H.; Moon, J. "Facile Route to Aligned One-Dimensional Arrays of Colloidal Nanoparticles." *Chem. Mater.* 2007, *19*, 1531-1533.

[7] Malaquin, L.; Kraus, T.; Schmid, H.; Delamarche, E.; Wolf, H. "Controlled Particle Placement through Convective and Capillary Assembly." *Langmuir* 2007, *23*, 11513-11521.

[8] Choi, T. Y. P., D.; Grigoropoulos, C. "Fountain-Pen-Based Laser Microstructuring with Gold Nanoparticle Inks." *Appl. Phys. Lett.* 2004, *85*, 13-15.

[9] Kuncicky, D. M.; Naik, R. R.; Velev, O. D. "Rapid Deposition and Long-Range Alignment of Nanocoatings and Arrays of Electrically Conductive Wires from Tobacco Mosaic Virus." *Small* 2006, *2*, 1462-1466.

[10] Yarin, A. L.; Szczech, J. B.; Megaridis, C. M.; Zhang, J.; Gamota, D. R. "Lines of Dense Nanoparticle Colloidal Suspensions Evaporating on a Flat Surface: Formation of Non-Uniform Dried Deposits." *J. Colloid Interface Sci.* 2006, *294*, 343-354.

[11] Yerushalmi, R.; Ho, J. C.; Jacobson, Z. A.; Javey, A. "Generic Nanomaterial Positioning by Carrier and Stationary Phase Design." *Nano Lett.* 2007, *7*, 2764-2768.

[12] Butter, K.; Bomans, P. H. H.; Frederik, P. M.; Vroege, G. J.; Philipse, A. "Direct Observation of Dipolar Chains in Iron Ferrofluids by Cryogenic Electron Microscopy." *Nat. Mater.* 2003, *2*, 88-91.

[13] Liao, J.; Zhang, Y.; Yu, W.; Xu, L.; Ge, C.; Liu, J.; Gu, N. "Linear Aggregation of Gold Nanoparticles in Ethanol." *Colloids and Surfaces A: Physicochem. Eng. Aspects* 2003, *223*, 177-183.

[14] Polavarapu, L.; Xu, Q.-H. "Water-Soluble Conjugated Polymer-Induced Self-Assembly of Gold Nanoparticles and its Application to SERS." *Langmuir* 2008, *24*, 10608-10611.

[15] Sardar, R.; Shumaker-Parry, J. S. "Asymmetrically Functionalized Gold Nanoparticles Organized in One-Dimensional Chains." *Nano Lett.* 2008, *8*, 731-736.

[16] Zhang, Y. X.; Zeng, H. C. "Template-Free Parallel One-Dimensional Assembly of Gold Nanoparticles." *J. Phys. Chem. B* 2006, *110*, 16812-16815.

[17] Zhang, Y. X.; Zeng, H. C. "Surfactant-Mediated Self-Assembly of Au Nanoparticles and Their Related Conversion to Complex Mesoporous Structures." *Langmuir* 2008, *24*, 3740-3746.

[18] Bhatt, K. H.; Velev, O. D. "Control and Modeling of the Dielectrophoretic Assembly of on-Chip Nanoparticle Wires." *Langmuir* 2004, *20*, 467-476.

[19] Hermanson, K. D.; Lumsdon, S. O.; Williams, J. P.; Kaler, E. W.; Velev, O. D. "Dielectrophoretic Assembly of Electrically Functional Microwires from Nanoparticle Suspensions." *Science* 2001, *294*, 1082-1086.

[20] Terray, A.; Oakey, J.; Marr, D. W. M. "Fabrication of Linear Colloidal Structures for Microfluidic Applications." *Appl. Phys. Lett.* 2002, *81*, 1555-1557.

[21] Deng, Z.; Mao, C. "DNA-Templated Fabrication of 1D Parallel and 2D Crossed Metallic Nanowire Arrays." *Nano Lett.* 2003, *3*, 1545-1548.

[22] Cai, Y.; Newby, B.-m. Z. "Marangoni Flow-Induced Self-Assembly of Hexagonal and Stripelike Nanoparticle Patterns." *J. Am. Chem. Soc.* 2008, *130*, 6076-6077.

[23] Cherniavskaya, O.; Adzic, A.; Knutson, C.; Gross, B. J.; Zang, L.; Liu, R.; Adams, D. M. "Edge Transfer Lithography of Molecular and Nanoparticle Materials." *Langmuir* 2002, *18*, 7029-7034.

[24] Kraus, T.; Malaquin, L.; Schmid, H.; Riess, W.; Spencer, N. D.; Wolf, H. "Nanoparticle Printing with Single-Particle Resolution." *Nat. Nanotechnol.* 2007, *2*, 570-576.

[25] Bieri, N. R.; Chung, J.; Poulikakos, D.; Grigoropoulos, C. P. "Manufacturing of Nanoscale Thickness Gold Lines by Laser Curing of a Discretely Deposited Nanoparticle Suspension." *Superlattices Microstruct.* 2004, *35*, 437-444.

[26] Chung, J.; Ko, S.; Bieri, N. R.; Grigoropoulos, C. P.; Poulikakos, D. "Conductor Microstructures by Laser Curing of Printed Gold Nanoparticle Ink." *Appl. Phys. Lett.* 2004, *84*, 801-803.

[27] Lee, D. Y.; Hwang, E. S.; Yu, T. U.; Kim, Y. J.; Hwang, J. "Structuring of Micro Line Conductor Using Electro-Hydrodynamic Printing of a Silver Nanoparticle Suspension." *Appl. Phys. A* 2006, *82*, 671-674.

[28] Lee, D.-Y.; Yu, J.-H.; Shin, Y.-S.; Park, D.; Yu, T.-U.; Hwang, J. "Formation of Ceramic Nanoparticle Patterns Using Electrohydrodynamic Jet Printing with Pin-to-Pin Electrodes." *Jpn. J. Appl. Phys.* 2008, *47*, 1723-1725.

[29] Taha, H.; Marks, R. S.; Gheber, L. A.; Rousso, I.; Newman, J.; Sukenik, C.; Lewis, A. "Protein Printing with an Atomic Force Sensing Nanofountainpen." *Appl. Phys. Lett.* 2003, *83*, 1041-1043.

[30] Taha, H.; Lewis, A.; Sukenik, C. "Controlled Deposition of Gold Nanowires on Semiconducting and Nonconducting Surfaces." *Nano Lett.* 2007, *7*, 1883-1887.

[31] Dockendorf, C. P. R.; Choi, T.-Y.; Poulikakos, D.; Stemmer, A. "Size Reduction of Nanoparticle Ink Patterns by Fluid-Assisted Dewetting." *Appl. Phys. Lett.* 2006, *88*, 131903-1-3.

[32] Adachi, E.; Dimitrov, A. S.; Nagayama, K. "Stripe Patterns Formed on a Glass Surface During Droplet Evaporation." *Langmuir* 1995, *11*, 1057-1060.

[33] Deegan, R. D.; Bakajin, O.; Dupont, T. F.; Huber, G.; Nagel, S. R.; Witten, T. A. "Capillary Flow as the Cause of Ring Stains from Dried Liquid Drops." *Nature* 1997, *389*, 827-829.

[34] Deegan, R. D. "Pattern Formation in Drying Drops." *Phys. Rev. E* 2000, *61*, 475-485.

[35] Nellimoottil, T. T.; Rao, P. N. G., S. S.; Chattopadhyay, A. "Evaporation-Induced Patterns from Droplets Containing Motile and Nonmotile Bacteria." *Langmuir* 2007, *23*, 8655-8658.

[36] Sommer, A. P.; Ben-Moshe, M.; Magdassi, S. "Size-Discriminative Self-Assembly of Nanospheres in Evaporating Drops." *J. Phys. Chem. B* 2004, *108*, 8-10.

[37] Kuncicky, D. M.; Velev, O. D. "Surface-Guided Templating of Particle Assemblies Inside Drying Sessile Droplets." *Langmuir* 2008, *24*, 1371-1380.

[38] Blossey, R.; Bosio, A. "Contact Line Deposits on cDNA Microarrays: A "Twin-Spot Effect"." *Langmuir* 2002, *18*, 2952-2954.

[39] Dugas, V. B., J.; Souteyrand, E. "Droplet Evaporation Study Applied to DNA Chip Manufacturing." *Langmuir* 2005, *21*, 9130-9136.

[40] Heim, T.; Preuss, S.; Gerstmayer, B.; Bosio, A.; Blossey, R. "Deposition from a Drop: Morphologies of Unspecificially Bound DNA." *J. Phys.: Condens. Matter* 2005, *17*, S703-S716.

[41] Deegan, R. D.; Bakajin, O.; Dupont, T. F.; Huber, G.; Nagel, S. R.; Witten, T. A. "Contact Line Deposits in an Evaporating Drop." *Phys. Rev. E* 2000, *62*, 756-765.

[42] Fischer, B. J. "Particle Convection in an Evaporating Colloidal Droplet." *Langmuir* 2002, *18*, 60-67.

[43] Hu, H.; Larson, R. G. "Evaporation of a Sessile Droplet on a Substrate." *J. Phys. Chem. B* 2002, *106*, 1334-1344.

[44] Hu, H.; Larson, R. G. "Analysis of the Microfluid Flow in an Evaporating Sessile Droplet." *Langmuir* 2005, *21*, 3963-3971.

[45] Hu, H.; Larson, R. G. "Marangoni Effect Reverses Coffee-Ring Depositions." *J. Phys. Chem. B* 2006, *110*, 7090-7094.

[46] Bourges-Monnier, C.; Shanahan, M. E. R. "Influence of Evaporation on Contact Angle." *Langmuir* 1995, *11*, 2820-2829.

[47] Erbil, H. Y.; McHale, G.; Newton, M. I. "Drop Evaporation on Solid Surfaces: Constant Contact Angle Mode." *Langmuir* 2002, *18*, 2636-2641.

[48] Poulard, C.; Benichou, O.; Cazabat, A. M. "Freely Receding Evaporating Droplets." *Langmuir* 2003, *19*, 8828-8834.

[49] Tsapis, N.; Dufresne, E. R.; Sinha, S. S.; Riera, C. S.; Hutchinson, J. W.; Mahadevan, L.; Weitz, D. A. "Onset of Buckling in Drying Droplets of Colloidal Suspensions." *Phys. Rev. Lett.* 2005, *94*, 018302-1-4.

[50] Slot, J. W.; Geuze, H. J. "A New Method of Preparing Gold Probes for Multiple-Labeling Cytochemistry." *Eur. J. Cell Biol.* 1985, *38*, 87-93.

[51] Denkov, N. D.; Velev, O. D.; Kralchevsky, P. A.; Ivanov, I. B.; Yoshimura, H.; Nagayama, K. "Mechanism of Formation of Two-Dimensional Crystals from Latex Particles on Substrates." *Langmuir* 1992, *8*, 3183-3190.

[52] Denkov, N. D.; Velev, O. D.; Kralchevsky, P. A.; Ivanov, I. B.; Yoshimura, H.; Nagayama, K. "2-Dimensional Crystallization." *Nature* 1993, *361*, 26.

[53] Dimitrov, A. S.; Nagayama, K. "Continuous Convective Assembly of Fine Particles into Two-Dimensional Arrays on Solid Surfaces." *Langmuir* 1996, *12*, 1303-1311.

Chapter 6. Summary

The goal of my research has been to develop techniques for assembling biologically active particles into technologically useful materials. Corollary to this was the need to understand the phenomena responsible for the particle assembly so that the methods could be controlled and optimized.

The first part of this dissertation discussed the deposition of live cells and particles via rapid convective assembly. By developing a “convective-sedimentation” assembly method, uniform, close-packed coatings of large cells and particles could be deposited in the presence of sedimentation. A computational model was developed to enhance our understanding of the phenomena. The process was optimized by examining cell profiles produced by the model in conjunction with those determined by experimentation. We found that large forward inclination with a small angle between the two slides resulted in the most uniform coatings. These results were then used to deposit composite coatings of large latex particles and live yeast cells. By allowing these coatings time to proliferate, introducing and then removing a contaminant, and allowing the coatings to regenerate, we showed proof-of-concept for a self-cleaning surface. Different types of robust cells, as well, could be used to develop coatings with additional functionalities. It is possible to envision these coatings being used for biocatalysis, bioreactor coatings, bioassays, biosensors, and implant coatings, in addition to self-cleaning applications.

The second part of this dissertation detailed the development of techniques for the deposition of gold nanoparticles into linear assemblies. The first technique uses a capillary pulled by a linear motor to draw a meniscus thereby depositing concentrated micro- and nanoparticles onto completely wettable substrates. The lines were deposited via viscous flow and convective assembly. The structure of the deposited lines was dependent upon both the withdrawal rate and the particle concentration. We also found that the heavy, parallel lines we deposited were electrically conductive. This gives credence to the possibility of using functionalized nanoparticle lines in sensors. The second technique we developed uses a wedge placed vertically on a moderately hydrophobic substrate to template the meniscus of a dilute micro- or nanoparticle suspension droplet. The particles assembled at the freely receding three-phase contact line, resulting in the movement of the particles with the meniscus. Continuous, ordered lines were deposited by controlling the substrate wettability and the particle concentration. As with the capillary-guided lines, the deposition of functionalized gold nanoparticles via wedge templating could also be used for the development of sensors.